AD NUMBER

AD820303

NEW LIMITATION CHANGE

TO

Approved for public release, distribution unlimited

FROM

Distribution authorized to U.S. Gov't. agencies and their contractors; Critical Technology; AUG 1967. Other requests shall be referred to Rome air Development Center, AFSC, Griffiss AFB, NY.

AUTHORITY

RADC USAF ltr, 17 Sep 1971

RADC-TR-67-370
Final Report

TRANSIENT BEHAVIOR OF MICROWAVE NETWORKS

G Ross
L. Allen
R. Smith
L. Susman
Sperry Rand Research Center

TECHNICAL REPORT NO. RADC-TR-67-370
August 1967

Rome Air Development Center
Air Force Systems Command
Griffiss Air Force Base, New York

When US Government drawings, specifications, or other data are used for any purpose other than a definitely related government procurement operation, the government thereby incurs no responsibility nor any obligation whatsoever; and the fact that the government may have formulated, furnished, or in any way supplied the said drawings, specifications, or other data is not to be regarded, by implication or otherwise, as in any manner licensing the holder or any other person or corporation, or conveying any rights or permission to manufacture, use, or sell any patented invention that may in any way be related thereto.

TRANSIENT BEHAVIOR OF MICROWAVE NETWORKS

G. Ross
L. Allen
R. Smith
L. Susman

Sperry Rand Research Center

FOREWORD

This final report has been prepared by Gerald F. Ross, Lamar Allen, Robert Smith, Leon Susman of Sperry Rand Research Center, Sudbury, Massachusetts, under Contract AF30(602)-4180, project number 4506, task number 450602. Secondary report number is SRRC-CR-67-29. RADC project engineer is Vincent C. Vannicola (EMATE).

This technical report has been reviewed by the Foreign Disclosure Policy Office (EMLI). It is not releasable to the Clearinghouse for Federal Scientific and Technical Information because it contains information from release to Sino-Soviet Eloc Countries by AFR 400-10, "Strategic Trade Control Program."

This report has been reviewed and is approved.

Approved: Vincent C. Vannicola
VINCENT C. VANNICOLA
Project Engineer
Electron Devices Section

Approved: Thomas S. Bond, Jr.
THOMAS S. BOND, JR.
Colonel, USAF
Chief, Surv. & Control Div.

FOR THE COMMANDER: Irving J. Gabelman
IRVING J. GABELMAN
Chief, Advanced Studies Group

ABSTRACT

The purpose of this study is to investigate the transient behavior of nonreciprocal ferrite devices and coupled networks which are used in wideband radar and communications systems to process signals having wideband spectral content. This investigation should lead to a better understanding of the limitations imposed by the use of these components.

This final report is divided into three major component study areas. They are:

(a) nonreciprocal ferrite devices (e.g., isolators, circulators)

(b) coupled TEM-mode networks (e.g., the quarter-wavelength or parallel-line coupler)

(c) coupled waveguide networks (e.g., the sidewall coupler).

In addition, a major subsection is devoted to determining the utility of describing the transient behavior of a microwave network by a single parameter in the frequency domain, namely, "the bandwidth."

New methods are introduced to evaluate transients in microwave networks in both the study of ferrite and waveguide networks; in the former area a microstrip circulator is suggested for wideband application. A new definition of effective bandwidth for microwave networks is offered which considers energy stored in the natural modes of the device. Finally, a novel class of parallel-line couplers whose impulse response is time limited is introduced: the impulse response consists of two delayed impulses.

Both the theoretical and experimental portions of this study employ a time domain analysis as opposed to the conventional frequency domain approach. It is shown that a time domain analysis yields considerable insight and suggests new network models. The measurement and analysis techniques presented in this study are outgrowths of efforts on two previous Air Force sponsored programs, namely, "The Transient Behavior of Large Arrays" (AF30(602)-3348) and "The Transient Behavior of Radiating Elements" (AF30(602)-4050).

TABLE OF CONTENTS

TABLE OF CONTENTS (cont.)

LIST OF ILLUSTRATIONS

LIST OF ILLUSTRATIONS (cont.)

LIST OF ILLUSTRATIONS (cont.)

EVALUATION

The objective of this contract is to establish optimum approaches for evaluating the performance of certain nonreciprocal and coupled broadband microwave networks. The contractor made extensive use of the time domain and the transient response in conducting these investigations. It is shown that such approaches give rise to effective methods of analysis and evaluation where conventional approaches tend to be laborious and unwieldy. The techniques established here will provide a time domain approach to microwave and systems engineers so that the design and evaluation of broadband components can be accomplished through an optimized procedure.

SECTION I

INTRODUCTION

(G. F. Ross, Sperry Rand Research Center)

1.1 GENERAL

This final technical documentary report covers work performed during the period 28 May thru 2 June 1967, under Contract No. AF30(602)-4180 for the Rome Air Development Center, Research and Technology Division, Air Force Systems Command, Griffiss Air Force Base, New York by the Sperry Rand Research Center, Sudbury, Massachusetts in cooperation with the Sperry Microwave Electronics Company, Clearwater, Florida and the Sperry Gyroscope Company, Great Neck, New York.

1.2 THE PURPOSE OF THIS PROGRAM

The purpose of this program is to study the transient behavior of certain nonreciprocal and coupled microwave networks in an attempt to understand their properties when excited by signals having wideband spectral content. Previous Air Force Sponsored programs have analyzed the transient behavior of reciprocal and connected TEM-mode and waveguide junctions used in the feed networks of array systems† and the properties of different radiating elements*.

In particular, this program contains an analysis of nonreciprocal ferrite networks (e.g., isolators, circulators, phase shifters etc.),

---

† G. Ross, L. Susman, G. Hanley, "The Transient Behavior of Large Arrays", RADC-TR-64-581 (June 1965).

* G. Ross, R. Bates, L. Susman, G. Hanley, et al, "Transient Behavior of of Radiating Elements", AF30(602)4050 (November 1966).

and an analysis of TEM-mode coupled networks, and the (waveguide) sidewall coupler. In addition, this study includes an investigation to determine the utility of describing the transient behavior of a network or a system of networks by a single parameter in the frequency domain, namely, the "bandwidth".

The results of this program, together with the results from previous programs provide additional insight, new analytical tools, and design data for the systems engineer. The contents of this report are described in the next subsection.

1.3 CONTENTS OF THIS REPORT

This report is divided into four major subsections. They are:

- Ferrite devices (Sec. II)
- Defining a "bandwidth" parameter (Sec. III)
- TEM "wideband" coupled networks (Sec. IV)
- Sidewall waveguide coupler (Sec. V)

Section II contains a literature survey of related work (Sec. 2.2.1) and a qualitative discussion of the intrinsic limitations on transient behavior in ferrite devices (Sec. 2.2.2). The theoretical problem of wave propagation in ferrite media and in ferrite-loaded transmission lines is analyzed in Section 2.2.3. This analysis starts with Maxwell's equations and develops an expression for the system function using Laplace transform techniques: an analytical and a computer solution for finding the inverse transform of the system function is presented in Appendix A. The results of the experimental studies are presented in Section 2.3. Here, the isolator, the circulator, the helical-line digital phase shifter, and the gyromagnetic coupler are experimentally evaluated.

In Section III the utility of describing the transient behavior of a microwave network by its "bandwidth" is discussed. In Section 3.2 some of the conventional lumped-circuit definitions of bandwidth are reviewed. New definitions, which may be applied to distributed microwave networks are discussed in Sec. 3.3. In particular, one definition involving a

new quality factor $\tilde{Q}_T$ is appealing: the ordinary definition of Q proves to be a narrow-band concept and must be extended for microwave network application. The concept of Q is reviewed in Appendix B and it is shown in Appendix C that the transfer function of a network is an implicit function of the quality factor. Also, in Section 3.3 several examples that show the deficiencies of conventional bandwidth definitions are offered. A time-frequency domain technique for analytically and experimentally evaluating the "wideband" Q factor is described in Section 3.4. The technique is applied to the analysis of commensurate-line TEM-mode networks in Section 3.5: applications to certain networks are offered in Section 3.6, while experimental results are given in Section 3.7. Conclusions are presented in Section 3.8.

In Section IV the transient behavior of coupled lines is investigated. In Sections 4.2 and 4.3 the impulse response constraints necessary for the conventional coupled-line directional coupler are derived and the transient response is carefully studied. In Section 4.4 a new directional coupler that has a time-limited impulse response is developed. Section 4.5 is a discussion of the experimental results for three different 1.35 GHz conventional coupled-line directional couplers; the results are then compared to theoretical predictions.

The transient response of sidewall couplers is considered in Section V. This particular waveguide component was chosen for detailed investigation because (1) it is commonly used in modern radar systems and (2) the mathematical techniques appropriate to its analysis are applicable to a very large class of microwave structures. In Section 5.2 the previous work on the transient response of straight sections of waveguide is briefly reviewed. In Section 5.3 the results for straight sections of waveguide are used to provide the basis for the analysis of the sidewall coupler. The sidewall coupler is considered as a cascade connection of straight sections of waveguide coupled together by a straight section of uniform guide capable of supporting higher order modes. Section 5.4 presents the experimental results for the impulse and step-modulated response of an L-band sidewall coupler.

1.4 PROGRAM ORGANIZATION

This program is directed by Dr. Gerard F. Ross, Department Head for Microwave Network and Antenna Research at the Sperry Rand Research Center, where Mr. Robert S. Smith, Research Staff Member, is a co-investigator. This center's investigative activities consisted of defining bandwidth for wide-band microwave systems and evaluating the performance of TEM-mode coupled networks.

At the Sperry Microwave Electronics Company, Clearwater, Florida, Dr. Lamar Allen, Research Staff Member, was responsible for the study of ferrite devices. This program included both a theoretical and an elaborate experimental effort.

At the Sperry Gyroscope Company, Mr. Leon Susman, Senior Engineer, was responsible for the theoretical and experimental studies relating to waveguide networks.

Since this study was a three-center effort involving several Scientists, it was decided to identify the contributions of the investigators by placing their names (in parenthesis) next to each major section.

SECTION II

FERRITE DEVICES

(L. Allen, Sperry Microwave Electronics Company)

2.1 INTRODUCTION

The objective of this phase of the study is to advance the understanding of the transient behavior of ferrite devices through a closely coordinated theoretical and experimental effort. Both the intrinsic limitations of the transient response of the ferrite itself and the transient behavior of several typical operational ferrite devices are examined.

2.2 THEORETICAL STUDIES

2.2.1 General

The theoretical effort is concentrated on the related areas of: (1) intrinsic transient phenomena in ferrites, and (2) transient behavior of typical ferrite devices. A literature survey carried out early in the program revealed few papers that were directly related to the rf transient behavior of ferrite devices. The most pertinent papers are those by Suhl, Schloemann, and Shaw et al. Suhl and Schloemann are both principally interested in high-power or nonlinear effects. Shaw and his colleagues are attempting to develop a short-pulse microwave generator based on transient phenomena in ferrites. (See references 1-8 in the bibliography.) During this program an effort was made to formulate the theoretical study of transients in ferrite devices directly in the time domain.

2.2.2 Some Comments on Intrinsic Transient Behavior

There are various intrinsic relaxation and excitation times associated with a ferrite. For example, there is a spin-lattice relaxation time (which is a measure of the length of time required to transfer energy from the uniform precession mode to the lattice) and there is a spin-spin relaxation time (which is a measure of the time required to transfer energy from the uniform precession mode to higher-order spin waves). The spin-spin relaxation time for a typical material might be of the order of a few

nanoseconds, while the spin-lattice relaxation time for the same material would be of the order of a hundred nanoseconds. An important parameter in the study of transient behavior of ferrite devices is the excitation time for the uniform precession. Excitation times for the uniform precession mode appear to be of the order of 100 picoseconds. From the time that the uniform precession is established until that time when loss of energy to spin waves occurs at a significant rate, the uniform precession is essentially an undamped mode of oscillation for the magnetic moments of material.

2.2.3 Transient Wave Propagation in an Infinite Ferrite

Before investigating the transient behavior of particular ferrite devices, consider the case of wave propagation in an infinite ferrite medium. An electromagnetic wave in a ferrite can be represented mathematically by the following three coupled equations:

$$\nabla \times \bar{e} = -\mu_o \left\{ \frac{\partial \bar{h}}{\partial t} + \frac{\partial \bar{m}}{\partial t} \right\} \tag{2.1}$$

$$\nabla \times (\bar{h} + \bar{H}_o) = \epsilon \frac{\partial \bar{e}}{\partial t} \tag{2.2}$$

$$\frac{\partial \bar{m}}{\partial t} = \gamma \left\{ (\bar{m} + \bar{M}_o) \times (\bar{h} + \bar{H}_o) \right\} - \frac{\alpha}{|\bar{M}|} \left\{ (\bar{m} + \bar{M}_o) \times \frac{\partial \bar{m}}{\partial t} \right\} \tag{2.3}$$

where $\bar{e}$ = time-varying electric field
$\bar{h}$ = time-varying magnetic field
$\bar{m}$ = time-varying magnetization
$\bar{H}_o$ = static magnetic field
ϵ = dielectric constant
μ_o = permeability of free space
γ = gyromagnetic ratio
α = damping parameter.
$\bar{M}_o$ = static magnetization

Assume that

$$\bar{M}_o = \bar{u}_z M_o$$
$$\bar{H}_o = \bar{u}_z H_o$$

where $\bar{u}_z$ is the unit vector in the z direction.

Then, in the small signal case Eq. 2.3 can be written in expanded form as

$$\frac{\partial m_x}{\partial t} = \gamma \left(H_o m_y - M_o h_y \right) + \alpha \frac{\partial m_y}{\partial t}$$
$$\frac{\partial m_y}{\partial t} = \gamma \left(-H_o m_x + M_o h_x \right) - \alpha \frac{\partial m_x}{\partial t} \qquad (2.4)$$
$$\frac{\partial m_z}{\partial t} = 0 \quad .$$

If it is further assumed that the time varying magnetization and magnetic field are zero at the initial instant, then $t = 0$. Then taking the Laplace transform with respect to time of Eq. 2.4 yields

$$s\hat{m}_x = \gamma \left(H_o \hat{m}_y - M_o \hat{h}_y \right) + \alpha \left(s\hat{m}_y \right)$$
$$s\hat{m}_y = \gamma \left(-H_o \hat{m}_x + M_o \hat{h}_x \right) - \alpha \left(s\hat{m}_x \right) \qquad (2.5)$$
$$s\hat{m}_z = 0$$

where s = Laplace transform parameter, $\hat{m}_x = L\left(m_x\right)$, etc. Solving for $\hat{m}_x$ and $\hat{m}_y$ in terms of $\hat{h}_x$ and $\hat{h}_y$ yields

$$\hat{m}_x = \chi_{xx} \hat{h}_x + \chi_{xy} \hat{h}_y \qquad (2.6a)$$

$$\hat{m}_y = \chi_{yx}\hat{h}_x + \chi_{yy}\hat{h}_y \tag{2.6b}$$

where

$$\chi_{yx} = -\chi_{xy} = \frac{s\gamma\mathfrak{M}_0}{s^2 + (\gamma H_0 + \alpha s)^2}$$

$$\chi_{xx} = \chi_{yy} = \frac{(\gamma M_0)(\gamma H_0 + \alpha s)}{s^2 + (\gamma H_0 + \alpha s)^2} \tag{2.7}$$

Thus,

$$\hat{\bar{m}} = \overleftrightarrow{\chi}\ \hat{\bar{h}} \tag{2.8}$$

where

$$\hat{\bar{m}} = L\left\{\bar{m}\right\}, \quad \hat{\bar{h}} = L\left\{\bar{h}\right\}, \quad \text{and}$$

$$\overleftrightarrow{\chi} = \begin{bmatrix} \chi_{xx} & \chi_{xy} & 0 \\ \chi_{yx} & \chi_{yy} & 0 \\ 0 & 0 & 0 \end{bmatrix}$$

Maxwell's equations can then be written in the form

$$\begin{aligned} \nabla x\hat{\bar{e}} &= -s(I + \overleftrightarrow{\chi})\,\hat{\bar{h}} = -s\overleftrightarrow{\mu}\,\hat{\bar{h}} \\ \nabla x\hat{\bar{h}} &= s\varepsilon\hat{\bar{e}} \end{aligned} \tag{2.9}$$

where $I + \overleftrightarrow{\chi} = \overleftrightarrow{\mu}$; I is the identity matrix.

Eliminating $\hat{\bar{e}}$ from Eq. 2.9 , we obtain

$$\nabla x\,\nabla x\hat{\bar{h}} = -s^2\varepsilon\overleftrightarrow{\mu}\hat{\bar{h}}$$

or

$$-\nabla^2\hat{\bar{h}} + \nabla(\nabla\cdot\hat{\bar{h}}) = -s^2\varepsilon\overleftrightarrow{\mu}\ \hat{\bar{h}} \tag{2.10}$$

(2.10)

The plane-wave solution has the form*

$$\hat{\bar{h}} = \hat{\bar{h}}_0 e^{-\xi(\bar{n} \cdot \bar{r})} \tag{2.11}$$

where ξ is a function of s and material parameters but not of the coordinates x, y, and z, and

$\bar{n}$ = unit vector in the direction of propagation

$\bar{r}$ = displacement vector .

Thus, for $\hat{\bar{h}}$ as given in Eq. 2.11

$$\begin{aligned} \nabla(\nabla \cdot \hat{\bar{h}}) &= \xi^2 (\bar{n} \cdot \hat{\bar{h}})\, \bar{n} \\ \nabla^2 \hat{\bar{h}} &= \xi^2 n^2 \hat{\bar{h}} \end{aligned} \tag{2.12}$$

Substituting Eq. 2.12 into Eq. 2.10 yields

$$\xi^2 \left[-n^2 \hat{\bar{h}} + (\bar{n} \cdot \hat{\bar{h}})\, \bar{n} \right] = -s^2 \varepsilon \overleftrightarrow{\mu}\, \hat{\bar{h}} \tag{2.13}$$

Assume that the applied dc magnetic field is in the z direction and the propagation vector is in the xz plane, so that $n_y = 0$, $n_x = \sin \phi$, and $n_z = \cos \phi$, where ϕ is the angle between the direction of propagation and the dc magnetic field. Expanding Eq. 2.13 into its three rectangular component equations yields three homogeneous linear equations in $\hat{h}_x$, $\hat{h}_y$, and $\hat{h}_z$. The determinant of the coefficients must vanish for a nontrivial solution; thus

$$\begin{vmatrix} -\xi^2 \cos^2 \phi + s^2 \mu_0 \mu & s\varepsilon\mu_0 K & \xi^2 \sin \phi \cos \phi \\ j s^2 \varepsilon \mu_0 K & -\xi^2 + s^2 \varepsilon \mu_0 \mu & 0 \\ \xi^2 \sin \phi \cos \phi & 0 & \xi^2 \sin^2 \phi + s^2 \varepsilon \mu_0 \end{vmatrix} = 0 \tag{2.14}$$

*See Reference 10 for a similar analysis in the frequency domain.

where $\mu = 1 + \chi_{xx}$ and $K = -j\chi_{yx}$.

Expanding the determinant and solving for ξ yields

$$\xi_{\pm}^2 = s^2 \mu_0 \epsilon \left\{ \frac{(\mu^2 - \mu - K^2)\sin^2\phi + 2\mu \pm \left[(\mu^2 - \mu - K^2)^2 \sin^4\phi + 4K^2\cos^2\phi\right]^{\frac{1}{2}}}{2(\cos^2\phi + \mu \sin^2\phi)} \right\} \tag{2.15}$$

The field is then

$$\hat{h} = \hat{h}_0 e^{-\xi \pm (\bar{n} \cdot \bar{r})} \tag{2.16}$$

where $\xi \pm$ is given by Eq. 2.15 . The transient response can be determined by taking the inverse Laplace transform of Eq. 2.16 . However, ξ is, in general, such a complicated function of s that inversion cannot be carried out analytically.

2.2.3.1 Transverse Field

A special case of particular interest is that in which the direction of the applied dc magnetic field is perpendicular to the direction of propagation. Then the value of ϕ in Eq. 2.15 is $\pi/2$ and ξ becomes

$$\xi_+ = s\sqrt{\mu_0 \epsilon} \left(\frac{\mu^2 - K^2}{\mu} \right)^{\frac{1}{2}} \tag{2.17a}$$

$$\xi_- = s\sqrt{\mu_0 \epsilon} \tag{2.17b}$$

Suppose propagation is in the y direction and the dc magnetic field is applied in the z direction. The solution ξ_- then represents a wave with the rf magnetic vector in the z direction and the rf electric vector in the x direction. In this case the rf magnetic field does not interact with the spin dipoles of the ferrite and the material resembles a simple dielectric.

Consider a plane wave which is zero for $t \leq 0$ propagating in the $+y$ direction. At $y = 0$ let the form of the wave be specified by $\bar{h}(0,t) = \bar{u}_z h_z(0,t) = \bar{u}_z f(t)$, so that

$$L\left\{ h_z(0,t) \right\} = \hat{f}(s) \quad .$$

If the ferrite has a conductivity σ, Eq. 2.17b becomes

$$\xi- = s \sqrt{\mu_o \epsilon + \frac{\mu_o \sigma}{s}}$$

Then

$$\hat{h}_z(y,s) = \hat{f}(s)\, e^{-\left(s\sqrt{\mu_o \epsilon + \frac{\mu_o \sigma}{s}}\right) y} \tag{2.18}$$

Stratton[9] has provided the necessary transform pairs for inverting this function. The result is

$$\hat{h}_z(y,t) = e^{-\left(\frac{\sigma}{2}\sqrt{\mu_o/\epsilon}\right) y} \quad f(t - \sqrt{\mu_o \epsilon}\, y) \tag{2.19}$$

$$- \frac{1}{\sqrt{\mu\epsilon}}\, e^{-\frac{\sigma}{2\epsilon}} \quad t \int_0^t - \sqrt{\mu_o \epsilon}\, y \; f(\beta) \exp \frac{\sigma}{2\epsilon} \beta \frac{2}{\partial y} \; Jo \left(\frac{\sigma}{2} \sqrt{\frac{\mu_o}{\epsilon}} \sqrt{z^2 - \frac{1}{\mu\epsilon}(t-\beta)^2} \right) d\beta$$

which represents a damped wave traveling in the $+y$ direction in a dissipative dielectric. For $y = 0$, $h_i(0,t) = f(t)$ for all $t > 0$. The first term results in a delayed, weighted replica of the input signal $f(t)$; the second term introduces the distortion.

If propagation is in the y direction and the rf magnetic field lies in the xy plane transverse to the applied dc magnetic field, interaction between the rf magnetic field and the spin dipoles does take place and $\xi+$ is the appropriate solution. In this case the wave is transverse electric and the x and z components of the rf fields can be expressed in terms of the y component of the rf magnetic field. The system function for

this wave corresponding to the ratio of h_y components at y and $y = 0$ is given by

$$\frac{\hat{h}_y(x,y,z,s)}{\hat{h}_y(x,0,z,s)} = e^{-s\sqrt{\mu_0\epsilon}\left(\frac{\mu^2 - K^2}{\mu}\right)^{\frac{1}{2}} y} \tag{2.20}$$

where $\mu = \chi_{xx}$, $K = -j\chi_{yx}$, and χ_{xx} and χ_{yx} are given by Eq. 2.7. The inverse Laplace transform of the right hand side of Eq. 2.20 is then the impulse response of the ferrite under the specified conditions. Unfortunately, this is a very complicated function of s and direct inversion has not been possible. It is, however, apparent that the impulse response will consist of a delayed replica of the input plus a series of Bessel function terms which represent distortion.

2.2.3.2 Longitudinal Field

Another special case of considerable interest is that in which the direction of propagation is parallel to the applied magnetic field. For this case $n_x = n_y = 0$, $n_z = 1$, and $\hat{h} = \hat{h}_0 e^{-\xi z}$. Eq. 2.15 then becomes

$$\xi_{\pm}^2 = s^2 \mu_0 \epsilon (\mu \pm K) \tag{2.21}$$

For this case the types of functions that must be inverted to obtain the impulse response are of the form

$$e^{-s\sqrt{\mu_0\epsilon(\mu \pm K)}} \tag{2.22}$$

where

$$\mu \pm K = \frac{s^2 + (\sqrt{H_0} + \alpha s)^2 + \gamma M_0 (\sqrt{H_0} + \alpha s) \mp j s \gamma M_0}{s^2 + (\sqrt{H_0} + \alpha s)^2}$$

This function is also quite complicated and a direct analytical inversion has not been possible. However, if H_0 is set equal to zero then Eq. 2.22 reduces to the form of Eq. 2.18 and can be inverted to yield a delayed and attenuated replica of the input signal plus distortion terms similar to the result shown in Eq. 2.19 . In the general case the response is more complicated but similar in form. An approach to the inversion of functions like Eq. 2.22 in terms of a series expansion is given in Appendix A. A computer program for inverting complicated unilateral Laplace transforms like Eq. 2.22 has just been completed under this contract. The details are not reported here because of time limitations. To check the technique, the inversion of Eq. 2.22 was accomplished and compared to the series solution (see Appendix A). It appears that this program should have considerable utility in future transient analyses.

2.2.4 Transient Behavior of Bounded Media

The exact analysis of the transient performance of microwave devices presents such formidable mathematical difficulties that one of necessity attempts various approximate calculations. Variational and perturbational techniques appear particularly interesting. Frequency-domain formulations of such techniques can be found in many books and articles.[10,11] Similar formulations in the s domain are also possible.

Let $L\{\bar{e}(x,y,z,t)\} = \hat{\bar{e}}(x,y,z,s)$, etc. Maxwell's equations for linear, isotropic homogeneous media, after Laplace transformation with respect to time (with $\rho = 0$, $\bar{J} = 0$), become

$$\begin{aligned} \nabla \times \hat{\bar{e}} &= -s\mu \hat{\bar{h}} \\ \nabla \times \hat{\bar{h}} &= s\epsilon \hat{\bar{E}} \\ \nabla \cdot \hat{\bar{h}} &= 0 \\ \nabla \cdot \hat{\bar{e}} &= 0 \end{aligned} \tag{2.23}$$

Suppose that the fields in a waveguide are of the form*

$$\hat{\bar{e}} = \bar{e}_z(x,y)\, e^{-\Gamma z} \tag{2.24}$$

* This is a crucial step for the work that follows. Often one assumes that in symmetric junctions the field can be expressed as the product of two terms: one a function of the coordinate system and one a function of time.

where Γ = function of s but not of coordinates.

$\hat{\underline{e}}$ = function of x, y but not of the complex variable s.

$$\nabla_{xe}\hat{\underline{e}} = e^{-\Gamma z}\left\{\nabla_{xe}\underline{\underline{e}} - \Gamma \bar{u}_z \times \underline{\underline{e}}\right\}$$

$$\nabla_{xh}\hat{\underline{h}} = e^{-\Gamma z}\left\{\nabla_{xh}\underline{\underline{h}} - \Gamma \bar{u}_z \times \underline{\underline{h}}\right\} \qquad (2.25)$$

Substituting Eq. 2.25 into Eq. 2.23 and scalar multiplying the first of equations 2.23 by $\underline{\underline{h}}$, the second by $\underline{\underline{e}}$, and then finding the difference between the two resulting equations, we obtain

$$\nabla \cdot \underline{\underline{e}} \times \underline{\underline{h}} + s\,(\mu \underline{\underline{h}} \cdot \underline{\underline{h}} + \epsilon \underline{\underline{e}} \cdot \underline{\underline{e}}) = 2\Gamma \underline{\underline{e}} \times \underline{\underline{h}} \cdot \bar{u}_z$$

Integrating over the cross section of the waveguide, we obtain

$$\Gamma = \frac{\iint (s\mu \underline{\underline{h}} \cdot \underline{\underline{h}} + s\epsilon \underline{\underline{e}} \cdot \underline{\underline{e}} + \nabla \cdot \underline{\underline{e}} \times \underline{\underline{h}})\, da}{2\iint \underline{\underline{e}} \times \underline{\underline{h}} \cdot \bar{u}_z\, da} \qquad (2.26)$$

From the identity

$$\iint \nabla \cdot \underline{\underline{e}} \times \underline{\underline{h}}\, da = \oint_c \underline{\underline{e}} \times \underline{\underline{h}} \cdot \bar{n}\, d\ell$$

the third term in the numerator of Eq. 2.26 vanishes if $\bar{n} \times \underline{\underline{e}} = 0$ on c. Hence,

$$\Gamma = \frac{s \iint \left[\mu \underline{\underline{h}} \cdot \underline{\underline{h}} + \epsilon \underline{\underline{e}} \cdot \underline{\underline{e}}\right] da}{2\iint \underline{\underline{e}} \times \underline{\underline{h}} \cdot \bar{u}_z\, da} \qquad (2.27)$$

This formula for Γ is stationary if the trial fields are selected so that $\bar{n} \times \check{\bar{e}} = 0$ on c. Equations similar to Eq. 2.27 involving $\check{\bar{e}}$ or $\check{\bar{h}}$ fields only can be obtained by eliminating $\check{\bar{h}}$ or $\check{\bar{e}}$, respectively, from Eqs. 2.23 and proceeding as above. The $\check{\bar{e}}$ - field result is

$$\Gamma^e = \frac{\iint \left\{ \mu^{-1} (\nabla \times \check{\bar{e}}) \cdot (\nabla \times \check{\bar{e}}) - s^2 \epsilon \check{\bar{e}} \cdot \check{\bar{e}} \right\} da}{\iint \left[\mu^{-1} (\bar{u}_z \times \check{\bar{e}}) \cdot (\bar{u}_z \times \check{\bar{e}}) \right] da} \tag{2.28}$$

which is stationary if $\bar{n} \times \bar{e} = 0$ on c . The result for the $\check{\bar{h}}$ - field is

$$\Gamma^h = \frac{\iint \left\{ \epsilon^{-1} (\nabla \times \check{\bar{h}}) \cdot (\nabla \times \check{\bar{h}}) - s^2 \mu \check{\bar{h}} \cdot \check{\bar{h}} \right\} da}{\iint \left[\epsilon^{-1} (\bar{u}_z \times \check{\bar{h}}) \cdot (\bar{u}_z \times \check{\bar{h}}) \right] da} \tag{2.29}$$

which is stationary with no boundary conditions required on $\check{\bar{h}}$. Similar results can be obtained for anisotropic media as illustrated by the frequency domain results of Berk.[12]

As an example of how these stationary formulas can be used to compute the transient response of microwave devices, consider a dielectric-loaded waveguide consisting of a single full-height dielectric slab in the center of a rectangular waveguide, as shown in Fig. 2.1.

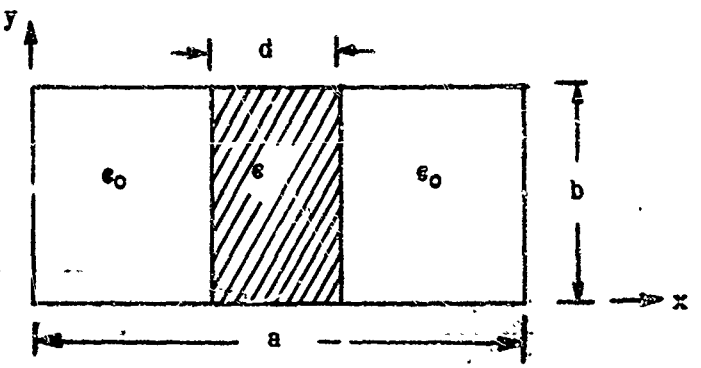

FIG. 2-1 A dielectric slab in the center of a rectangular waveguide.

As a trial field, take

$$\bar{e} = \bar{u}_y \sin \frac{\pi x}{a} e^{-\Gamma z}$$

corresponding to the dominant TE-mode propagation and use Eq. 2.28 . The result is

$$\Gamma^2 = s^2 \mu_0 \epsilon_0 \left[1 + \frac{\epsilon - \epsilon_0}{\epsilon_0} \left(\frac{d}{a} + \frac{1}{\pi} \sin \frac{\pi d}{a}\right)\right] + \left(\frac{\pi}{a}\right)^2 \tag{2.30}$$

$$\Gamma = c_1 \sqrt{s^2 + \left(\frac{c_2}{c_1}\right)^2}$$

where

$$c_1^2 = \mu_0 \epsilon_0 \left[1 + \frac{\epsilon - \epsilon_0}{\epsilon_0} \left(\frac{d}{a} + \frac{1}{\pi} \sin \frac{\pi d}{a}\right)\right]$$

$$c_2^2 = \left(\frac{\pi}{a}\right)^2$$

The transverse field can be obtained from the longitudinal magnetic field through Maxwell's equations. The "transfer function" for the longitudinal magnetic field is

$$\frac{h_z(x,y,z,s)}{h_z(x,y,0,s)} = e^{-c_1\left(\sqrt{s^2 + \left(\frac{c_2}{c_1}\right)^2}\right)z} \tag{2.31}$$

If $d = 0$ then Eq. 2.31 reduces to

$$\frac{h_z(x,y,z,s)}{h_z(x,y,0,s)} = e^{-z\sqrt{\mu_0 \epsilon_0}\sqrt{s^2 + \left(\frac{\pi}{a}\right)^2}} \tag{2.32}$$

which is the exact equation for the empty waveguide case.

The impulse response corresponding to Eq. 2.31 is

$$\frac{h_z(x,y,z,t)}{h_z(x,y,0,t)} = \delta(t - c_1 z) - \frac{c_2 z}{\sqrt{t^2 - (c_1 z)^2}} J_1\left(\frac{c_2}{c_1}\sqrt{t^2 - (c_1 z)^2}\right) u(t - c_1 z) \qquad (2.33)$$

The transfer functions and impulse responses for the transverse components can be determined in the manner indicated in Sec. 5.2.1. The frequency domain formula corresponding to Eq. 2.30 was found by Berk to yield 0.5% accurac when the dielectric constant of the loading slab was relatively small. The dielectric-loaded waveguide example given above illustrates the powe the variational technique when applied to the transient analysis icrowave devices.

Perturbation techniques such as those discussed by Lax and Button[12] for the frequency domain can also be applied in the s domain. As an example, consider the change in transient response due to the introduction of a transversely magnetized ferrite rod into a rectangular waveguide, as in Fig. 2-2.

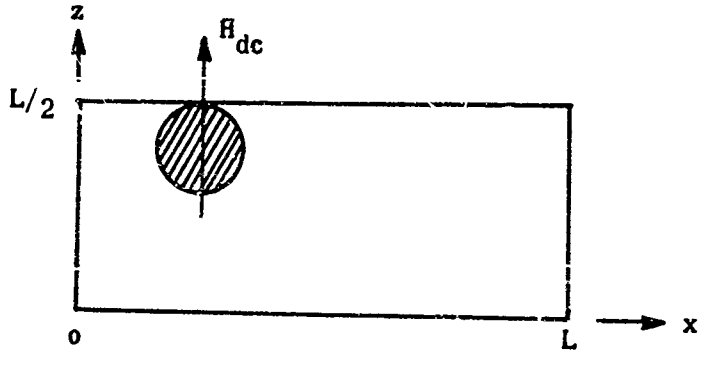

FIG. 2-2 A transversely magnetized ferrite rod in a rectangular waveguide.

The fields of the unperturbed waveguide are assumed to be those of the TE_{10} mode. The propagation factor of the perturbed guide as a function of s is found to be

$$\Gamma \pm = \Gamma_o + \frac{s^2 \mu_o \epsilon_o \Delta A}{\Gamma_o A} \left(\frac{\epsilon - \epsilon_o}{\epsilon_o} \right) \sin^2 k\chi$$

$$+ \frac{\Delta A}{A \Gamma_o} (\chi_{xx} \Gamma_o^2 \sin^2 k\chi - \chi_{yy} k^2 \cos^2 k\chi \pm \chi_{xy} k \Gamma_o \sin^2 k\chi) \qquad (2.34)$$

where $\Gamma_o = \sqrt{\mu_o \epsilon_o} \sqrt{s^2 + k^2}$

$k = \pi / L$

ΔA = cross-sectional area of ferrite rod

A = cross-sectional area of waveguide

$\chi_{xx} = \chi_{yy}$ and χ_{xx} and χ_{yx} are given by Eq. 2.7 .

The longitudinal h-field transfer function for the ferrite-loaded guide is

$$\frac{\check{h}_y(x,y,z,s)}{\check{h}_y(x,o,z,s)} = e^{-\Gamma \pm y} \qquad (2.35)$$

where $\Gamma \pm$ is given by Eq. 2.34 and Γ_+ is for a dc bias field in the $+z$ direction, while Γ_- is for a dc bias field in the $-z$ direction. Since χ_{xx} and χ_{xy} are complicated functions of s, Eq. 2.35 will be quite difficult to invert. If inversion can be achieved, the inverse transform will be the impulse response for the longitudinal h field of the ferrite-loaded waveguide. Note that in the case where ΔA is zero, Eq. 2.34 reduces to Γ_o, the propagation factor for the unperturbed or empty waveguide.

It certainly appears that variational and perturbational methods will be very useful in transient analysis. However, the general validity of the methods in the s domain needs to be carefully examined. In a brief literature survey no publications were found in which transient analysis was carried out by such techniques.

2.3 EXPERIMENTAL STUDIES

2.3.1 General

A number of ferrite devices were studied experimentally. Device types were selected such that the effect of the ferrite on transient response could be examined with the ferrite operating in a variety of magnetization states (i.e., below resonance, at resonance, in the remanent state, etc.).

The transient response of each ferrite device selected for study was determined utilizing the pulse generator furnished by SRRC and a time-domain reflectometer. The experimental apparatus configuration is shown in Fig. 2-3. The devices examined were coaxial resonance isolators, stripline and microstrip circulators, a helical-line ferrite digital phase shifter, a dielectric-loaded helical line, and a gyromagnetic coupler filter.

2.3.2 Isolators

The transient behavior of resonance isolators has been probed by determining the response of two coaxial resonance isolators to 8 cycles of a 1500 MHz pulse-modulated signal and to a very short spike or impulse of energy. The measured frequency response of each of the two isolators is as follows:*

* Also see Fig. 2-8.

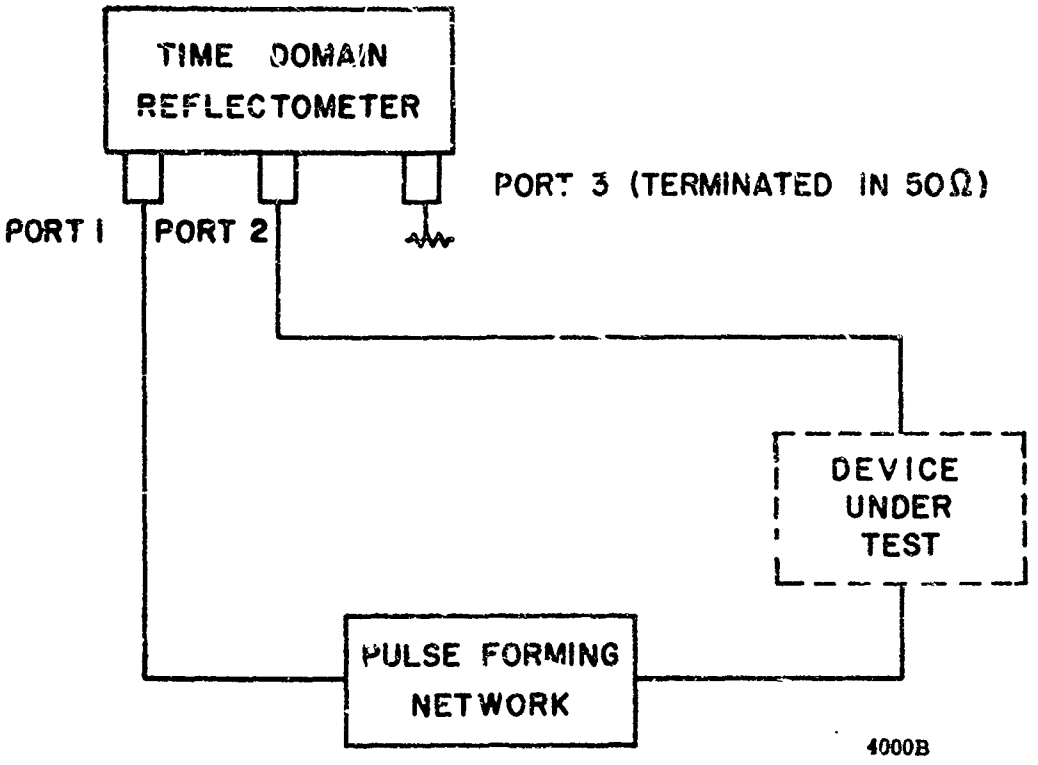

FIG. 2-3 Block diagram of experimental apparatus.

D44L15 Frequency (GHz)	"Broadband" Coaxial Resonance Isolator Isolation (dB)	Insertion Loss (dB)	VSWR
1.0	11.3	0.35	1.06
1.2	18.6	0.50	1.02
1.4	12.4	0.50	1.05
1.6	12.2	0.78	1.12
1.8	12.8	0.62	1.04
2.0	20.2	0.90	1.08

D44L17 Frequency (GHz)	"Narrow Band" Coaxial Resonance Isolator Isolation (dB)	Insertion Loss (dB)	VSWR
1.25	24.3	0.57	1.17
1.40	16.6	0.60	1.02
1.55	15.9	0.75	1.05

Oscilloscope pictures of the reference pulse and the forward and reverse response of the broadband (D44L15) isolator are shown in Fig. 2-4. The forward response indicates that the pulse is transmitted in the forward direction essentially unchanged in form and attenuated by an amount corresponding to the steady-state attenuation (i.e., about 0.6 dB at 1.5 GHz). That first half-cycle of the forward output is attenuated more than the steady-state value is probably due to the tenth of a nanosecond or so required to establish the uniform precession mode in the ferrite.

The reverse direction response of the isolator exhibits an isolation lower than the steady-state value for the initial few tenths of a nanosecond because of the time required to excite the uniform precession mode. For somewhat more than a nanosecond after the uniform precession mode is established, there is essentially no damping by energy transfer to spin waves, and the uniform precession apparently builds up to a large value, making the isolation greater than its steady-state value. After

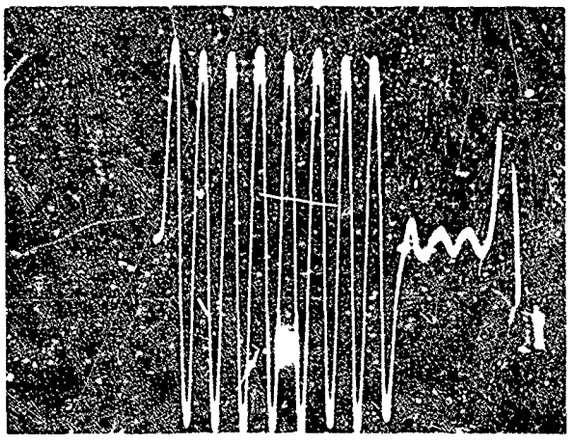

(a) Reference Pulse (Vert x20, Hor 1 nsec/cm)

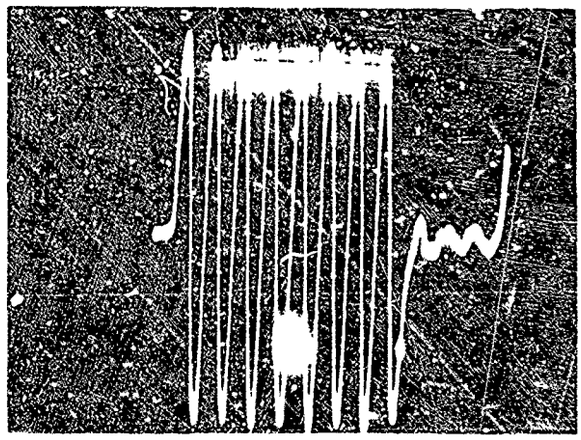

(b) Response of Adapters Used in Test (Vert x20, Hor 1 nsec/cm)

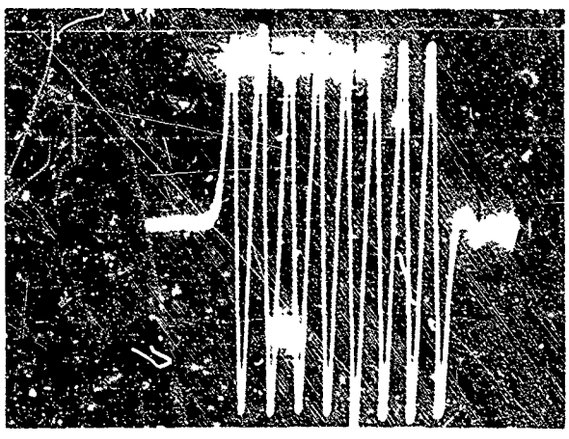

(c) Forward Pulsed Sinusoid Response, D44L15 (Vert x20, Hor 1 nsec/cm)

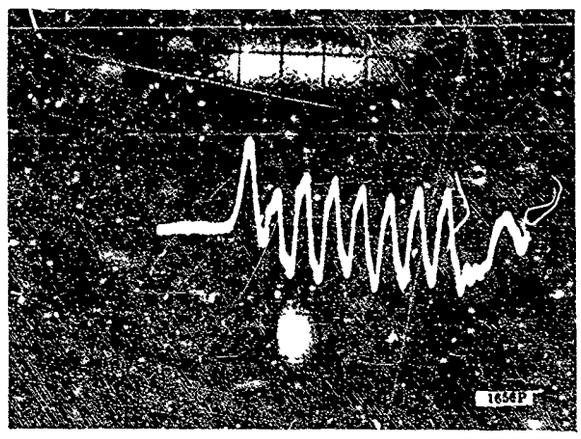

(d) Reverse Pulsed Sinusoid Response, D44L15 (Vert x20, Hor 1 nsec/cm)

two or three nanoseconds the isolation settles down to its steady-state value. These comments are consistent with the plot of measured isolation vs. time depicted graphically in Fig. 2-5. The behavior of the isolation is strikingly similar to the behavior of the precession angle θ, as illustrated in Fig. 2 of reference 10 in the bibliography.

The response of the broadband isolator to a very short spike of energy is shown in Fig. 2-6. In the forward direction the spike is transmitted with little attenuation but with some trailing edge distortion in the form of ringing. In the reverse direction, the pulse is attenuated by about 6 dB. This corresponds to the attenuation of the first half-cycle of the pulsed sinusoid, as shown in Fig. 2-5.

Figure 2-7 shows the impulse and pulse-modulated response of a commercially available narrow-band coaxial resonance isolator (D44L17). Both the forward and reverse responses are similar to those of the commercially available broadband unit. The bandwidths of these components are commonly specified with respect to tolerance levels on the isolation and the insertion losses. However, as can be seen from Fig. 2-8, although the characteristics of the D44L17 isolator do not meet the specifications necessary for classification as broadband, the frequency-domain characteristics are not significantly different from those of the broadband D44L15 unit. This leads one to question the utility of the conventionally accepted definition of bandwidth. This topic is discussed in detail in Sec. III.

2.3.3 Circulators

The transient behavior of Y-junction circulators has been probed by determining the response of four stripline circulators and a microstrip circulator to an impulse and to a pulse-modulated signal of 8 cycles of rf energy at 1500 MHz.

The measured frequency response of three of the stripline circulators is as follows:

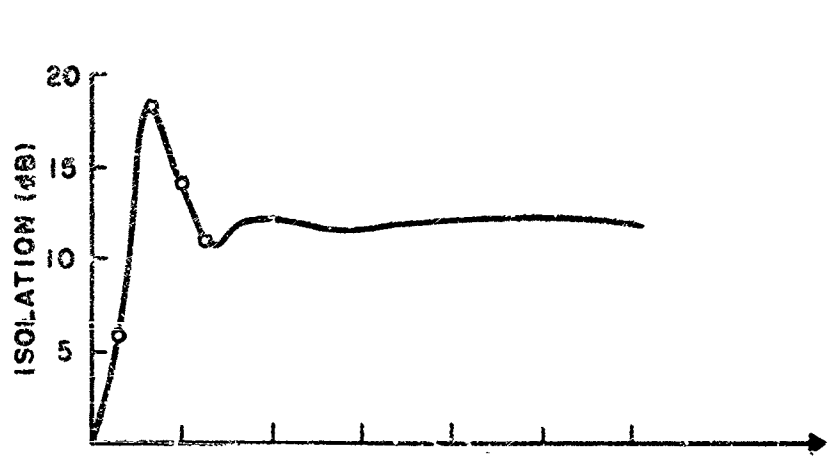

FIG. 2-5 Measured isolation vs time.

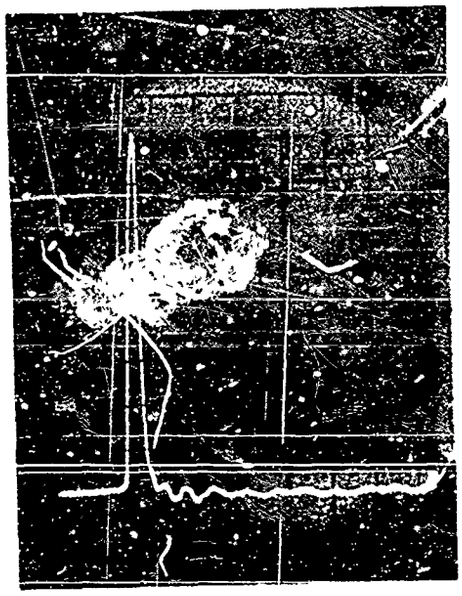

(a) Reference Pulse (Vert x40, Hor 1 nsec/cm)

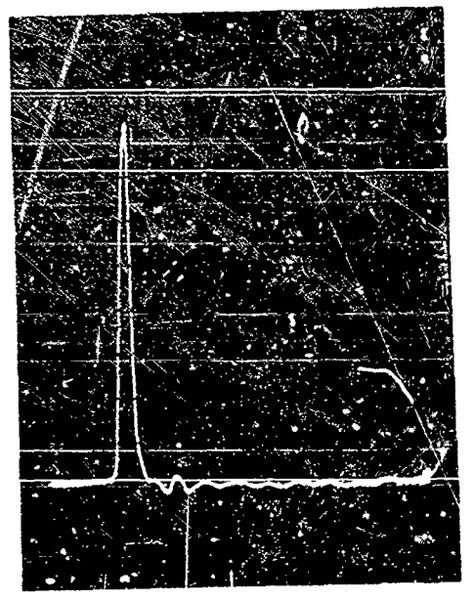

(b) Response of Adapters Used in Test (Vert x40, Hor 1 nsec/cm)

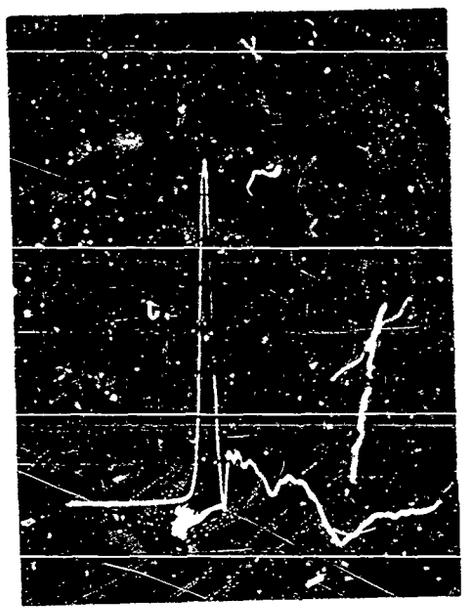

(c) Forward Impulse Response, D44L15 (Vert x40, Hor 1 nsec/cm)

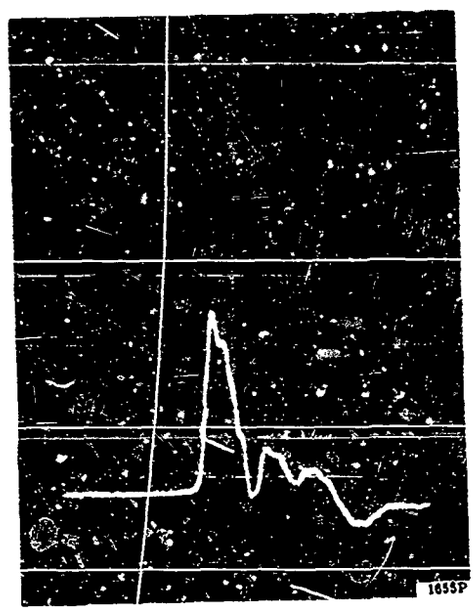

(d) Reverse Impulse Response, D44L15 (Vert x40, Hor 1 nsec/cm)

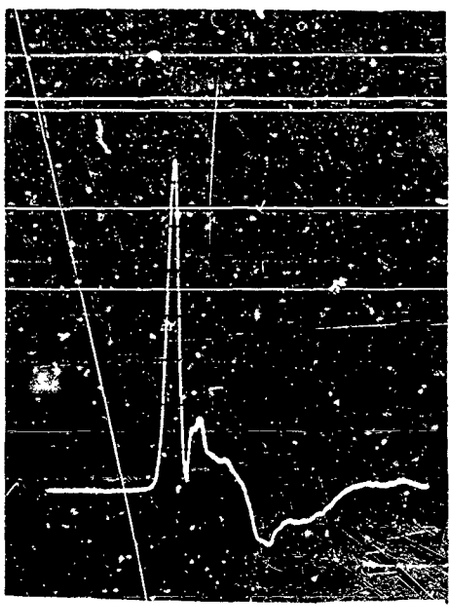

(a) Forward Impulse Response, D44L17 (Vert x40, Hor 1 nsec/cm)

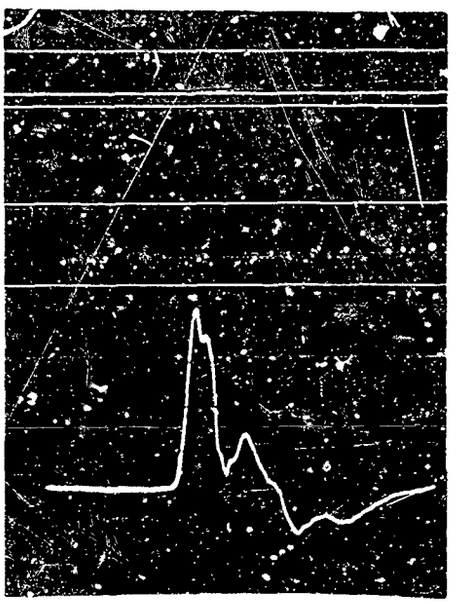

(b) Reverse Impulse Response, D44L17 (Vert x40, Hor 1 nsec/cm)

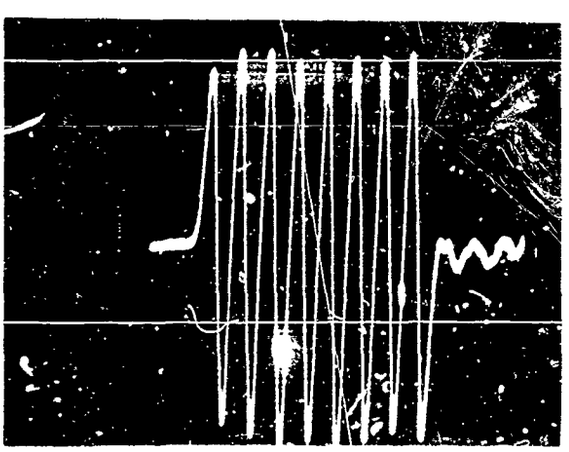

(c) Forward Pulsed Sinusoid Response, D44L17 (Vert x40, Hor 1 nsec/cm)

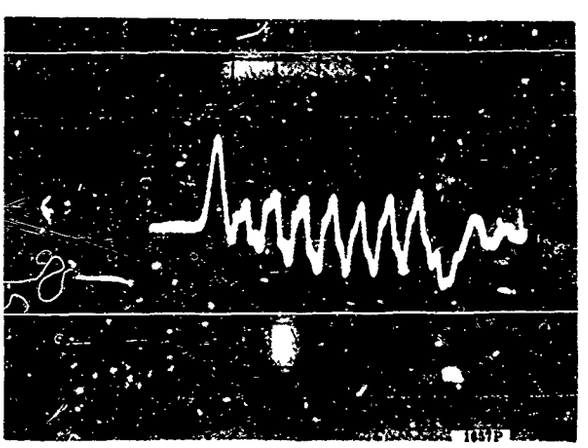

(d) Reverse Pulsed Sinusoid Response, D44L17 (Vert x40, Hor 1 nsec/cm)

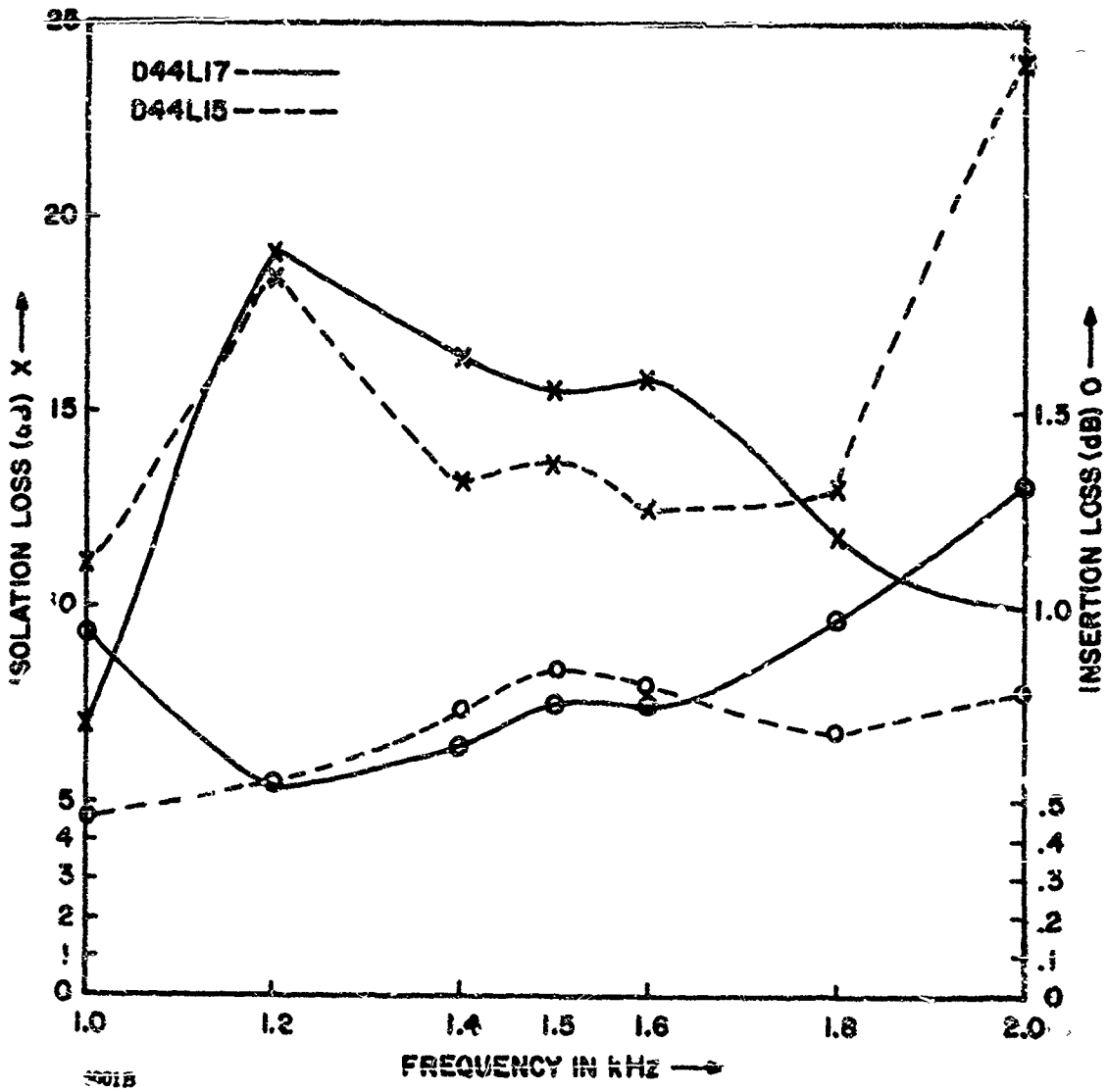

FIG. 2-8 Isolator characteristics.

D52L21	S/N 103		Circulator	
Frequency (GHz)	T-A(dB)	T-R(dB)	A-R(dB)	A-T(dB)
1.0	0.40	18.2	0.40	18.6
1.2	0.35	23.8	0.30	25.2
1.4	0.26	21.8	0.25	22.8
1.5	0.28	20.0	0.28	19.0
1.6	0.20	27.0	0.15	24.5
1.8	0.15	26.0	0.20	26.0
2.0	0.10	19.5	0.35	22.9

D52L11	S/N 1		Circulator	
Frequency (GHz)	T-A(dB)	T-R(dB)	A-R(dB)	A-T(dB)
1.40	0.23	22.8	0.18	23.7
1.45	0.12	24.2	0.16	24.8
1.50	0.14	24.4	0.14	25.5
1.55	0.13	23.0	0.18	24.0
1.60	0.13	20.0	0.18	21.1

D52L11	S/N 20		Circulator	
Frequency (GHz)	T-A(dB)	T-R(dB)	A-R(dB)	A-T(dB)
1.40	0.28	25.4	0.23	24.8
1.45	0.26	27.0	0.20	27.2
1.50	0.23	32.2	0.18	30.0
1.55	0.20	35.5	0.18	30.0
1.60	0.20	26.1	0.18	24.7

The frequency response of the fourth stripline circulator is shown in Figure 2-9.

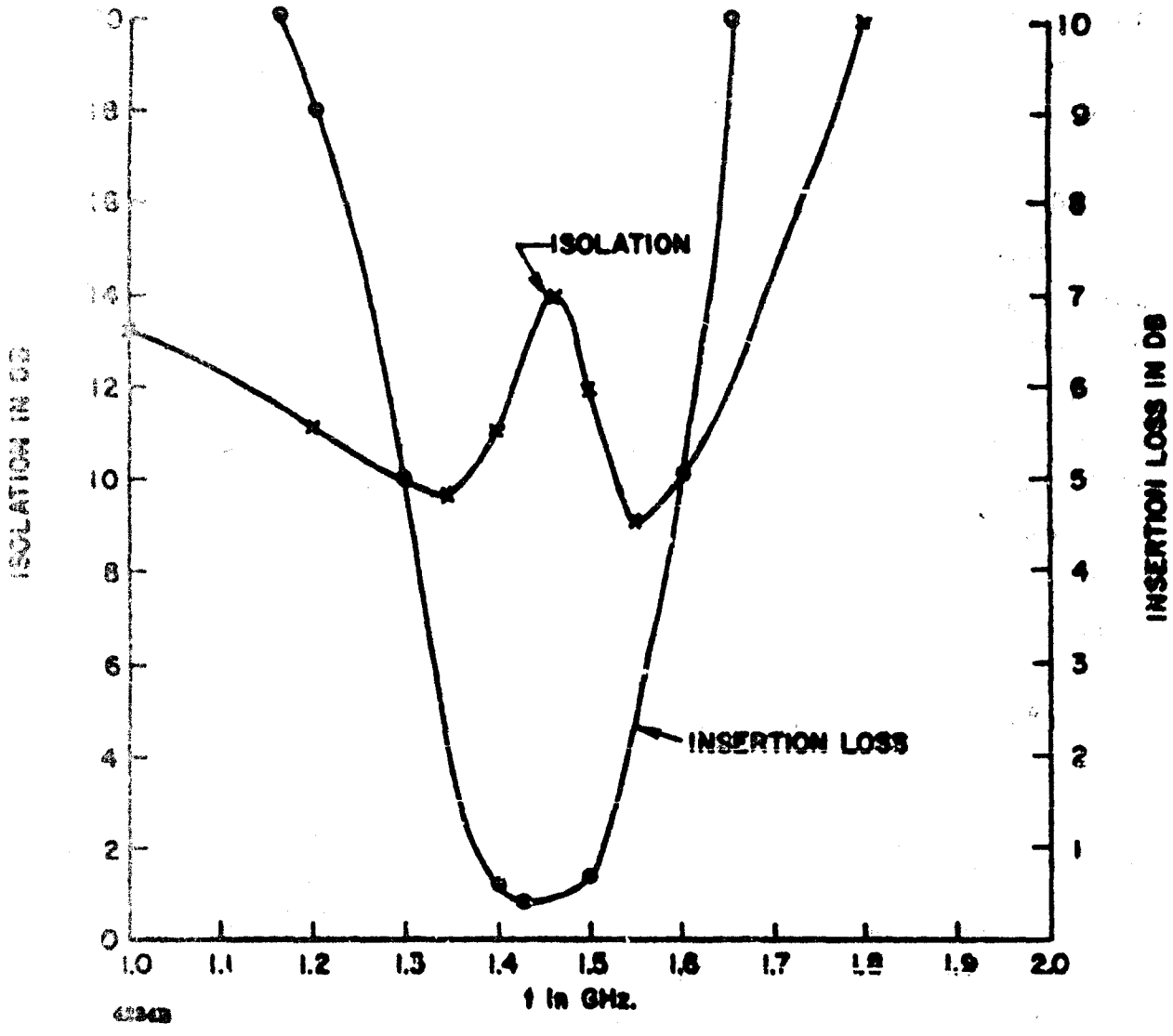

FIG. 2-9 Insertion loss and isolation for a standard-size narrow-band stripline circulator.

Photographs of the two stripline circulator types are shown in Fig. 2-10. Figures 2-11a, 2-11b, and 2-11c are oscilloscope pictures of the input-pulse, the transmitter-to-antenna-port, and the antenna-to-transmitter-port response, respectively, with the receiver port terminated in 50 ohms for the D52L21 S/N 103 circulator with a pulse-modulated input. Figure 2-11d is an overlay of Figs. 2-11a and 2-11b. The transmitted pulse in the low-loss direction (T-A) exhibits substantially more attenuation than the steady-state value for the initial cycle, but for the remaining 7 cycles the attenuation is approximately that for steady-state operation. On the trailing edge of the pulse an "extra" half cycle of energy can be seen; this probably arises from the release of stored energy from the precessing magnetic moments. In the reverse direction (A-T) the pulse is heavily attenuated. Again, initially the attenuation is somewhat greater than the steady-state value, but after a cycle or two (i.e., 1-2 nanoseconds) the attenuation settles down to its steady-state value. As expected, the responses for various port combinations exhibit three-fold symmetry. Thus, the response in the direction of circulation between any two ports is indistinguishable from the response in the direction of circulation between any other pair of ports. Similar comments apply to the response between any pair of ports in the direction opposite to that of circulation.

The pulse-modulated responses for all three circulators were very similar except for the initial cycle or so, as can be seen by comparing Figs. 2-11 and 2-12. There are noticeable differences in the impulse response for the two different circulator models, as shown in Fig. 2-13. Two circulators of the same model have nearly identical impulse responses (Figs. 2-13b and 2-13c). Comparing the initial cycles of the pulsed-sinusoid responses given in Figs. 2-11 and 2-12 with the impulse responses of Fig. 2-13, reveals that the initial response of each circulator to the pulse-modulated signal seems in every feature to be very similar to the impulse response for that circulator. The differences in impulse response between the two circulator models (D52L21 and D52L11) which have similar steady-state characteristics arise from the mechanically different schemes utilized in matching the devices over the band of interest. Note that an "impulse" theoretically contains all frequencies with equal

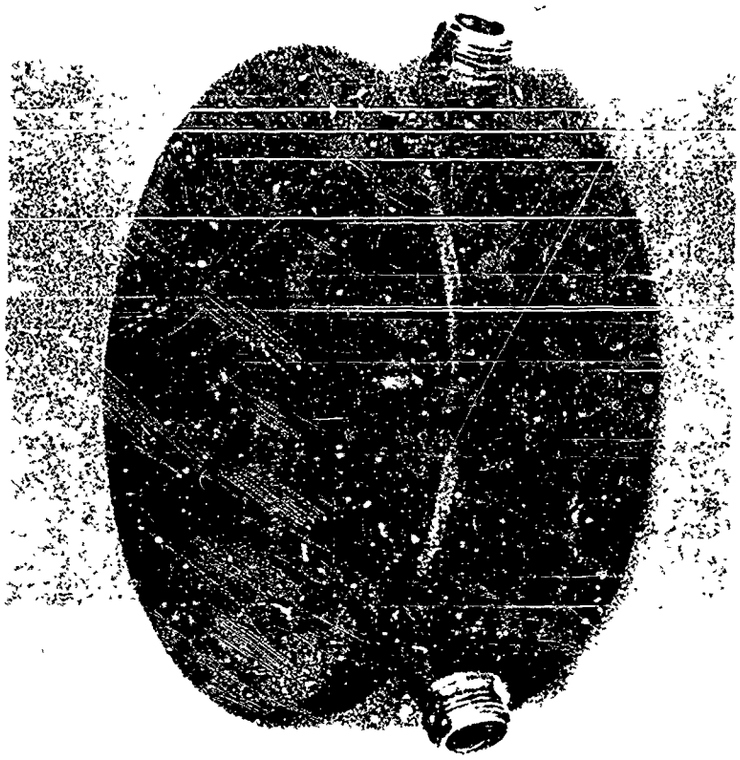

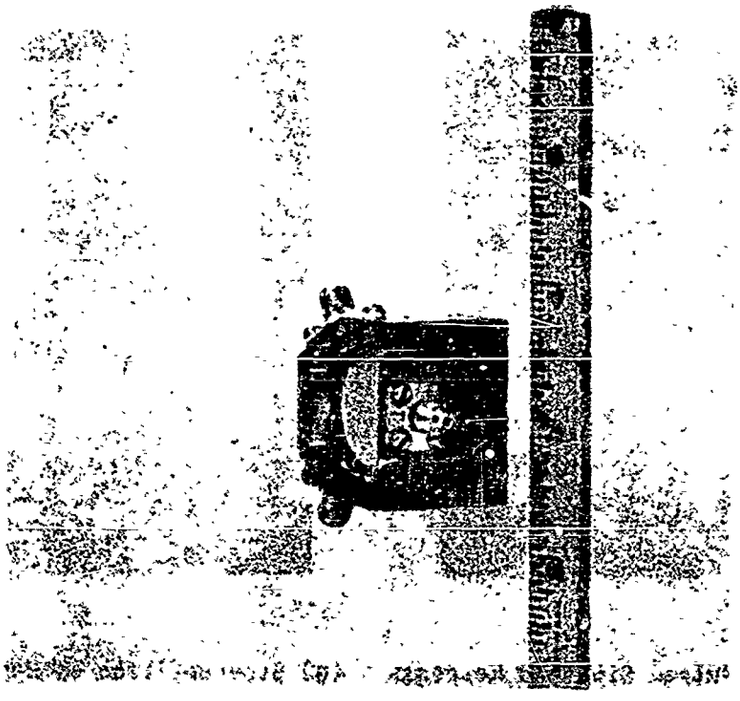

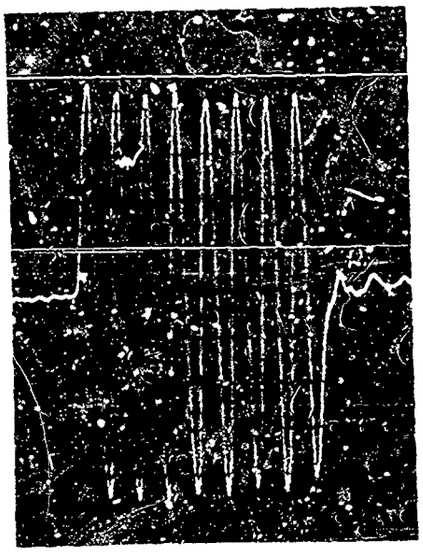

(a) Reference Pulse (Vert x20, Hor 1 nsec/cm)

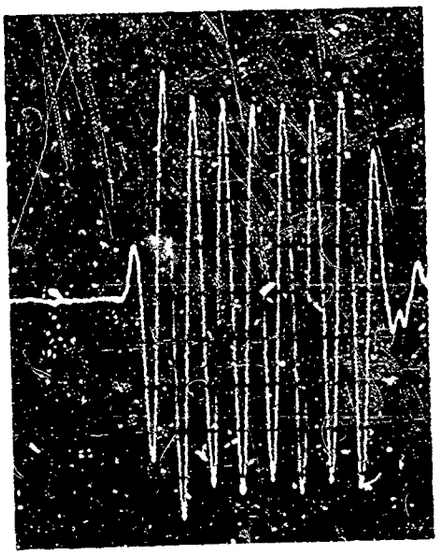

(b) T → A Pulsed Sinusoid Response, D52L21 S/N103 (Vert x20, Hor 1 nsec/cm)

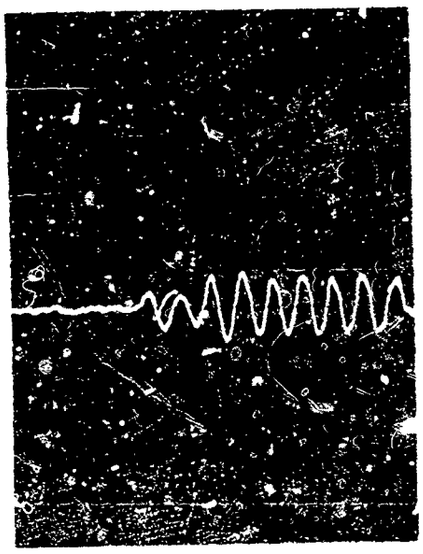

(c) A → T Pulsed Sinusoid Response D52L21 S/N103 (Vert x20, Hor 1 nsec/cm)

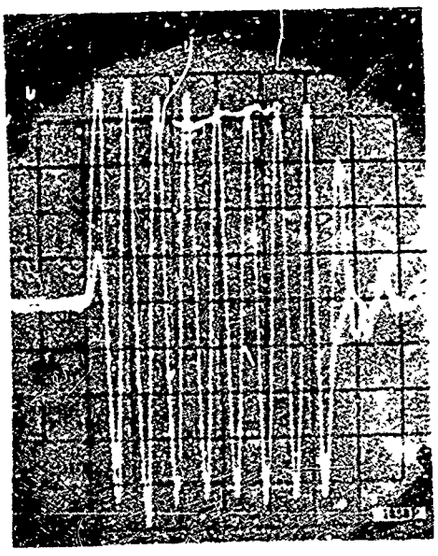

(d) Superposition of Reference and T → A Response, D52L21 S/N103 (Vert x20, Hor 1 nsec/cm)

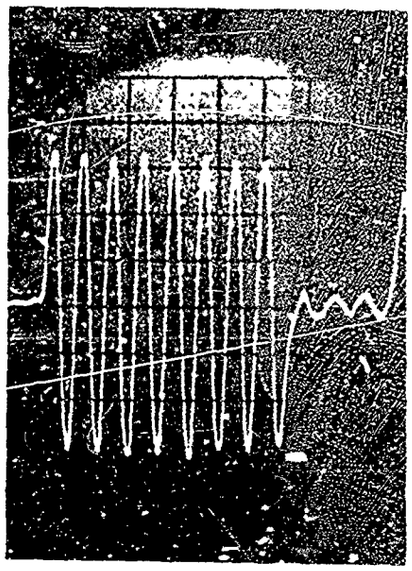

(a) Reference Pulse (Vert. x20, Hor 1 nsec/cm)

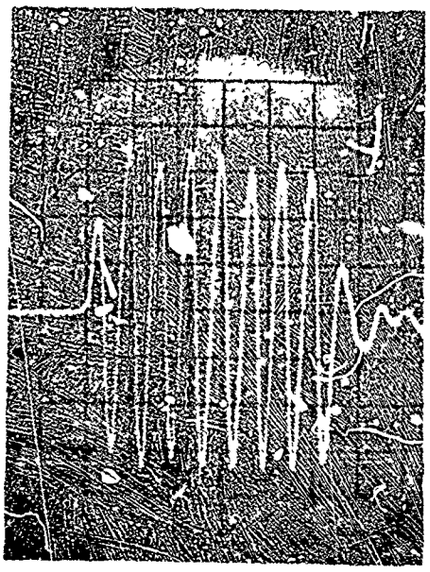

(b) T → A Pulsed Sinusoid Response, D52L21 S/N20 (Vert x20, Hor 1 nsec/cm)

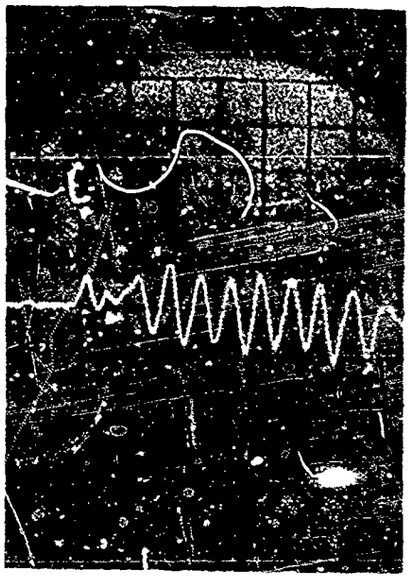

(c) A → T Pulsed Sinusoid Response, D52L11 S/N 20 (Vert x20, Hor 1 nsec/cm).

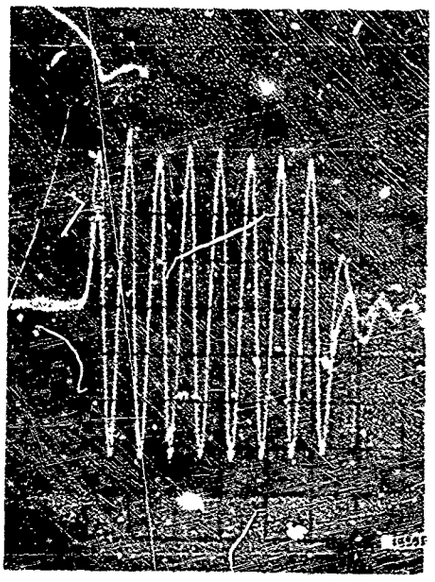

(d) Superposition of Reference and T → A Response, D52L11 S/N 20 (Vert x20, Hor 1 nsec/cm)

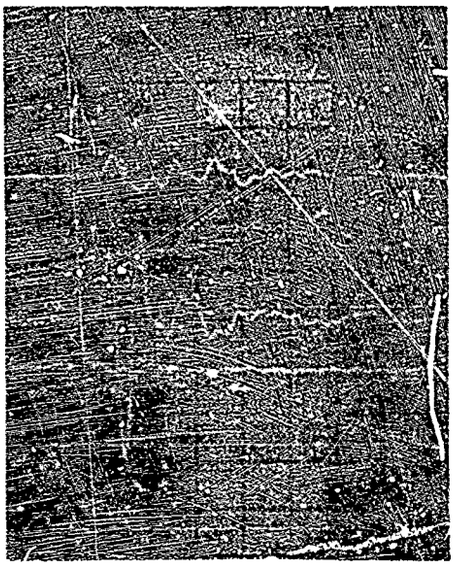

(a) From Bottom to Top Curves are Reference and T → A, A → T Impulse Responses, Respectively, D52L?i S/N 103 (Vert x20, Hor 1 nsec/cm)

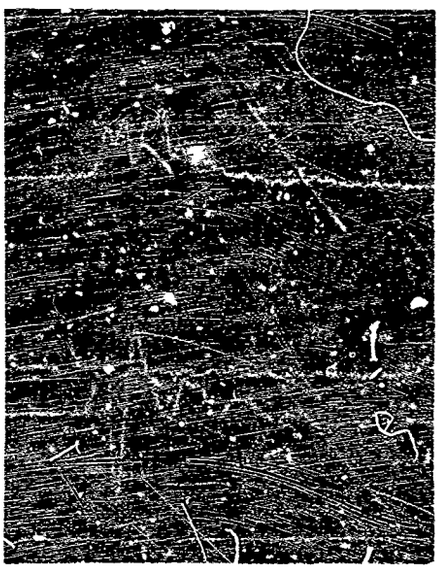

(b) From Bottom to Top Curves are Reference and T → A, A → T Impulse Responses, Respectively, D52L11 S/N 1 (Vert x 20, Hor 1 nsec/cm)

(c) From Bottom to Top Curves are Reference and T → A, A → T Impulse Responses, Respectively, D52L11 S/N 20 (Vert x20, Hor 1 nsec/cm)

weighting: the pulse-modulated signal heavily weights the frequencies in the band of interest.

Figure 2-14 shows the impulse and pulsed-sinusoid response of the narrowband stripline circulator whose frequency response is shown in Fig. 2-9. The response shows the expected differences when compared to the behavior of the broader-band units. The primary difference is in the slower rise time, the pulsed sinusoid response requiring about 3 rf cycles to reach full amplitude.

The frequency characteristics of a microstrip circulator are shown in Fig. 2-15. The frequency response is seen to be quite narrow band. To provide a convenient basis for comparison, the frequency response characteristics of the narrow-band stripline circulator discussed earlier were adjusted to be nearly identical to those of the microstrip unit. The characteristics of the narrow-band stripline unit are given in Fig. 2-9. The same type of ferrimagnetic material was used in both circulators.

A comparison of the time-domain response of the microstrip circulator (Fig. 2-16) with that of the stripline unit (Fig. 2-14) reveals striking similarities. Indeed, the only real difference is in transmission time delay, which is much less for the microstrip circulator. Thus, it appears that circulators with radically different structures but the same frequency characteristics will have very similar transient characteristics.

The pulsed-sinusoid response of these units shows a "peculiarity" in the response of the isolated port in the fourth rf cycle. The same peculiarity is found in broadband structures. This behavior appears to be relatively independent of both material and structural parameters. The cause of this interesting effect is not yet understood.

2.3.4 Helical-Line Ferrite Digital Phase Shifter

A helical-line phase shifter is shown in a cutaway view in Fig. 2-17. The transient response of this device to a 1500 MHz pulse-modulated signal and a short spike of energy has been experimentally determined.

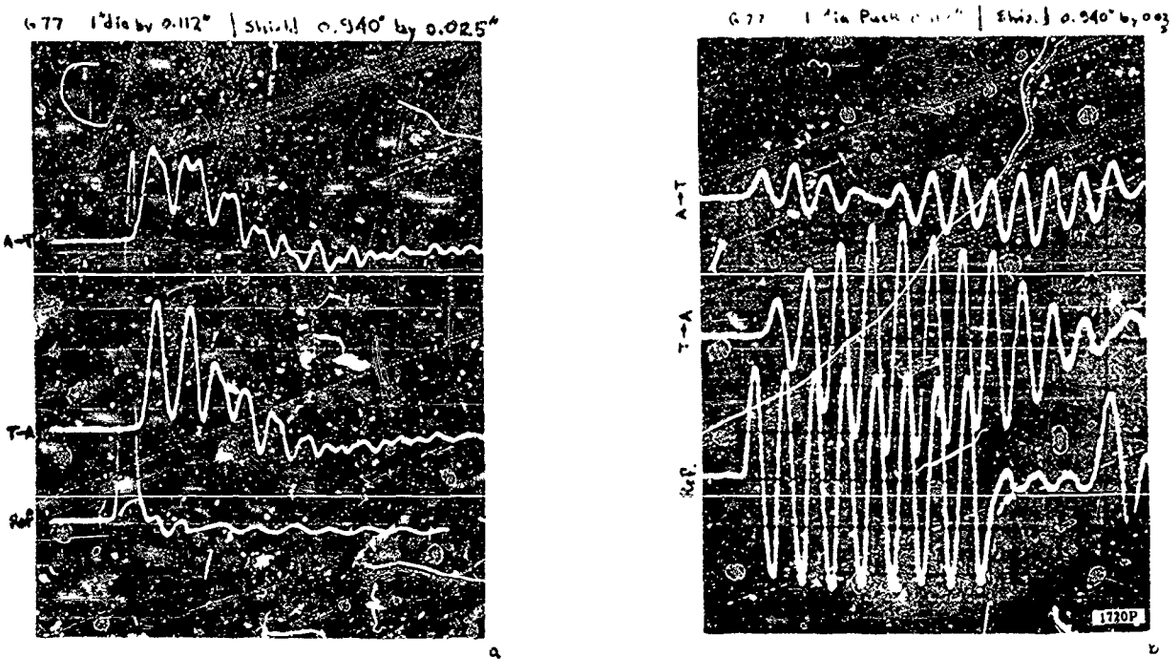

(a) Impulse Response
(Vert x 2; Hor x 1 nsec/cm)

(b) Step-Modulated Response
(Vert x 20; Hor x 1 nsec/cm)

FIG. 2-14 The transient response of the standard-size narrow-band circulator.

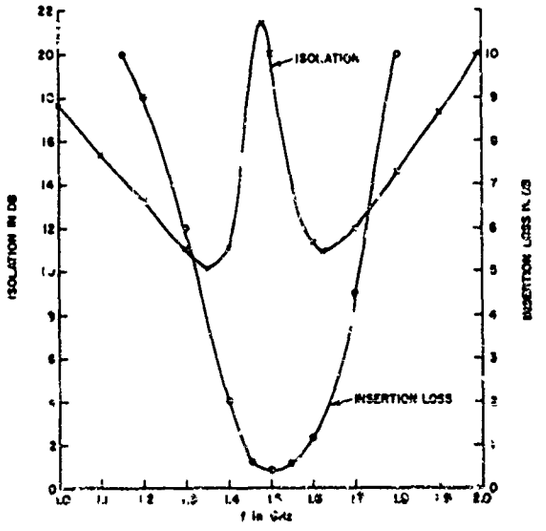

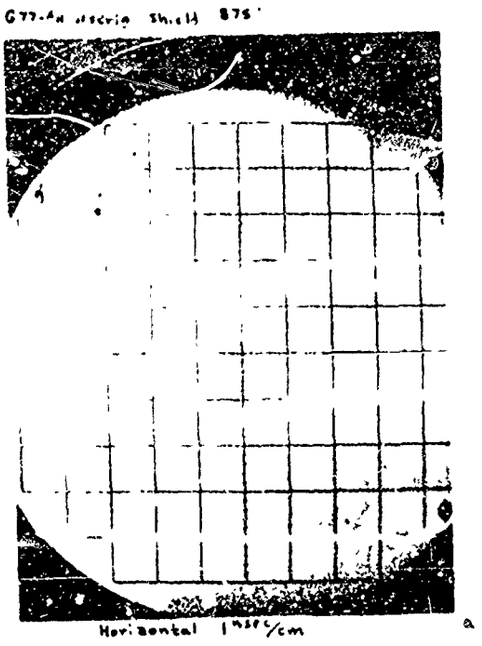

(a) Impulse Response
(Vert x 2; Hor x 1 nsec/cm)

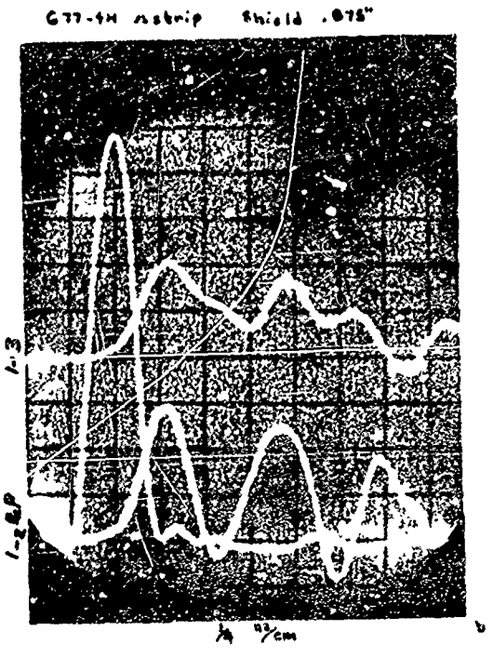

(b) Expanded Impulse Response
(Vert x 2; Hor x 0.25 nsec/cm)

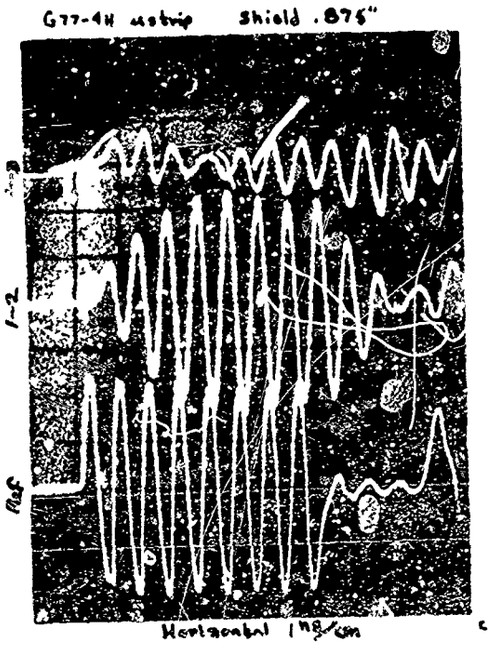

(c) Step-Modulated Response
(Vert x 20; Hor x 1 nsec/cm)

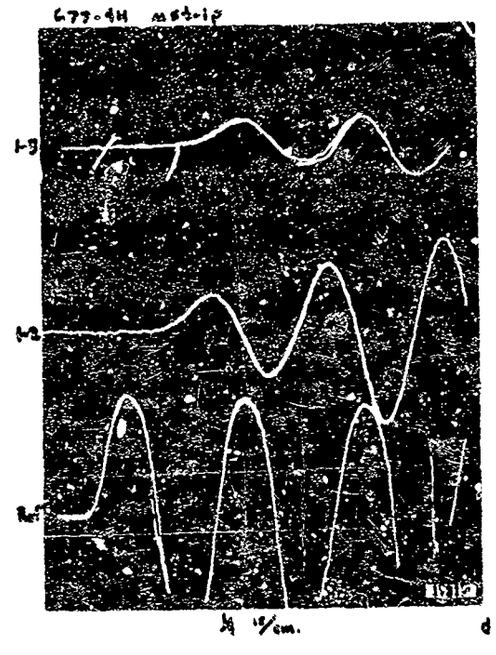

(d) Expanded Step-Modulated Response
(Vert x 20; Hor x 1 nsec/cm)

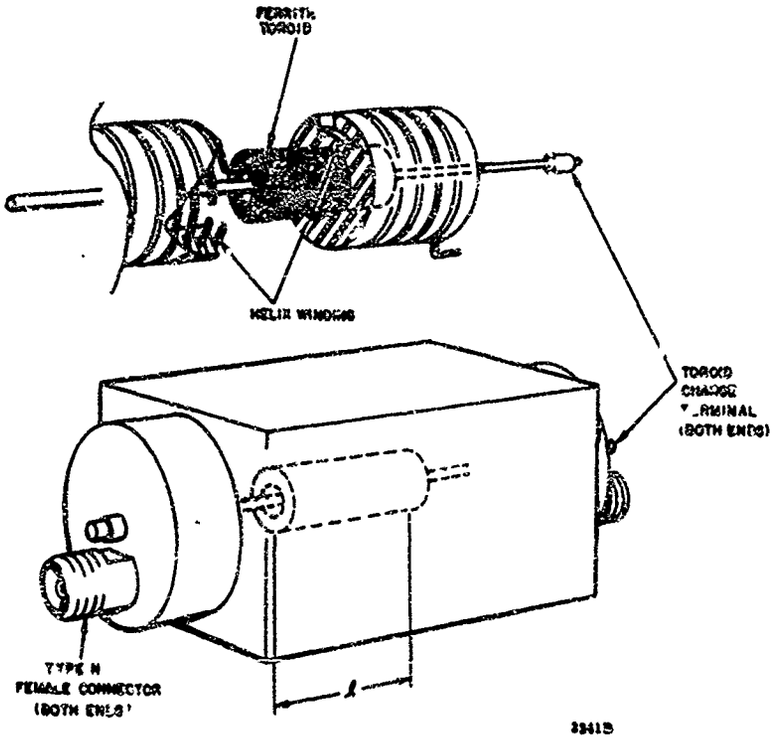

FIG. 2-17 A cutaway view of a helical-line digital phase shifter.

The pulse-modulated responses are given in Fig. 2-18. The response of the helical line with all the ferrite replaced by a dielectric having the same dielectric constant as the ferrite and the response of the ferrite-loaded line with the ferrite toroid latched in the forward and reverse directions are also shown. The time delay is different for the forward and reverse directions. When the ferrite is in the line, the difference in insertion loss between the first half-cycle and following cycles increases compared to the difference in insertion loss observed with dielectric only in the line. This is due to the ferrite magnetic losses that are in effect after a nanosecond or so.

Figure 2-19 shows the responses of the dielectric-loaded helix and of the ferrite-loaded helix to a short spike of energy. These impulse responses closely resemble the first cycle of the pulse-modulated responses. It is again apparent that essentially steady-state operation is achieved within roughly three cycles.

2.3.5 Gyromagnetic Coupler Filter

The transient response of a gyromagnetic coupler filter to a pulse-modulated signal and a short spike of energy has been experimentally determined. The steady-state characteristics of the filter are:

3 dB bandwidth at center frequency of 1.5 GHz ≈ 20 MHz
Insertion loss at 1.5 GHz ≈ 2 dB
Coupling element 0.030-inch diameter GaYBiFe garnet sphere, ΔH = 1.92 Oe, $4\pi M_s$ = 520 G .

Figure 2-20a shows an oscilloscope trace of the filter bandpass. The 3 dB bandwidth is about 20 MHz. Figures 2-20b and 2-20c are the input impulse and the impulse response of the filter, respectively. After the first couple of nanoseconds the impulse response is simply a slightly damped sinusoid, as would be expected for this high-Q circuit. The portion of the response to the right of the center line of the oscilloscope face appears to be due to reflection in the measurement set-up.

Figures 2-20d and 2-21a-c show the input and the pulse-modulated response of the filter, respectively. Eight to ten nanoseconds after the initial response the oscilloscope trace is most likely a superposition of

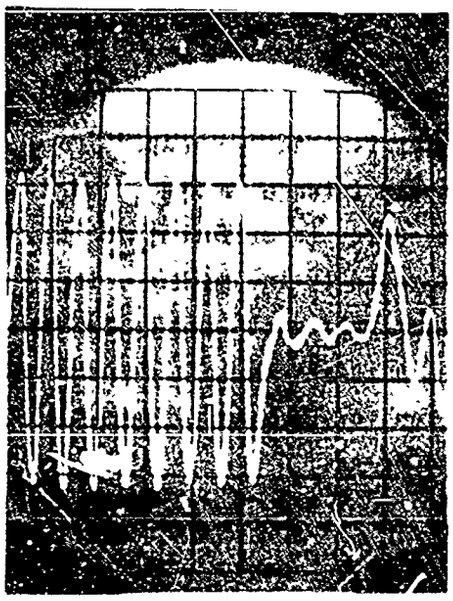

(a) Reference Pulse (Vert x20, Hor 1 nsec/cm)

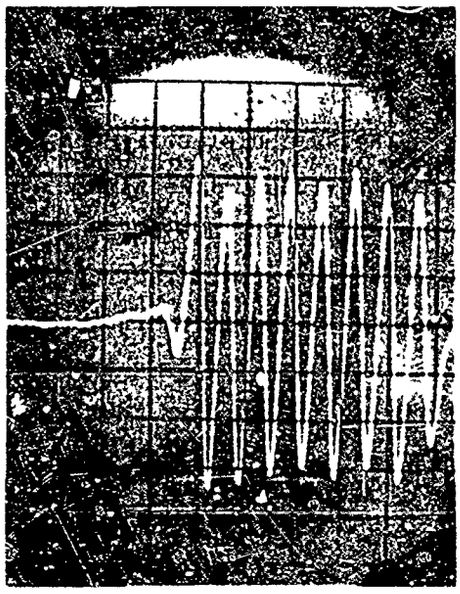

(b) Pulsed Sinusoid Response Helical Line with Ferrite Replaced by Dielectric (Vert x20, Hor 1 nsec/cm)

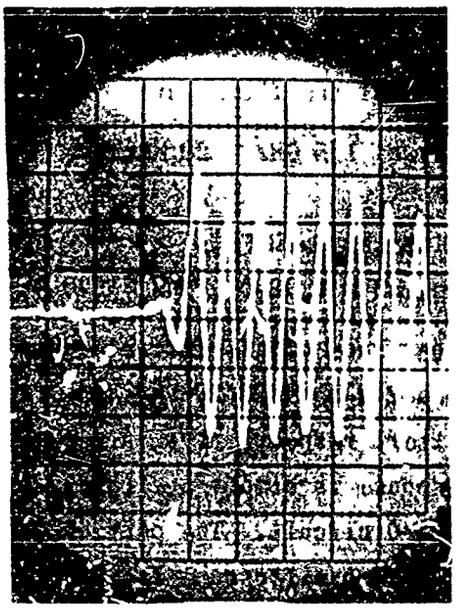

(c) Forward Pulsed Sinusoid Response of Ferrite Loaded Helical Line (Vert x20, Hor 1 nsec/cm)

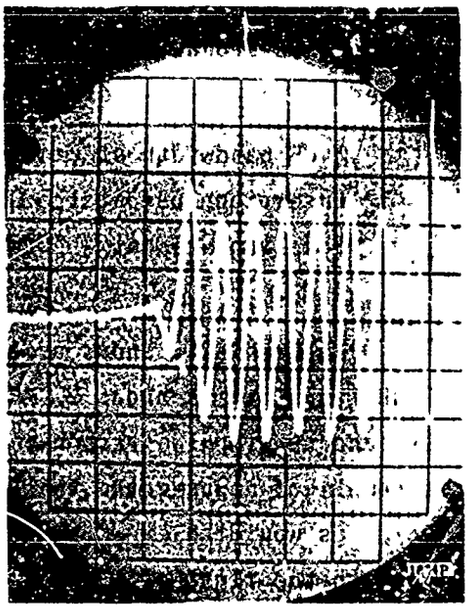

(d) Reverse Pulsed Sinusoid Response of Ferrite Loaded Helical Line (Vert x20, Hor 1 nsec/cm)

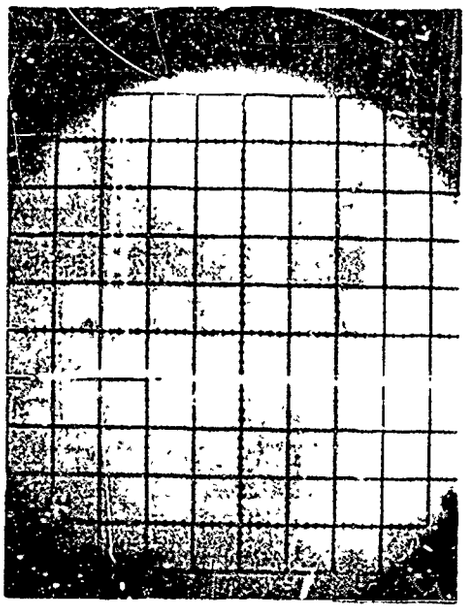

(a) Reference Pulse (Vert x20, Hor 1 nsec/cm)

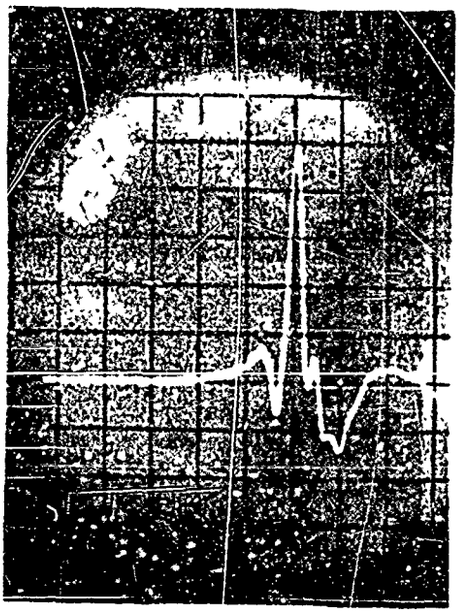

(b) Impulse Response of Helical Line with Ferrite Replaced by Dielectric (Vert x20, Hor 1 nsec/cm)

(c) Reference Pulse (Vert x20, Hor 1 nsec/cm)

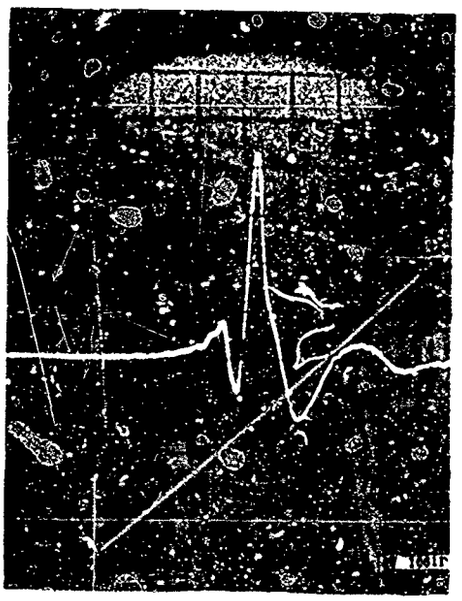

(d) Impulse Response of Ferrite Loaded Helical Line (Vert x20, Hor 1 nsec/cm)

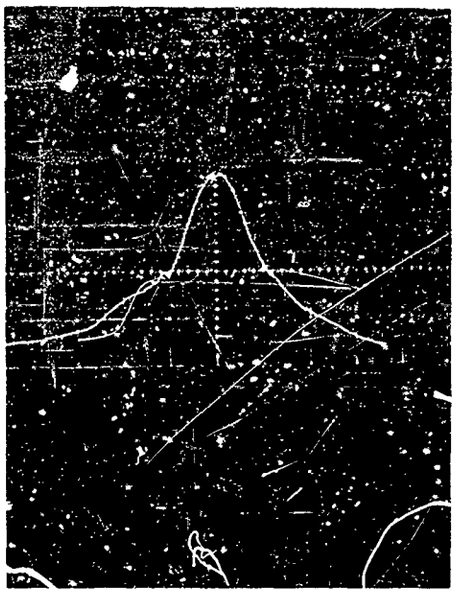

(a) Filter Bandpass 4 dB BW $\approx$ 20 MHz, $f_o = 1.5$ GHz.

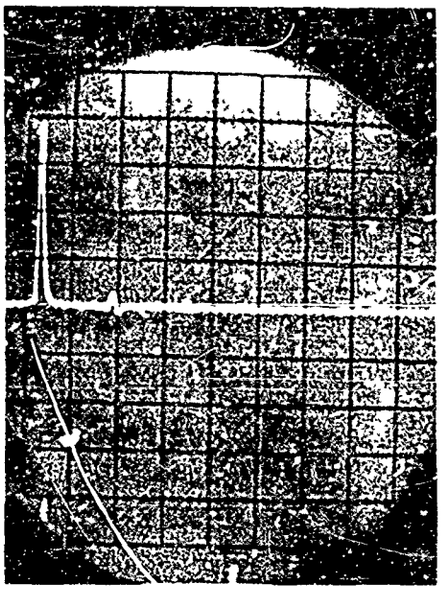

(b) Reference Pulse (Vert x20, Hor 1 nsec/cm)

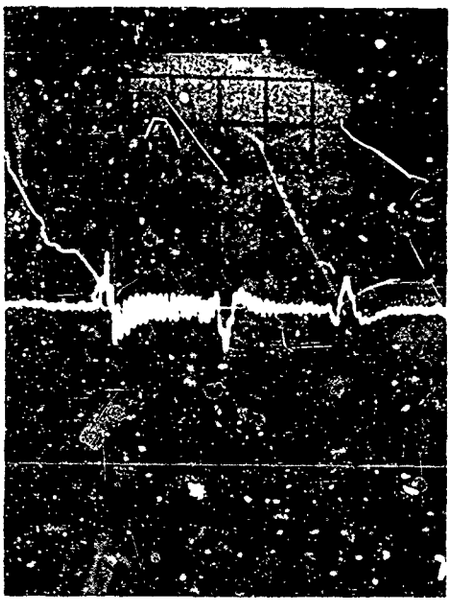

(c) Impulse Response of Filter (Vert x20, Hor 1 nsec/cm)

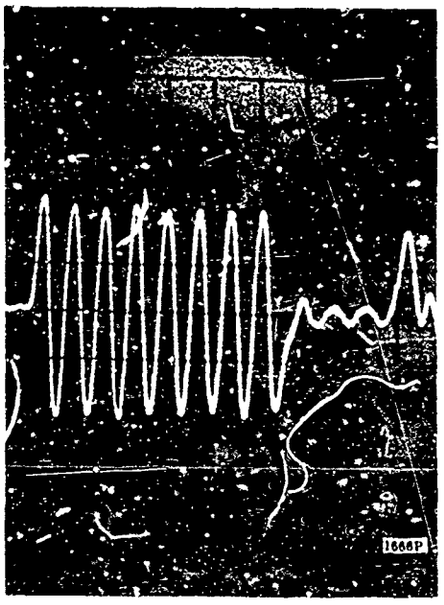

(d) Reference Pulse (Vert x10, Hor 1 nsec/cm).

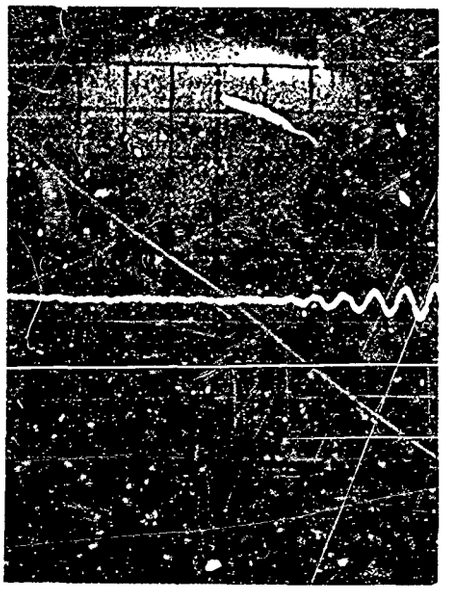

(a) Pulsed Sinusoid Response of Filter (Vert x10, Hor 1 nsec/cm)

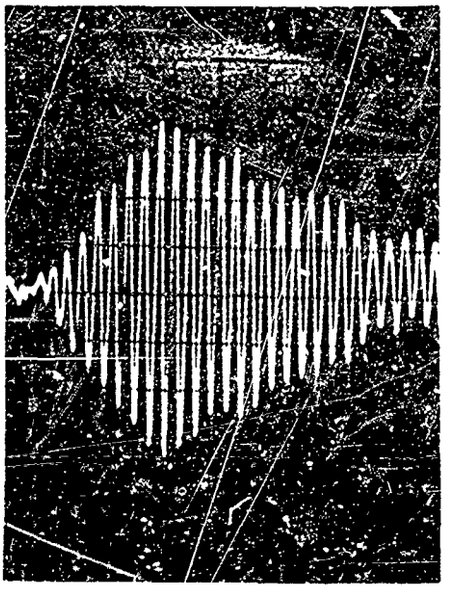

(b) Shifted Pulsed Sinusoid Response of Filter (Vert x40, Hor 2 nsec/cm)

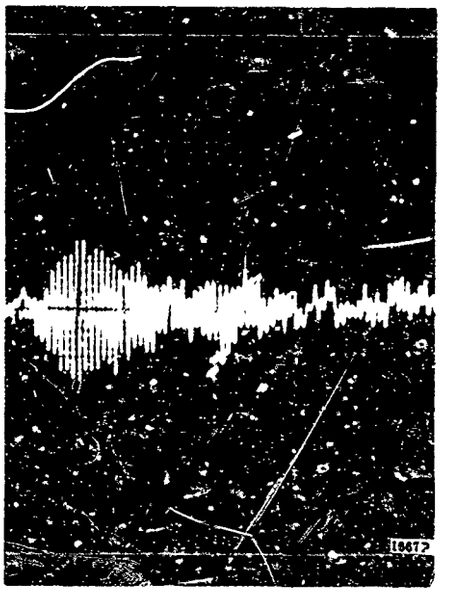

(c) Expanded Shifted Pulsed Sinusoid Response of Filter (Vert x40, Hor 5 nsec/cm)

the desired response, reflections, and response to spurious signals following the main test pulse. In the approximately ten nanosecond "viewing window", the envelope of the pulse-modulated response is an integrated response that reaches a peak of only about 0.4 of the height of the exciting pulse. This response is in line with that expected for a circuit having a bandwidth of 20 MHz when excited by a 5.33 nsec pulse; i.e., $BW_{3dB} \approx \frac{1}{10} \tau$, where τ is the width of the pulsed sinusoid.

The results of the experimental investigation of ferrite device excitation times are summarized below to facilitate comparison.

TABLE 2-I

Summary of Ferrite Device Response Characteristics

DEVICE*	EXCITATION TIME**
Broadband Resonance Isolator	Forward Direction - ≈ 0.5 rf cycle Reverse Direction - ≈ 0.5 rf cycle
Broadband Circulator	Transmitter Port to Antenna Port - ≈ 1 rf cycle Antenna Port to Transmitter Port < 0.5 rf cycle
Narrow-Band Circulator	Transmitter Port to Antenna Port - ≈ 3 rf cycles Antenna Port to Transmitter Port - 0.5 rf cycle
Helical-Line Digital Phase Shifter	Principal delay characteristics realized "instantaneously", but dispersive nature of line produces considerable pulse distortion.
Gyromagnetic Coupler Filter (20 MHz 3 dB BW)	> 10 rf cycles

*All components tested at 1500 MHz.

**This differs from the conventional "settling time" since the back loss, for example, is greater than the specification value for $t < t_{settling}$. Hence, for this class of components the "excitation time" may be a more significant quantity.

2.4 SUMMARY

The transient behavior of ferrite devices has been investigated through a closely coordinated theoretical and experimental effort. The influence of the various intrinsic "relaxation" and "excitation" times of the ferrite on device performance has been probed. In an effort to clarify the principles of transient wave propagation in ferrites the case of propagation in an infinite ferrite medium has been attacked analytically. This problem, which appears at first to be rather simple, gives rise to a very complicated function whose inverse Laplace transform must be evaluated.

Variational and perturbational techniques have been investigated and applied to the solution of some dielectric- and ferrite-loaded waveguide problems. These techniques appear to have considerable promise in providing solutions to otherwise unmanageable problems. A brief literature search failed to reveal publications dealing with variational or perturbational techniques in the Laplace transform domain. The justification of the validity of the techniques as applied in this report has thus far been largely intuitive. Additional work should be devoted both to providing a rigorous justification of the validity of the methods in the s domain and to the application of the techniques to the solution of specific problems.

A number of typical operational ferrite devices have been investigated experimentally. Device types were selected such that the effect of the ferrite on transient response could be examined with the ferrite operating in a variety of magnetization states (i.e., below resonance, at resonance, and in the remanent state). The approximate excitation times are summarized in Table 2-1.

One of the most interesting devices studied was the ferrite circulator. The circulator is an extremely versatile device and finds a multitude of applications in radar and communications systems. With one port terminated in a matched load, a 3-port circulator becomes an isolator; with a filter on one port and the conjugate filter on another port, a 3-port circulator becomes a diplexer; provided with a controlled means of changing the direction of circulation, a 3-port circulator becomes a

single-pole double-throw switch, etc., etc. Because of its great versatility, the ferrite circulator has many possible applications in wideband systems, and it seems that some effort should be directed towards optimizing it for wideband operation.

To be satisfactory for many wideband applications, circulator transient response should be such that steady-state isolation and insertion-loss values are achieved within one-half rf cycle. None of the designs tested was fully capable of meeting this requirement. From the data currently available on the transient behavior of ferrite circulators, it appears that circulator transient response is influenced by the intrinsic properties of the ferrite material, the volume of ferrite, the type of matching structure, etc. Precisely how to adjust the various parameters to optimize the transient response requires further study. The available data on circulator transient behavior shows many interesting features which are not at this time clearly understood. A more thorough investigation of circulator transient response should lead to a more complete interpretation of these effects and should provide the necessary design information to optimize the transient response of ferrite circulators.

SECTION III

THE CONCEPT OF BANDWIDTH IN MICROWAVE SYSTEMS

(G. F. Ross, Sperry Rand Research Center)

3.1 INTRODUCTION

With the present day emphasis on the use of wideband signals for high-resolution radar, considerations imposed by distributed microwave structures have become increasingly important. It is the purpose of this section to investigate the value of using a single number, for example the "bandwidth", to describe the transient properties of a microwave network, especially when such a network is used to process signals having wide spectral content. Since phase information is lacking, it is felt, intuitively, that any definition of bandwidth derived from the amplitude or power spectrum alone must be lacking, at least when transient behavior is important.

It is shown in this section that a "single number" criterion has merit if one considers the energy storage of the network (involving the "natural modes") as the basic starting point and carefully examines a related quantity defined as the transmission quality factor Q_T. It is found that this number is a good measure of the "rise time" of a network when excited by a step-modulated signal at resonance. To determine the "setting time" T_S, or the time required for the step-modulated response to settle to within ±5% of its steady-state value, one must also specify the phase function of the network.

This section starts with a discussion of bandwidth definitions as employed in lumped network theory (Sec. 3.2). These definitions are then extended to a particular class of important microwave networks in Sec. 3.3. None of the conventional definitions, however, proves to be very satisfying.

In Sec. 3.4.1 a definition of the new transmission quality factor, Q_T, (which is later used to define an "effective" bandwidth) is presented. An interpretation of the conventional Q factor and applications of this factor via the scattering matrix notation for networks

is presented in Appendices B and C, respectively. The conventional Q factor is defined as being proportional to the time average of the stored energy, $\langle W \rangle$, and inversely proportional to the time average of the power dissipated, $\langle P_d \rangle$, in the network at resonance: The new quality factor $\tilde{Q}_T$ involves a new quantity $\langle \tilde{W} \rangle$ which is a measure of the time average of the stored energy of the system, and is therefore related to the natural modes of the network. A discussion of how one obtains $\langle \tilde{W} \rangle$ in the laboratory is presented in Section 3.4.2, and a mathematical derivation of $\langle \tilde{W} \rangle$ for TEM-mode line networks follows in Section 3.4.3.

The theory is applied to evaluating $\tilde{Q}_T$ for TEM-mode line networks using Z-transform techniques in Section 3.5. Applications to a line and a short-circuited stub and a parallel-line or quarter-wavelength coupler are presented in 3.6.1 and 3.6.2, respectively. Experimental results are reported in Section 3.7, and conclusions follow in Section 3.8.

3.2 THE DEFINITION OF BANDWIDTH

It is constructive to review some of the definitions of bandwidth that are used in conventional lumped network theory. The first and perhaps most familiar definition is shown in Fig. 3-1a[13]. The system function $H(\omega)$ of a transmission network is given by

$$H(\omega) = A(\omega)e^{-j\phi(\omega)} \tag{3.1}$$

where $A(\omega)$ is the amplitude spectrum
and $\phi(\omega)$ is the phase function

The magnitude of $A(\omega)$ is plotted as a function of frequency. The bandwidth of a low-pass filter (LPF) is defined as the frequency bw_1 at which $A(\omega)$ is reduced to 0.707 of its value at zero frequency: In terms of the power spectrum or $A^2(\omega)$, bw_1 is the so-called half-power frequency. This definition ignores any "ripple" in the passband.

The second definition is that of the equivalent rectangular bandwidth and is shown in Fig. 3-1b[14]. It is obtained as follows: we integrate the function $A(\omega)$ over the frequency band, i.e.,

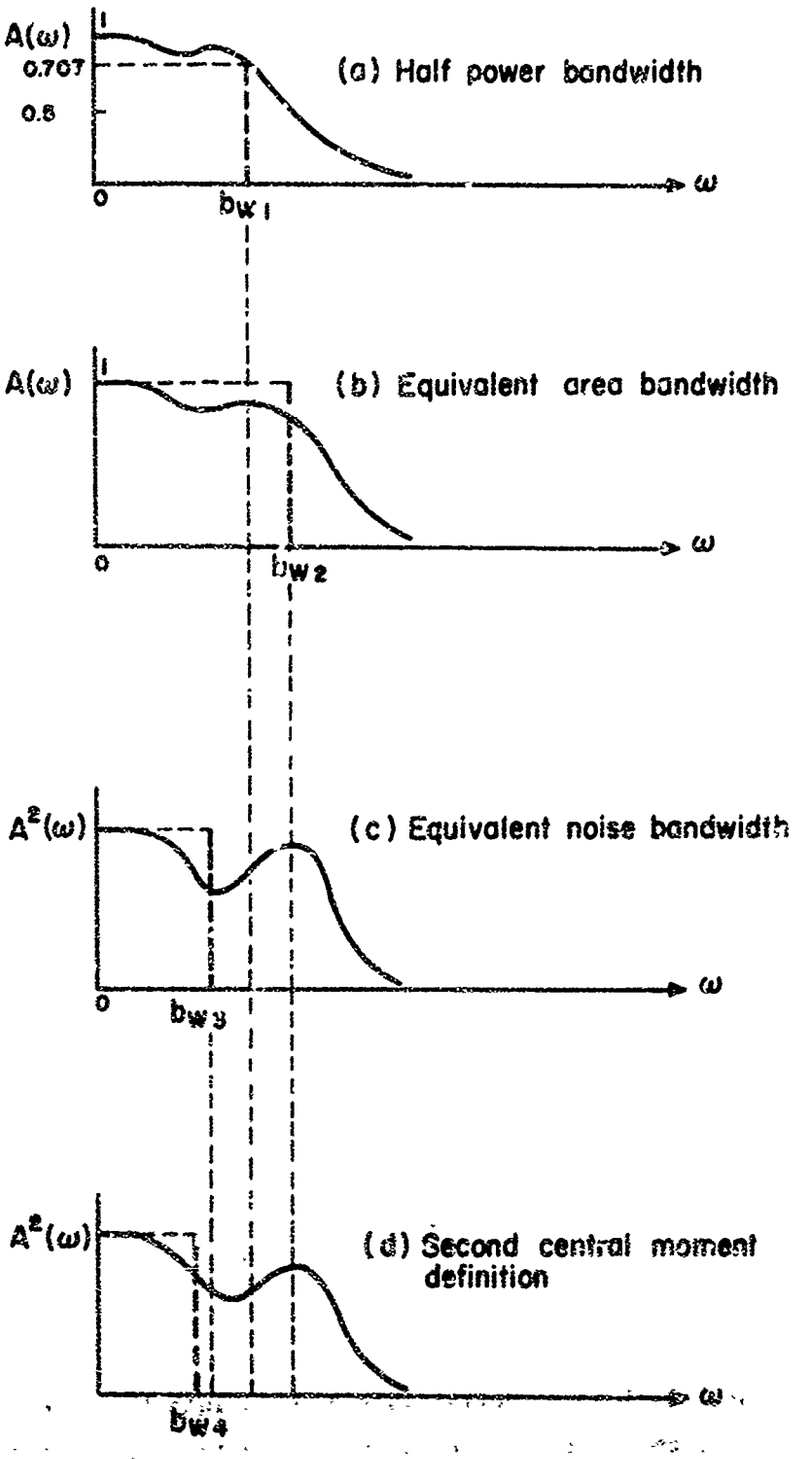

FIG. 3-1 Definitions of bandwidth in lumped networks.

$$\int_0^\infty A(\omega)d\omega = N \tag{3.2}$$

and obtain a numeric answer N. We now define the bandwidth bw_2 as the equivalent rectangle having an amplitude $A(\omega)|_{\omega=0}$ at zero frequency and a bandwidth bw_2 such that the relationship

$$bw_2 \cdot A(0) = N \quad \text{or} \quad bw_2 = \frac{\int_0^\infty A(\omega)d\omega}{A(0)} \tag{3.3}$$

is satisfied.

Still another definition (and one popular in statistical detection problems) is the "equivalent noise bandwidth," defined in a fashion similar to Eq. (3.2) but with respect to the power spectrum $|H(\omega)|^2$ or $A^2(\omega)$.[15] Here, the height of the equivalent rectangle is $A^2(0)$ and the area under the power spectrum is given by

$$\int_0^\infty A^2(\omega)d\omega = M \tag{3.4}$$

The noise bandwidth bw_3 is then defined as

$$bw_3 \cdot A^2(0) = M \quad \text{or} \quad bw_3 = \frac{\int_0^\infty A^2(\omega)d\omega}{A^2(0)} \tag{3.5}$$

and is shown in Fig. 3-1c.

There are still other definitions of bandwidth that are employed. For example, a measurement of the spread around the mean or centroid of the power spectrum, $\bar{\omega}$, can be defined as

$$bw_4 = \frac{\int_0^\infty (\omega - \bar{\omega})^2 A^2(\omega) d\omega}{\int_0^\infty A^2(\omega) d\omega} \tag{3.6}$$

as shown in Fig. 3-1d.[16]

Note that, in general, each definition yields a <u>different number</u> describing the bandwidth of the system. The measure of signal bandwidth in terms of a single number is an appealing concept, but intuitively we feel that it may not be a sufficient measure, since the phase function of the network has been neglected—especially in nonminimum phase networks where the phase function is not uniquely related to the amplitude spectrum. This is explicitly illustrated by the examples presented in the next section.

3.3 THE BANDWIDTH CONCEPT AS APPLIED TO MICROWAVE NETWORKS

3.3.1 <u>Example 1</u>

When lengths of waveguide or TEM-mode lines are interconnected to form couplers or hybrid junctions, the system functions of these networks become quite complicated.[17] In one particularly useful class of TEM-mode networks where the impulse response between any two ports i and j is given by

$$h_{ji}(t) = \sum_{k=1}^{\infty} a_k^{(ij)} \delta(t - k\tau) \tag{3.7}$$

the system function

$$H_{ji}(\omega) \overset{\mathcal{F}}{\longleftrightarrow} h_{ji}(t) \tag{3.8}$$

is periodic; that is,

$$H_{ji}(\omega) = H_{ji}\left(\omega + \frac{2\pi}{T}\right) \tag{3.9}$$

Networks of this type are the branch-line coupler, the ring hybrid, the quarter-wavelength coupler, etc. A plot of $|H(\omega)| = A(\omega)$ is shown in Fig. 3-2a. The network exhibits its hybrid properties around ω_0 (the design center frequency) and $(2k-1)\omega_0$ because, theoretically, the characteristics of the network "around" these frequencies are identical, neglecting loss.

The bandwidth of this network is conventionally defined by microwave engineers as "the spread" between the half-power points around ω_0. When the spectrum of the signal applied to the coupler is very narrow (with respect to the half-power bandwidth), negligible distortion is introduced. This definition certainly has utility in "frequency diversity systems" where one is required to process a narrow-band signal over a large band of frequencies, but we suspect that it is not as useful when wideband signals are employed. For example, the equivalent rectangular bandwidth or the noise bandwidth of this class of networks is infinite; that is, the area under $A(\omega)$ or $A^2(\omega)$ is infinite by inspection of Fig. 3-2a.

It is instructive to investigate the area under the power spectrum in a more physical sense. Assume that we excite this class of networks with a rectangular pulse of width Δ and amplitude V such that

(1) the pulse width Δ is less than T, the spacing between impulses

(2) the <u>energy</u> in the incident pulse equals unity: i.e.,

$$(V)^2 \cdot \Delta = 1$$

Then the output pulse train is given by

$$r(t) = \sum_{k=1}^{\infty} V \cdot a_k \, p(t - kT) \tag{3.10}$$

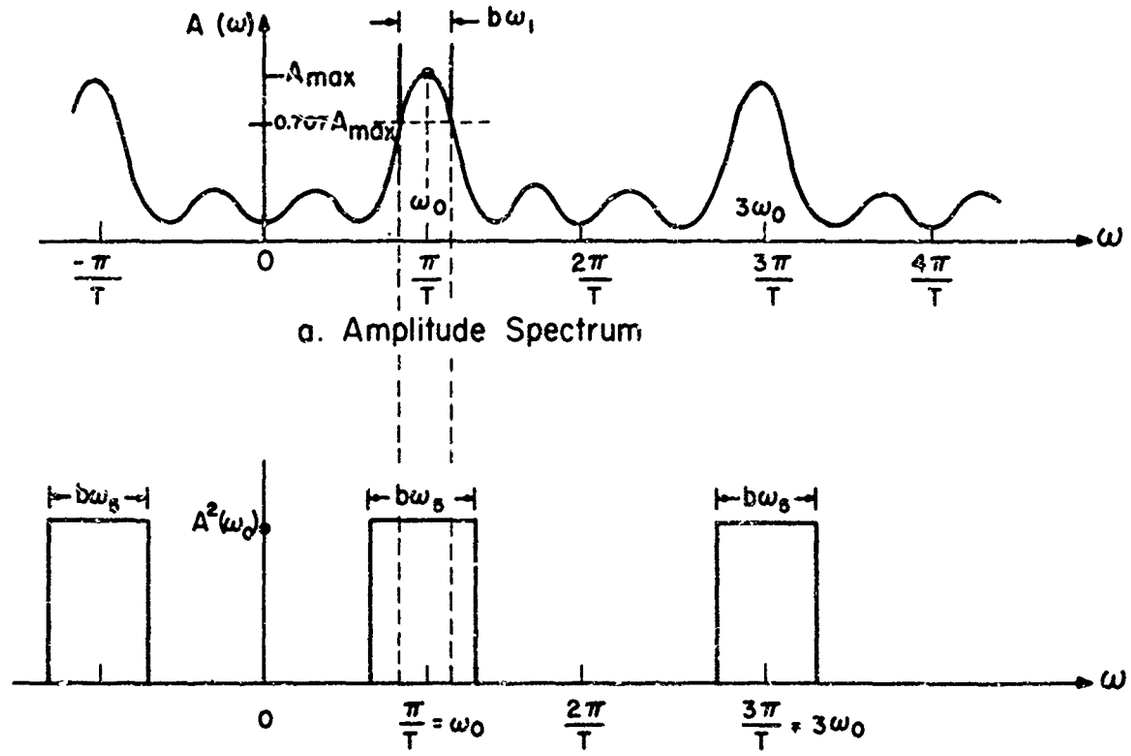

FIG. 3-2 Properties of Hybrid TEM mode couplers.

where

$$p(t) = 1 \quad , \quad 0 \le t \le \Delta$$
$$p(t) = 0 \quad , \quad t > \Delta$$
$$p(t) = 0 \quad , \quad t < 0$$

We can now use Eq. 3.10 to find the energy in the response. From Parseval's theorem,

$$\frac{1}{2\pi}\int_{-\infty}^{+\infty} |R(\omega)|^2 d\omega = \int_0^{\infty} \sum_{k=1}^{\infty} V^2 a_k^2 \, p(t - kT)dt$$
$$= V^2\Delta \sum_{k=1}^{\infty} a_k^2 \qquad (3.11)$$

Since $V^2\Delta$ equals unity, we have

$$\frac{1}{2\pi}\int_{-\infty}^{+\infty} |R(\omega)|^2 d\omega = \sum_{k=1}^{\infty} a_k^2 \qquad (3.12)$$

It is interesting to note that for excitation by a <u>unit energy pulse</u> the number given by the right-hand side of Eq. 3.12 also corresponds to the total energy within any period $\frac{2\pi}{T}$ of the energy spectrum of the system function (or the response to a <u>unit impulse</u>). This can be shown in the following manner. From Eq. 3.7,

$$h(t) \overset{\mathcal{F}}{\longleftrightarrow} H(\omega) = \sum_{0}^{+\infty} a_k e^{-j\omega kT} = \sum_{-\infty}^{+\infty} a_k e^{-j\omega kT} \qquad (3.13)$$

Over the interval $-\Omega \le \omega \le +\Omega$

we have

$$\int_{-\Omega}^{+\Omega} |H(\omega)|^2 d\omega = \sum_{-\infty}^{+\infty}\sum a_k a_\ell^* \int_{-\Omega}^{+\Omega} e^{-j\omega(k-\ell)T} d\omega$$

$$= \sum_{-\infty}^{+\infty}\sum a_k a_\ell^* \left[\frac{e^{-j\Omega(k-\ell)T}}{j(k-\ell)T} - \frac{e^{+j\Omega(k-\ell)T}}{j(k-\ell)T}\right] \qquad (3.14)$$

$$= \sum_{-\infty}^{+\infty}\sum a_k a_\ell^* \left[\frac{2\sin[\Omega(k-\ell)]T}{(k-\ell)T}\right]$$

The coupling in Eq. 3.14 vanishes for all $k \neq \ell$ only when $\Omega = \frac{n\pi}{T}$, where n is an integer other than zero. Hence,

$$\int_{-\frac{n\pi}{T}}^{-\frac{n\pi}{T}} |H(\omega)|^2 d\omega = 2n\pi \sum_{-\infty}^{+\infty} |a_k|^2 \qquad (3.15)$$

and it follows that the spectral energy within any period $\frac{2\pi}{T}$ is given by

$$e = \frac{1}{2\pi} \int_0^{\frac{2\pi}{T}} |H(\omega)|^2 d\omega = \sum_{-\infty}^{+\infty} |a_k|^2$$

$$= \sum_{k=1}^{\infty} a_k^2 \qquad (3.16)$$

for the case of real coefficients and a causal impulse response.

The results presented above suggest a different definition of bandwidth for this class of microwave networks—a definition similar to that given for the noise bandwidth in Eq. 3.5. Here the bandwidth is defined as the equivalent rectenge in a given period $\frac{2\pi}{T}$; the peak value occurs at odd multiples of $\omega_0 = \frac{\pi}{T}$. Thus,

$$|H(\omega_0)|^2 \cdot bw_5 = \sum_{k=1}^{\infty} a_k^2 \tag{3.17}$$

or

$$bw_5 = \frac{\sum_{k=1}^{\infty} a_k^2}{|H(\omega_0)|^2}$$

It follows from Eq. 3.7 that $|H(\omega_0)|^2$ is given by[17]

$$|H(\omega_0)|^2 = \left| \sum_{k=1}^{\infty} (-1)^{k+1} a_k \right|^2 \tag{3.18}$$

while the null frequency and periodic repetitions of the null frequency occur at

$$|H(0)|^2 = \left| \sum_{k=1}^{\infty} a_k \right|^2 \tag{3.19}$$

Then, from Eqs. 3.17 and 3.18, we have

$$bw_5 = \frac{\sum_{k=1}^{\infty} a_k^2}{\left| \sum_{k=1}^{\infty} (-1)^{k+1} a_k \right|^2} \qquad (3.20)$$

This definition is illustrated in Fig. 3-2b.

One might also define the bandwidth in a manner similar to Eq. 3.20, but in terms of the normalized second central moment of $|H(\omega)|^2$ in a given period, as discussed in Section 3.2 where it was applied to the entire ω domain. Both this definition and the one given in Eq. 3.20 result in different equivalent system bandwidths. Neither definition appears very satisfying. The various definitions described in the earlier sections also either fail when applied to certain microwave networks or at best seem artificial.

3.3.2 Example 2

A length of rectangular waveguide has a system function which resembles a high-pass filter for each possible mode and depends upon the manner of launching and retrieving the signal. The impulse response of a rectangular waveguide network is given by the sum of a delayed impulse and a second term, imvolving Bessel functions, which results in signal distortion. By any of the definitions bw_1 through bw_4 discussed in Section 3.2, however, the bandwidth is infinite.

3.3.3 Example 3

A section of lossless coaxial line whose characteristic impedance is invariant with length has an all-pass, linear-phase system function; the impulse response is simply a delayed impulse and hence introduces no distortion. It too has an infinite bandwidth. How do we distinguish between Examples 2 and 3?

Examples 1 through 3 illustrate that either the definitions of bandwidth as described earlier are inadequate and a new definition is required, or the characteristics of wideband networks should be defined

in a different domain; for example the time domain—the domain of eventual interest. Here, specifications such as rise time, build-up time, settling time, time residues, etc., have more significance.

We feel that a more fundamental (and satisfying) description of bandwidth might be obtained through the definition of the familiar Q or quality factor.[18] A detailed derivation of the Q factor via scattering matrix notation is presented in Appendices B and C. This factor depends on the time rate of change of the stored energy and the power dissipated in a network, and must be finite and, indeed, on the order of unity for wideband networks. Unfortunately, the conventional definition of Q involves certain inherent narrow-band approximations. In Appendix C these approximations are investigated to see how they apply first to narrow-band systems and later to wideband transmission networks. It will be shown in the next section that for certain classes of wideband networks the description of an effective bandwidth defined by a modified Q factor is meaningful.

3.4 A PROPOSED DEFINITION FOR THE TRANSMISSION QUALITY FACTOR

It is proposed to define a new transmission quality factor for wideband networks—one which is closely related to that used in narrow-band systems (see Appendix C). As indicated in Appendix B, it is clear that any such definition must involve the fundamental quantities of energy stored and power dissipated in the network. The effective bandwidth of the network will then be defined as the resonant frequency divided by the transmission Q .

3.4.1 Definition

The transmission Q of a transmission network, from a fixed input port to any other port i , is defined as

$$\tilde{Q}_T = \frac{\omega_0 \langle \tilde{W},\ i^{th} \text{ port} \rangle}{\langle \text{Pd, excluding source termination} \rangle \big|_{\omega=\omega_0}} \qquad (3.21)$$

where $\langle \tilde{W},\ i^{th} \text{ port} \rangle$ is defined as the time average of the total stored energy in the network (as observed at port i) when excited by a sinusoidal source at ω_0 and includes the effects of the "natural modes" of the

network. This quantity is "weighted" mainly by the contribution to stored energy at ω_0, but also includes transient contributions (see Sec. 3.4).

The effective transmission bandwidth of a two-port network is defined as

$$BW_{eff} \equiv \frac{f_0}{\tilde{Q}_T} \tag{3.22}$$

3.4.2 Finding $\langle \tilde{W} \rangle$

In the previous section a definition of $\tilde{Q}_T$ was presented that involved a quantity described as $\langle \tilde{W} \rangle$, the time average of the energy stored in the network due to the natural modes of the circuit. It is the purpose of this section to describe the meaning of this term and how it can be measured.

Consider the linear, passive, time-invariant two-port network shown in Fig. 3-3. This configuration might be a multi-port lossy network as described in Appendix B or C, where one is interested in evaluating the transfer function between a given input and output port. Two cw signal generators whose EMF's are e_{g1} and e_{g2} are connected in series at the input port. Here

$$e_{g1} = -\, e_{g2} = -\, 2 \sin(2\pi f_0 t) \tag{3.23}$$

where f_0 is the resonant frequency of the network. The source impedances of the generators are combined into one resistor, as shown in the figure. Generator two is normally not connected so that the total EMF in the circuit is supplied by e_{g1} and is equal to $-2 \sin(2\pi f_0 t)$ volts; the incident voltage at the network terminals is simply

$$\begin{aligned} E_{inc} &= -\sin(2\pi f_0 t) \quad \text{(switch closed)} \\ E_{inc} &= 0 \qquad\qquad\ \ \text{(switch open)} \end{aligned} \tag{3.24}$$

and depends on the time t_i when the switch is opened. Alternately, the incident voltage can be expressed as

$$E_{inc} = -\{\sin \omega_o t\}u(t_i - t) \tag{3.25}$$

where $u(t)$ is a unit step function. A picture of E_g, the equivalent generator voltage for several different switching times, is shown in Fig. 3-4. Note that after the switch is opened the network is passive. The voltage appearing across the load and terminations after $t=t_i$ is due only to the energy stored in the network at the natural modes of the system. Once the driving voltage $\sin \omega_o t$ is removed, the network is given "initial conditions"; the poles and zeros of the system in the complex p plane determine the response for $t > t_i$. The magnitude and the rate of decay of the voltage depend, of course, upon when the switch is opened. The energy absorbed by the source termination is determined by squaring the voltage across the resistance and integrating the result from zero to infinity. When this computation is done for all possible times t_i in the interval $0 \le t_i \le T = \frac{1}{f_o}$, the result is a series of numbers $W_0, W_1, W_2, \ldots, W_i$ corresponding to a measure of the stored energy for each time the switch is opened; i.e., for $t = t_0$, $t = t_1$, $t = t_2, \ldots, t = t_i$. It is clear from Parseval's theorem that the operation of squaring and integrating the response after $t > t_i$ corresponds to integrating the stored energy over the entire ω domain and not just at ω_o. From the description of the method used to turn off the input signal, we suspect that the contribution to the stored energy is greatest at ω_o: this is also later verified in Fig. 3-5. The result of averaging these numbers as a function of time over the period T is defined as $\langle \widetilde{W} \rangle$, the time average of the stored energy absorbed by the termination.

3.4.3 Stored Energy in TEM-Mode Networks

Assume that the impulse response between ports in a class of microwave networks is given by a train of unequally weighted but uniformly spaced impulses.* That is,

* For example, the branch-line coupler, the ring hybrid, the quarter wavelength coupler, etc.

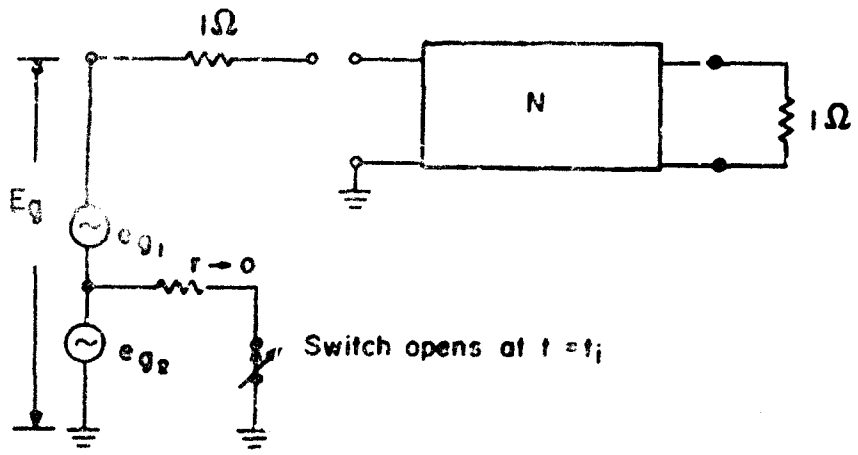

FIG. 3-3 The network configuration of the input circuit.

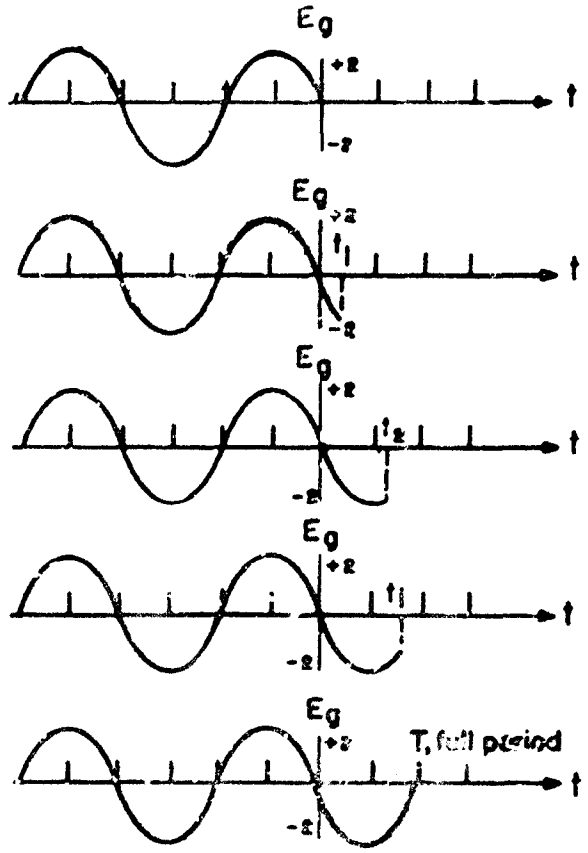

FIG. 3-4 The generator voltage for the circuit in Fig. 3-3.

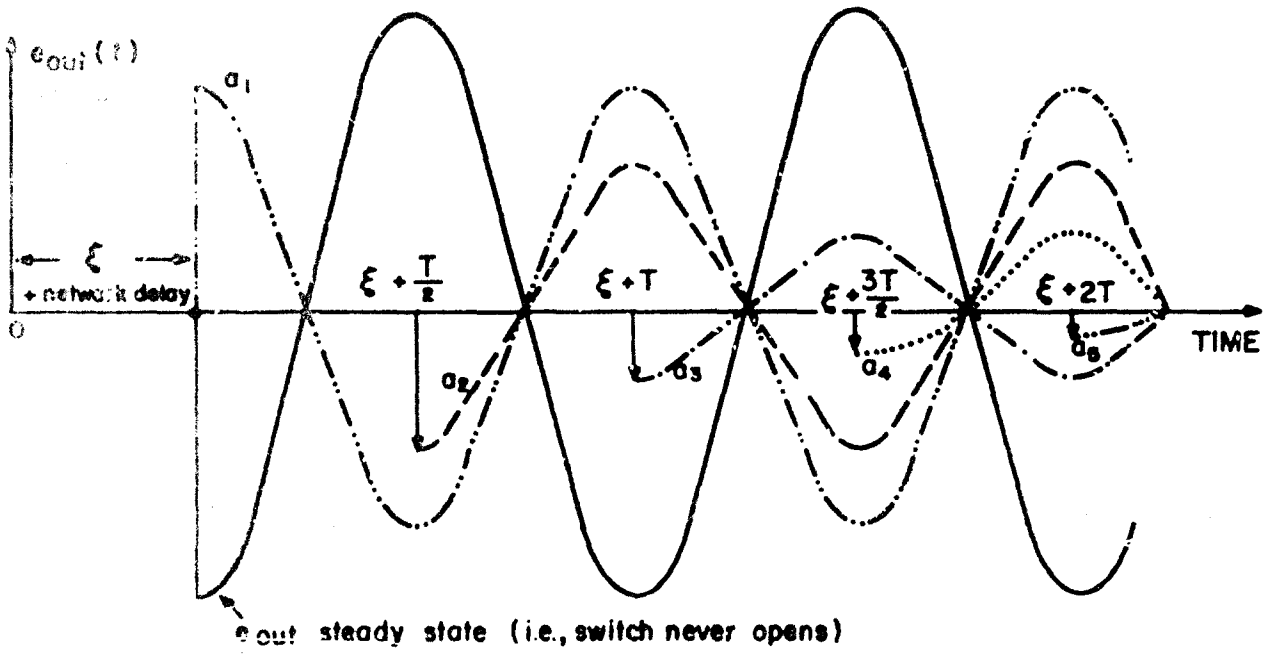

FIG. 3-5 The stored energy given by the sum of sinusoids.

$$h(t) = \sum_{k=0}^{\infty} a_k \delta\left(t - k\frac{T}{2} - t_i\right) \tag{3.26}$$

where
- k is an integer
- T is the reciprocal of the resonant frequency of the network
- t_i is a constant corresponding to the time the switch in Fig. 3-4 is opened

Then the response of the network to an incident voltage

$$\mathcal{E}_{inc} = \{\sin \omega_0 t\}\, u(t_i - t) \tag{3.27}$$

is given by the superposition of sinusoidal signals shown in Fig. 3-5. In any half period the incident voltage has the form of a simple sinusoidal signal whose amplitude depends on k and a_k : the portion of the sine wave to be considered depends upon t_i . Mathematically, if the switch opens at $t = \xi$, then after a suitable delay the total stored energy $\tilde{W}(\xi)$ is given by

$$\tilde{W}(\xi) = \int_{\xi}^{\xi+\frac{T}{2}} [a_{ss} - a_0]^2 \sin^2(\omega_0 t)dt + \int_{\xi+\frac{T}{2}}^{\xi+T} [a_{ss} - \{a_0 - a_1\}]^2 \sin^2(\omega_0 t)dt$$

$$+ \int_{\xi+T}^{\xi+\frac{T}{2}} [a_{ss} - \{a_0 - a_1 + a_2\}]^2 \sin^2(\omega_0 t)dt + \ldots \tag{3.28}$$

where a_{ss} is the peak steady-state voltage across the load due to generator 1.

Since

$$\int_{\xi}^{\xi+\frac{T}{2}} \sin^2(\omega_0 t)dt = \int_{\xi+\frac{T}{2}}^{\xi+T} (\sin^2\omega_0 t)dt = \int_{\xi+T}^{\xi+\frac{3T}{2}} (\sin^2\omega_0 t)dt = \ldots \qquad (3.29)$$

one obtains

$$\widetilde{W}(\xi) = \left\{\sum_{n=0}^{\infty}\left[a_{ss} - \sum_{k=0}^{n}(-1)^k a_k\right]^2\right\}\int_{\xi}^{\xi+\frac{T}{2}} \sin^2(\omega_0 t)dt \qquad (3.30)$$

Now the time average of $\widetilde{W}(\xi)$ can be found by averaging Eq. 3.30 over a half period $\frac{T}{2}$. This follows, since it is not difficult to deduce (from physical reasoning) that $\widetilde{W}(\xi)$ must be periodic with a period $\frac{T}{2}$, i.e.,

$$\langle\widetilde{W}(\xi)\rangle = \left\{\ \right\}\frac{2}{T}\int_{0}^{\frac{T}{2}} \widetilde{W}(\xi)d\xi \qquad (3.31)$$

where $\left\{\ \right\}$ is given in Eq. 3.30. Indeed, for the class of networks described by Eq. 3.26 the integral given on the right side of Eq. 3.30 is a constant for all ξ and can be shown by a direct integration to be equal to $\frac{T}{4}$. In particular, a convenient value of ξ, namely $\xi = 0$, corresponds to a sinusoidal input signal originating at $t = -\infty$ and stopping abruptly at $t = 0$. This waveform can be approximated using, for example, the generator being developed for the Floyd Site Radar System.[21] The final answer, therefore, is given by

$$\langle\widetilde{W}(\xi)\rangle\Big|_{\substack{\xi=0\\ \omega=\omega_0}} = \frac{T}{4}\left\{\sum_{n=0}^{\infty}\left[a_{ss} - \sum_{k=0}^{n}(-1)^k a_k\right]^2\right\} \qquad (3.32)$$

and can be found graphically by viewing an oscilloscope trace or exactly if the system function of a component is known. Finally, it is interesting to note (and not difficult to prove) that Eq. 3.32 is equal to the same constant at all the $(2k-1)f_o$ odd harmonics of f_o at which the network is resonant.

3.5 THE QUALITY FACTOR, $\tilde{Q}_T$, FOR TEM-MODE NETWORKS

In this section we will derive the transmission quality factor, $\tilde{Q}_T$, for TEM-mode transmission line networks and use the results to find BW_{eff}, the effective bandwidth. We will use the results given in the previous section and introduce Z-transform techniques in order to obtain a closed-form expression for $\tilde{Q}_T$ and BW_{eff}. The procedure is as follows. Using (3.21) and (3.32) we have

$$\tilde{Q}_T = \frac{\omega_o\{\langle\tilde{W}\rangle\}}{\langle Pd_{load}\rangle\big|_{\omega=\omega_o}}$$

$$= \frac{\frac{\pi}{T}\cdot\frac{T}{4}\left\{\sum_{n=0}^{\infty}\left[a_{ss} - \sum_{k=0}^{n}(-1)^k a_k\right]^2\right\}}{\left(\frac{a_{ss}}{\sqrt{2}}\right)^2} \qquad (3.33)$$

Simplifying,

$$\tilde{Q}_T = \frac{\pi}{2a_{ss}^2}\left\{\sum_{n=0}^{\infty}\left[a_{ss} - \sum_{k=0}^{n}(-1)^k a_k\right]^2\right\}$$

$$= \frac{\pi}{2a_{ss}^2}\sum_{n=0}^{\infty} c_n^2 \qquad (3.34)$$

where

$$c_n = a_{ss} - \sum_{k=0}^{n} (-1)^k a_k \tag{3.35}$$

Assume that the Z transform of c_n is defined as

$$Z[c_n] = \sum_{n=0}^{\infty} c_n Z^{-n} = C(Z) \tag{3.36}$$

where

$$Z = e^{+p}$$

$$p = \sigma + j\omega$$

In effect, we are artificially representing c_n (Eq. 3.35) as a sequence of impulses of area c_n volt-seconds starting at $t=0$ and spaced one second apart for mathematical convenience. Then it is not difficult to show that[22]

$$\sum_{n=0}^{\infty} c_n^2 = \frac{1}{2\pi_j} \oint_{\text{unit}\,\odot} C(Z)\, C\left(\frac{1}{Z}\right) Z^{-1}\, dZ \tag{3.37}$$

where we evaluate the contour integral by summing the residues of the integrand at the poles located <u>within</u> the unit circle.

The next task is to find $C(Z) \overset{Z}{\longleftrightarrow} c_n$. Let us define the system function of a network whose impulse response is a train of weighted and delayed impulses such as the Z transform of $h(t)$ given in Eq. 3.26; that is, $H(Z) \overset{Z}{\longleftrightarrow} h(t)$. For convenience we shall once again assume the impulses are spaced one second apart and begin at $t=0$. Then the term $\sum_{k=0}^{n}(-1)^k a_k$ represents the peak value of the response in any half-period k when excited by a step-modulated signal whose carrier frequency is equal to the resonant frequency of the device; namely, $f_o = \frac{1}{2}$ hertz. The term $\{a_{ss} - \sum_{k=0}^{n}(-1)^k a_k\}^2$

is proportional to the energy dissipated in the load resistance in any half period k after the switch is opened (and after a time equal to the signal-front delay[24] of the network has elapsed). Note that the peak value of the steady-state solution a_{ss} alternates in sign each half period; the sign of the peak value of the transient contribution, $\sum_{k=0}^{n}(-1)^k a_k$ also alternates, algebraically. Using this information one can find the Z transform of the c_n coefficient defined in Eq. 3.35 as follows:

$$C(Z) = Z[c_n] = Z[a_{ss}]_{sgn\text{-}rep} - Z\left[\sum_{k=0}^{n}(-1)^k a_k\right]_{sgn\text{-}rep} \tag{3.38}$$

Here,

$$Z[a_{ss}]_{sgn\text{-}rep} = \frac{a_{ss}Z}{1+Z} \tag{3.39}$$

represents an equal-amplitude alternating series.

The term $Z\left[\sum_{k=0}^{\infty}(-1)^k e_k\right]_{sgn\text{-}rep}$ can be found in two steps. First, we find the peak value in any half-period k as[23]

$$Z\left[\sum_{k=0}^{n}(-1)^k a_k\right] = P(Z) = \frac{Z}{Z-1}H(-Z) \tag{3.40}$$

Alternation in sign can be accomplished by substituting $-Z$ for Z in Eq. 3.40. Hence,

$$Z\left[\sum_{k=0}^{n}(-1)^k a_k\right]_{sgn\text{-}rep} = \frac{-Z}{-Z-1}H(Z) = \frac{Z}{Z+1}H(Z) \tag{3.41}$$

Substituting Eqs. 3.39 and 3.41 into Eq. 3.38 yields

$$C(Z) = \frac{Z}{Z+1}\left[a_{ss} - H(Z)\right] \tag{3.42}$$

Substituting Eq. 3. into Eq. 3.37 we obtain

$$\sum_{n=0}^{\infty} a_n^2 = \frac{1}{2\pi j} \oint_{\text{within}\odot} \frac{\frac{Z}{Z+1}\left[a_{ss} - H(Z)\right]\left(\frac{1}{1+Z}\right)\left[a_{ss} - H\left(\frac{1}{Z}\right)\right]dZ}{Z}$$

$$= \frac{1}{2\pi j} \oint_{\text{within}\odot} \frac{1}{(Z+1)^2}\left\{a_{se}^2 - a_{ss}\left[H(Z) + H\left(\frac{1}{Z}\right)\right] + H(Z)\,H\left(\frac{1}{Z}\right)\right\}dZ \tag{3.43}$$

Finally, substituting Eq. 3.43 into Eq. 3.34 we obtain

$$\tilde{Q}_T = \frac{\pi}{2a_{ss}^2}\left[\frac{1}{2\pi j} \oint_{\text{within}\odot} \frac{1}{(Z+1)^2}\left\{a_{ss}^2 - a_{ss}\left[H(Z) + H\left(\frac{1}{Z}\right)\right] + H(Z)\,H\left(\frac{1}{Z}\right)\right\}dZ\right] \tag{3.44}$$

The effective bandwidth is given by

$$BW_{eff} = \frac{f_o}{\tilde{Q}_T} \tag{3.45}$$

3.6 APPLICATIONS

3.6.1 Two-Port Lossless Network

Consider the single short-circuited stub shown in Fig. 3-6a: the stub has a characteristic impedance of d ohms while the main line is normalized to 1 ohm. The flow graph for the network is shown in Fig. 3-6b. The transmission through the network, neglecting the signal-front delay, can be found from the graph by inspection and is given by

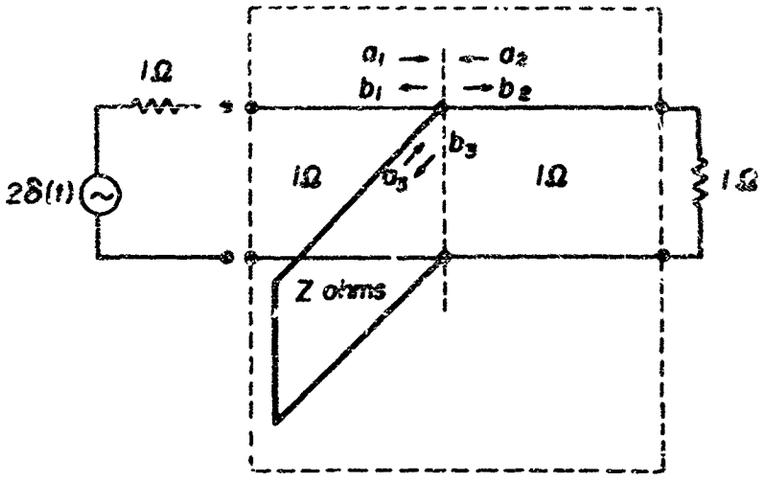

(a) Two Port Configuration

$\Gamma_1 \equiv$ 1 ohm line driving a 1 ohm line || Z ohm line

$\Gamma_2 \equiv$ Z ohm line driving a 1Ω || 1Ω line

(b) Flow graph

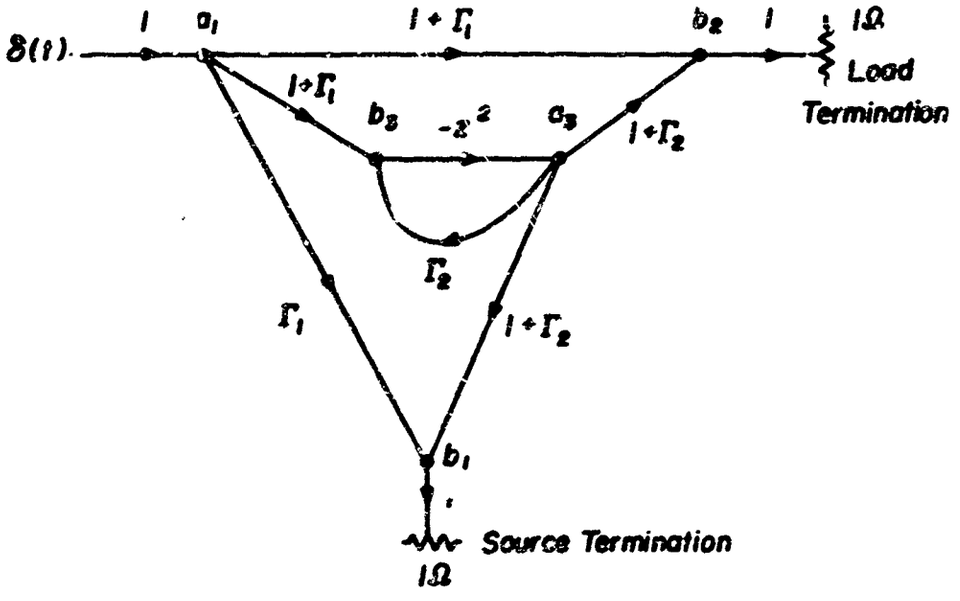

FIG. 3-6 A simple two-port.

$$H_{21}(z) = \frac{b_2}{a_1} = (1 + \Gamma_1) + \frac{(1 + \Gamma_1)(1 + \Gamma_2)(-z^2)}{1 + \Gamma_2 z^2}$$

$$= \frac{(1 + \Gamma_1)(1 - z^2)}{1 + \Gamma_2 z^2} \qquad (3.46)$$

where

$$z^2 = e^{-2p\tau} \approx e^{-\Gamma \frac{2s}{c}}$$

$$\Gamma_1 \equiv \frac{d/(d + 1) - 1}{d/(d + 1) + 1} = -\frac{1}{2d + 1}$$

$$\Gamma_2 = \frac{\frac{1}{2} - d}{\frac{1}{2} + d} = \frac{1 - 2d}{1 + 2d}$$

Letting

$$Z = \frac{1}{z^2} \qquad (3.47)$$

we have

$$H_{21}(Z) = \frac{(1 + \Gamma_1)(Z - 1)}{Z + \Gamma_2} \qquad (3.48)$$

and

$$C(Z) = \frac{Z}{Z + 1}\left[a_{ss} - H_{12}(Z)\right]$$

$$= \frac{Z}{Z + 1}\left[\frac{(1 + \Gamma_1 + \Gamma_2) \quad \Gamma_2 Z}{Z + \Gamma_2}\right] \qquad (3.49)$$

since $a_{ss} = 1$ for a lossless network. Similarly,

$$C\left(\frac{1}{Z}\right) = \frac{1}{1 + Z}\left[\frac{-\Gamma_1 + Z(1 + \Gamma_1 + \Gamma_2)}{1 + \Gamma_2 Z}\right] \tag{3.50}$$

Substituting Eqs. 3.49 and 3.50 into Eq. 3.37 directly yields

$$\sum_{n=0}^{\infty} c_n^2 = \frac{1}{2\pi j} \oint_{\text{within } \odot} \frac{1}{(Z+1)^2}\left[\frac{(1 + \Gamma_1 + \Gamma_2) - \Gamma_1 Z}{Z + \Gamma_2}\right]\left[\frac{-\Gamma_1 + Z(1 + \Gamma_1 + \Gamma_2)}{1 + \Gamma_2 Z}\right] dZ$$

$$= \frac{1}{(Z+1)^2} \frac{\left[(1 + \Gamma_1 + \Gamma_2) - \Gamma_1 Z\right]\left[-\Gamma_1 + Z(1 + \Gamma_1 + \Gamma_2)\right]}{(1 + \Gamma_2 Z)}\Bigg|_{Z=-\Gamma_2} \tag{3.51}$$

and from Eq. 3.34

$$\mathcal{T}_T = \frac{\pi}{2} \frac{1}{(Z+1)^2} \frac{\left[(1 + \Gamma_1 + \Gamma_2) - \Gamma_1 Z\right]\left[-\Gamma_1 + Z(1 + \Gamma_1 + \Gamma_2)\right]}{\left[1 + \Gamma_2 Z\right]}\Bigg|_{Z=-\Gamma_2}$$

$$= \frac{\pi}{2}\left(\frac{\Gamma_1^2}{1 + \Gamma_2^2}\right) \tag{3.52}$$

Assume the characteristic impedance of the stub is 1 ohm. Then from Eq. 3.46

$$\Gamma_1 = \Gamma_2 = -\frac{1}{3} \tag{3.53}$$

Substituting Eq. 3.53 into Eq. 3.52 we find

$$\mathcal{T}_T\Big|_{d=1\ \Omega} = \frac{\pi}{16} = 0.197 \tag{3.54}$$

It is instructive to plot the amplitude spectrum of the function $H_{21}(z^2 = e^{-2p\tau})$: this is shown in Fig. 3-7 for a stub with d = 1 ohm. The conventional quality factor, defined as

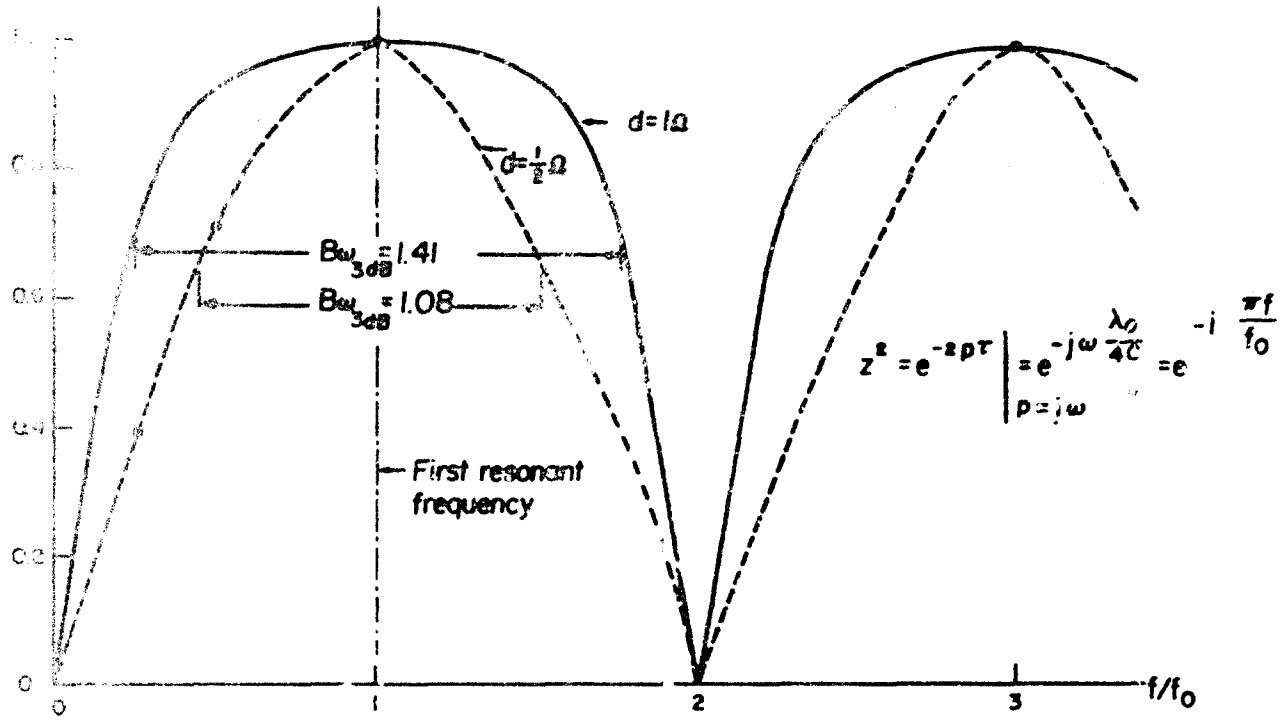

FIG. 3-7 The amplitude spectrum for a d-ohm stub across a 1-ohm line.

$$Q_{CONV} \equiv \frac{f_o}{BW_{3dB}} \quad \text{or} \quad BW_{3dB} = \frac{f_o}{Q_{CONV}} \tag{3.55}$$

yields

$$Q_{CONV} = \frac{1}{\sqrt{2}} = 0.707$$

Comparing the result of Eq. 3.54 with the conventional figure given by Eq. 3.55, we find that the new definition yields a smaller Q ; this yields a larger "effective" bandwidth if we employ the relationship given in Eq. 3.55 and substitute Q_T for Q_{CONV} . Intuitively this appears reasonable, since we are now including the contributions from all the periodic (and infinitely denumerable) passbands of the transfer function of the network.

We can plot the step-modulated response a(t) of this network for d = 1 ohm using Eq. 3.40. The results are shown in Fig. 3-8. The peak envelope of the magnitude of this response, $|a(t)|$, is plotted in Fig. 3-9 where it is shown that it exhibits a settling time T_{sl} equal to approximately 1.25T , where T is the time for 1 rf period.

It is interesting to investigate also the case for the particular value of d for which the impulse response is time limited. The impulse response for this case is given by

$$\begin{aligned} h_{21}(t) &= \frac{1}{2}\,\delta(t) - \frac{1}{2}\,\delta\left(t - \frac{T}{2}\right) \\ h_{21}(t) &\overset{z}{\longleftrightarrow} H_{21}(z) = \frac{1}{2}\,(1 - z^2) \end{aligned} \tag{3.56}$$

and corresponds (in the network) to setting $\Gamma_2 = 0$. It can be seen by examining the amplitude spectrum (shown dotted in Fig. 3-7) that the conventional 3 dB bandwidth for this case has decreased by about a factor of 1.3. Using Eq. 3.52, that is, by setting $\Gamma_2 = 0$ and $\Gamma_1 = -\frac{1}{2}$, we obtain

$$\tilde{Q}_{T}\Big|_{d=\frac{1}{2}\,\Omega} = \frac{\pi}{8} \tag{3.57}$$

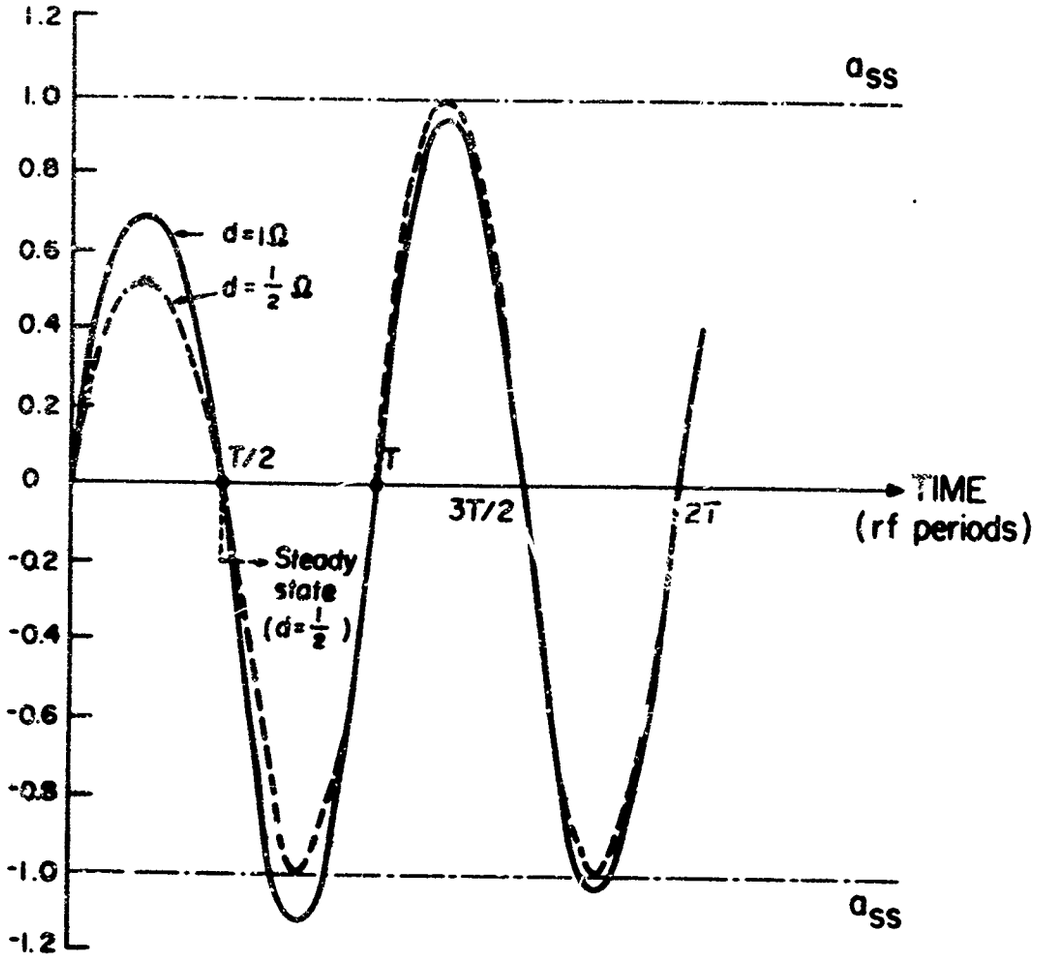

FIG. 3-8 The step-modulated response a(t) for a d-ohm stub across a 1-ohm line.

A comparison with Eq. 3.54 indicates that the effective $\tilde{Q}_T$ has increased by a factor of two. An increase in $\tilde{Q}_T$ is accompanied by a decrease in the rise time of the positive envelope of the step-modulated response as shown in Fig. 3-9. The settling time, however, has improved from 1.25 T to 0.62 T., We conclude that although the rise time of the response varies as a function of the effective bandwidth, the settling time does not! Indeed, the settling time is a measure of the overshoot and ringing behavior of the network and must depend on both the amplitude spectrum and the phase function. Thus, specifying the bandwidth by either Eq. 3.46 or Eq. 3.55 is not sufficient; one must also specify the settling time. Note that the effective bandwidth defined using $\tilde{Q}_T$ is a more sensitive function than the conventional 3 dB bandwidth.

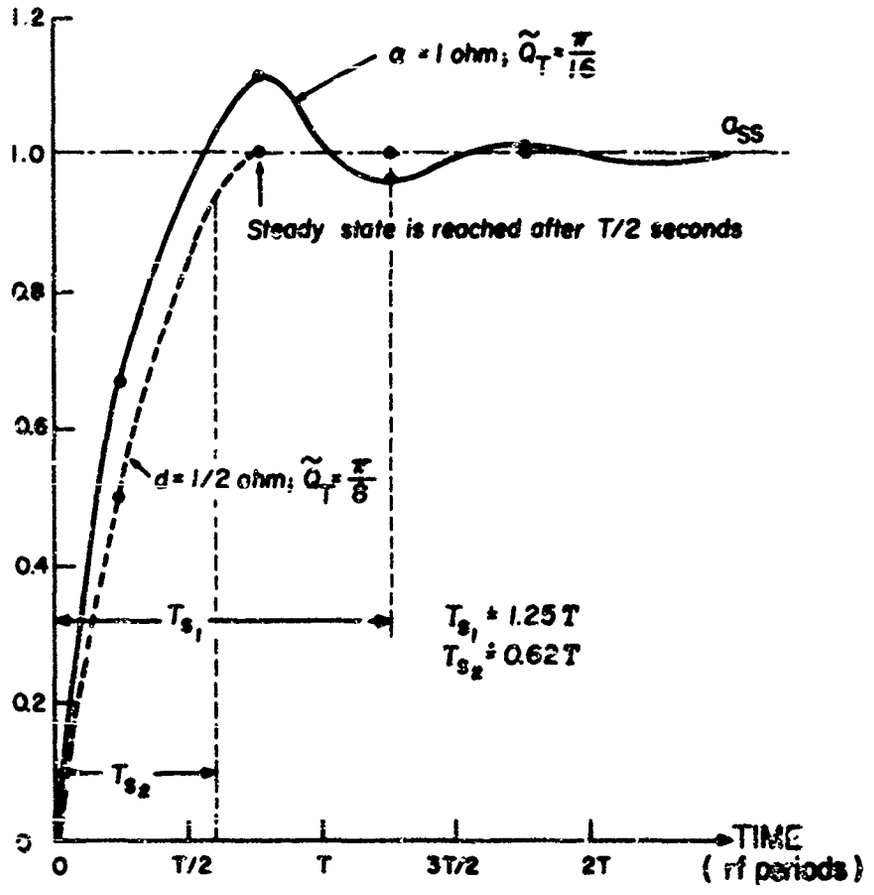

FIG. 3-9 Envelope of $|a(t)|$ for a d-ohm stub across a 1-ohm line.

3.6.2 Two-Port Lossy Network

As a second example we will consider the familiar four-port lossless parallel-line (quarter-wavelength) coupler described in Section IV. We are interested in evaluating the transmission between the direct colinear path $H_{21}(z)$ and the coupled path $H_{41}(z)$. In either case the overall two-port network formed by considering either $H_{21}(z)$ or $H_{41}(z)$ is lossy. This is shown in Fig. 3-10.

The system functions for these couplers were derived in a classic paper by Oliver.[26] He also plotted the impulse response (i.e., the inverse Laplace transform of $H_{21}(z)$ and/or $H_{41}(z)$) and the amplitude spectrum of $H_{41}(z)$ as a function of the coupling coefficient k. The resonant frequency of the device corresponds to the frequency for which the line lengths are $\frac{\lambda_0}{4}$ meters, where $\lambda_0 f_0 = c$. Since the impulse response of this class of networks is a train of uniformly spaced impulses, we know that resonance may be interpreted as the frequency corresponding to

$$f_0 = \frac{1}{2T} \tag{3.58}$$

where T is the spacing between impulses. Also, we note that the amplitude spectrum is periodic in the frequency domain, with resonance occurring at each frequency

$$f = (2k - 1)f_0$$

where k is an integer.

The system function to the coupled port is given by

$$H_{41} = \Gamma - \frac{\Gamma(1 - \Gamma^2)z^2}{1 - \Gamma^2 z^2} = \frac{\Gamma(1 - z^2)}{1 - \Gamma^2 z^2} \tag{3.59}$$

where

$$\Gamma = \frac{\xi - 1}{\xi + 1}$$
$$\xi = \frac{1 + k}{1 - k} \tag{3.60}$$

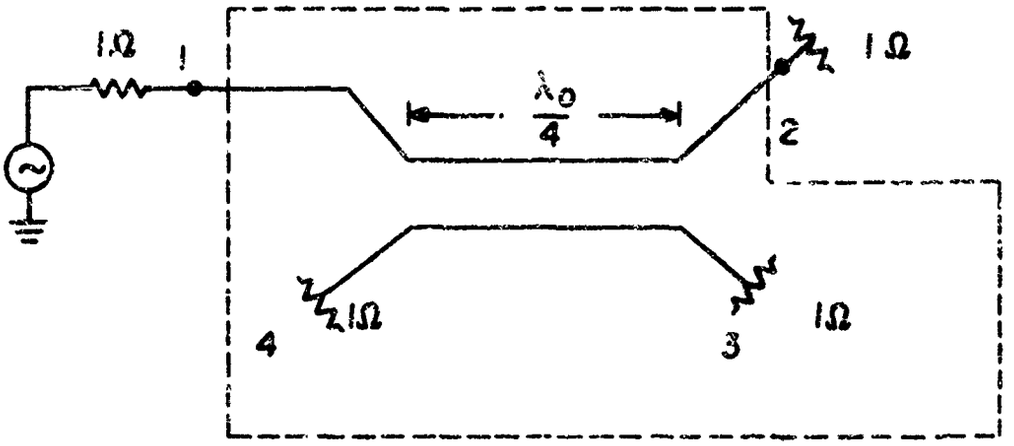

(a) $H_{21}(z)$; Direct or colinear arm

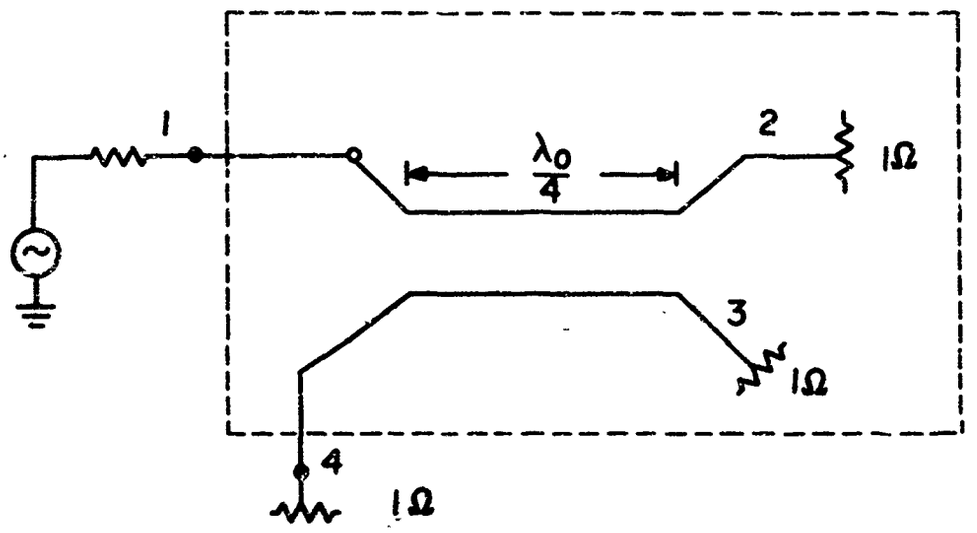

(b) $H_{41}(z)$; Coupled arm

FIG. 3-10 Quarter wavelength coupler as a two port.

k is the coefficient of coupling

$$z^2 = e^{-p2\tau} = e^{-pT}$$

$$\tau = \frac{\lambda_0}{4c} \qquad \text{(3.60 cont.)}$$

The normalized amplitude spectrum can be found by letting $p = j\omega$ and plotting $|H_{41}(e^{-j\omega t})|$. This is given in Fig. 11a for various values of the parameter k. In Fig. 11b Oliver also plotted the inverse transform of Eq. 3.59. Note that for small k the impulse response is essentially time limited: for large k (i.e., $k > \frac{1}{2}$) the impulse response is a train of impulses whose areas are weighted exponentially, and the transmission is dispersive.

We next find $\tilde{Q}_{T_{41}}$ by substituting Z for $\frac{1}{z^2}$, forming $C(Z)$, and evaluating the contour integral given in Eq. 3.37. Thus,

$$H_{41}(Z) = \frac{\Gamma(Z - 1)}{Z - \Gamma^2} \qquad (3.61)$$

and

$$C(Z) = \frac{Z}{1 + Z}\left[a_{ss} - H(Z)\right] \qquad (3.62)$$

where

$$a_{ss} = H(z)\Big|_{z=-1} \quad \frac{2\Gamma}{1 + \Gamma^2} \qquad (3.63)$$

Hence

$$C(Z) = \frac{\Gamma(1 - \Gamma^2)Z}{(1 + \Gamma^2)(Z - \Gamma^2)} \qquad (3.64a)$$

$$C\left(\frac{1}{Z}\right) = \frac{\Gamma(1 - \Gamma^2)}{1 + \Gamma^2} \quad \frac{1}{(1 - \Gamma^2 Z)} \qquad (3.64b)$$

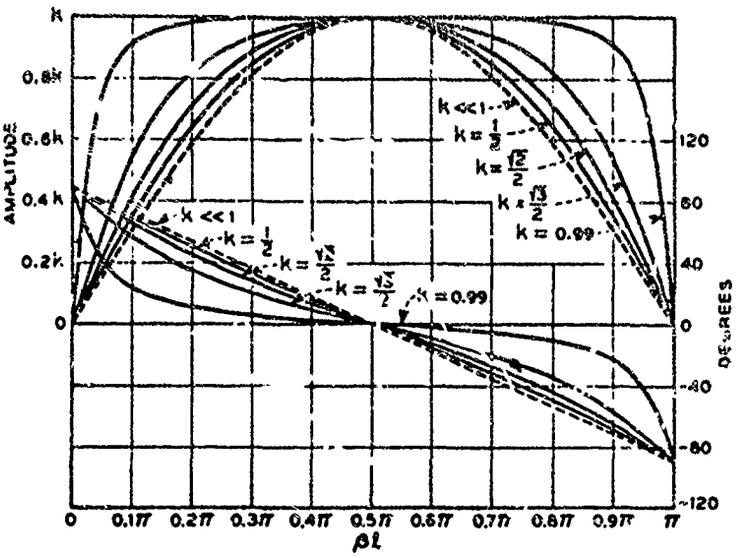

a. Amplitude spectrum.

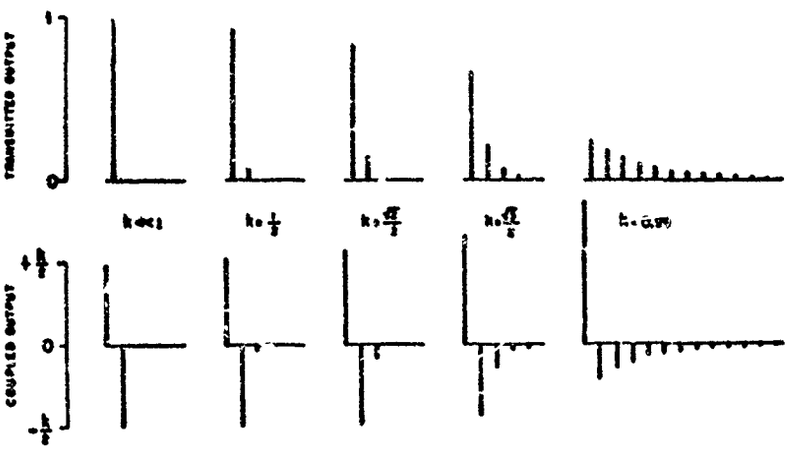

b. Impulse response.

FIG. 3-11 Amplitude spectrum and impulse response of Oliver's contra-directional coupler with constant coupling.

and

$$\tilde{Q}_{T_{41}} = \frac{\pi}{2} \frac{(1 + \Gamma^2)^2}{4\Gamma^2} \frac{\Gamma^2(1 - \Gamma^2)^2}{(1 + \Gamma^2)^2(1 - \Gamma^4)}$$

$$= \frac{\pi}{8} \frac{(1 - \Gamma^2)}{(1 + \Gamma^2)} \tag{3.65}$$

In a similar fashion, after the signal-front delay has been factored,

$$H_{21}(Z) = \frac{4\xi}{(\xi + 1)^2} \frac{1}{(1 - \Gamma^2 z^2)}$$

$$H_{21}(Z) = \frac{(1 - \Gamma^2)Z}{Z - \Gamma^2} \tag{3.66}$$

since

$$1 - \Gamma^2 = \frac{4\xi}{(\xi + 1)^2} \tag{3.67}$$

as can be verified at zero frequency. We then find $C(Z)$ as before, and obtain

$$C(Z) = - \frac{\Gamma^2(1 - \Gamma^2)}{(1 + \Gamma^2)} \frac{Z}{(Z - \Gamma^2)} \tag{3.68a}$$

$$C\left[\frac{1}{Z}\right] = - \frac{\Gamma^2(1 - \Gamma^{-2})}{(1 + \Gamma^2)} \frac{1}{(1 - \Gamma^2 Z)} \tag{3.68b}$$

and

$$\tilde{Q}_{T_{21}} = \frac{\pi}{2} \cdot \frac{\Gamma^4}{1 - \Gamma^4} \tag{3.69}$$

The results using Eqs. 3.66 and 3.69 for different values of k are given in Table 3-1.

TABLE 3-1

$\tilde{Q}_T$ vs k

k	$\tilde{Q}_{T_{41}}$	$\tilde{Q}_{T_{21}}$
0.99	0.0545	2.08
$1/\sqrt{2}$	0.278	0.049
$1/\sqrt{10}$	0.374	0.017
1/10	0.392	$\ll 0.1$

Referring to the amplitude spectrum shown in Fig. 11b it can be seen that as $k \to 1$ the bandwidth in any given period approaches π and the effective bandwidth approaches ∞. This result agrees with the computed value of $\tilde{Q}_{T_{41}}$. In a similar fashion it can be seen by examining Fig. 11a that for very small k the direct transmission is virtually an impulse and hence, it's effective bandwidth is very large (e.g., as $k \to 0$, $\tilde{Q}_{T_{21}} \to 0$ and $BW_{eff} \to \infty$).

The settling times of the direct and coupled arms are both excellent for small k. There is virtually no distortion in the direct branch since the impulse response is essentially an impulse. Due to the increased effective bandwidth in the coupled arm the rise time is superior when the coupling coefficient k approaches unity: the settling time, however, is poorer because of the increased distortion in the phase function.

3.7 EXPERIMENTAL RESULTS

In Section 3.6 we theoretically evaluated $\tilde{Q}_T$ for a line and a stub, and for a quarter-wavelength coupler. It is the purpose of this section to investigate the response of these networks experimentally. A more detailed experimental analysis of 3 dB, 10 dB, and 20 dB quarter-wavelength couplers is presented in Section IV.

3.7.1 A Line-Stub Configuration

A pulse modulated input shown in Fig. 3-12 at f_0 =1.35 GHz is fed into a 50-ohm length of RG9/U cable connected in series with a tee connector. A 50-ohm stub, electrically equal to $\frac{\lambda_0}{4}$ meters and short-circuited, is connected to one end of the tee, while the other end is routed to the HP 12 GHz oscilloscope. The pulse-modulated source is generated by the pulse-forming network described in previous reports.

The leading edge of the response is identical to the results predicted in [3-8 (d=1 ohm). It is difficult to examine the trailing edge, however, because the signal level is considerably reduced and, after the second period, becomes comparable to the time residues after the incident pulse.

Note that to obtain the c_n coefficient desceibed in Eq. 3.35 one can examine the leading edge of the response. The constant a_{ss} can be determined by inspection of the response: the leading edge reveals the term $\sum_{k=0}^{n}(-1)^k a_k$ given in Eq. 3.35.

3.7.2 The Quarter Wavelength Coupler

The experimental results for the quarter wavelength coupler are presented in Fig. 3-13. The particular case here shows the leading and trailing edges for both the colinear and coupled arms for $k = \frac{1}{\sqrt{2}}$. The pulse-modulated responses are also evaluated at the resonant frequency of the device; namely f_0 =1.35 GHz. The time-domain results are in close agreement with the results predicted by Eqs. 3.59 and 3.61 and shown in Fig. 3-11. Once again it should be noted that the preferred method for evaluating the c_n coefficient would be to use leading-edge rather than trailing-edge data for the reasons given in Section 3.7.1.

3.8 CONCLUSIONS

We conclude that specifying the transient behavior of a microwave network by a single number, for example its "effective bandwidth" or its transmission quality factor $\tilde{Q}_T$, is not sufficient. This number, however, is a good measure of how quickly the network (after the signal front delay has been factored) responds to a step-modulated input at resonance. If

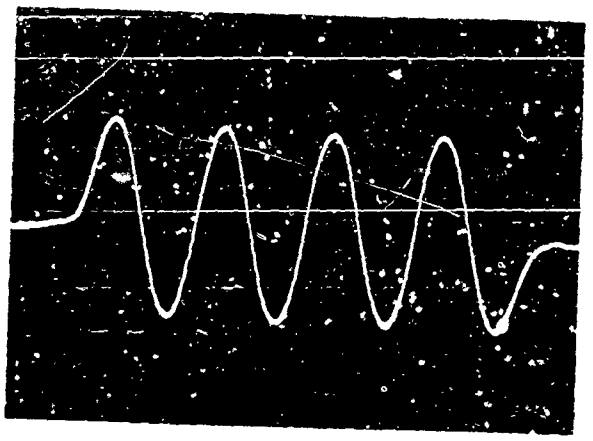

Input signal

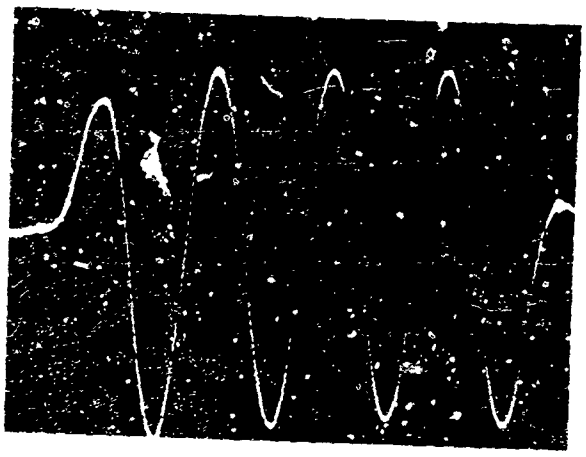

Leading edge
Compiete response

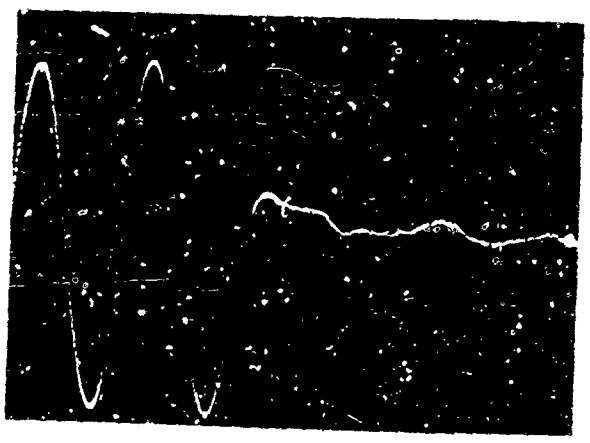

Trailing edge
1.35 GHz signal

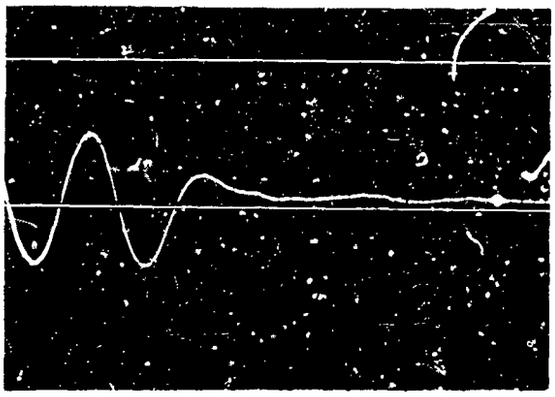

Coupled output Trailing edge

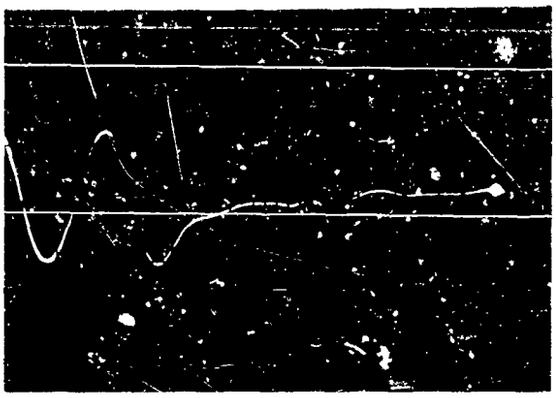

Direct output Trailing edge

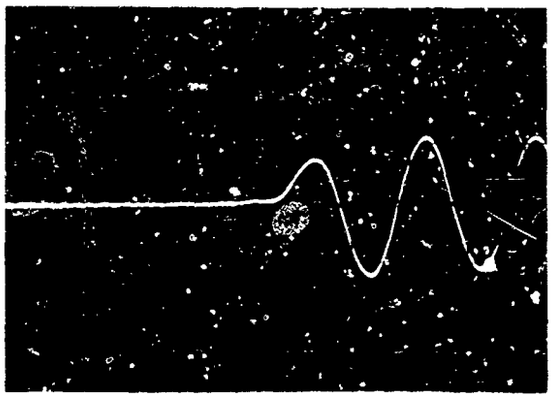

Coupled output Leading edge

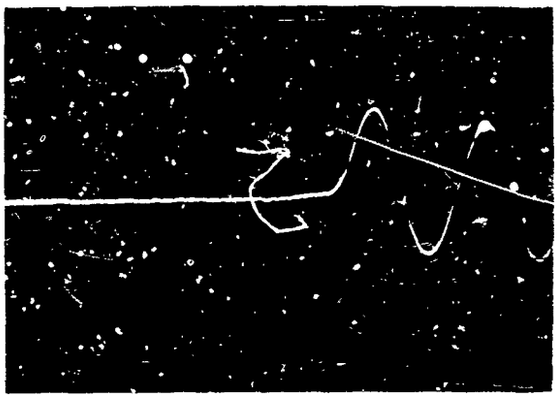

Direct output Leading edge

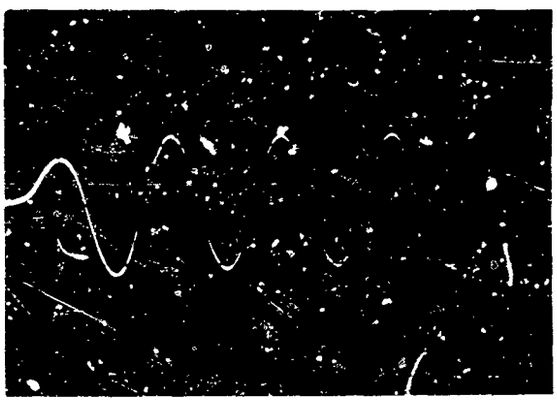

Coupled output Complete signal

one plots the envelope of the magnitude of this response, then the rise time (defined in the conventional manner) is directly proportional to $\tilde{\theta}_T$. The settling time, T_s, must be specified independently. Indeed, for very wide-band distributed systems, it seems more appropriate to specify three quantities; namely,

(1) the signal-front delay
(2) the rise time
(3) the settling time

in contrast to specifying bounds on the amplitude spectrum and phase function in the frequency domain. Practically, specifications on bounds in the frequency domain (especially for small deviations from linearity) are difficult to measure and their verification is time consuming. In addition they must be related, mathematically, to the eventual domain of interest, namely, the time domain. Instead, a set of three measurements in the time domain is sufficient to specify the response of the system to a step-modulated input. For a pulse-modulated input, a bound on the time-residue level may also be desirable.

SECTION IV

COUPLED TEM-MODE NETWORKS

(R. Smith, Sperry Rand Research Center)

4.1 INTRODUCTION

The analysis of the transient response of coupled TEM-mode networks is presented in this section. Starting from the well known matrix approach as it applies to multiconductor lines, we derive the impulse response of several commonly used coupled structures. In general, it is found that the impulse response is a periodic train of impulses. When certain constraints on the coupler are removed (namely the need for a perfect match at all frequencies at the input), it is found that the transient response can be made to be time limited. This result is significant in that it leads to a new type of directional coupler which has near optimum properties in the time domain.

4.2 CONVENTIONAL COUPLED TEM-MODE NETWORKS

The mathematical tools needed to analyze any TEM-mode device are available in the literature.[25] We shall illustrate the use of these tools in the analysis of a pair of coupled lines terminated at both ends by uncoupled transmission lines (Fig. 4-1). This particular configuration has been analyzed in the past from the frequency domain point of view and has led to coupled-line directional couplers.[26,27,28] It is interesting to note, however, that the original paper[26] on the transmission-line directional coupler found the frequency response from the time-domain impulse response, but since that paper no analysis of the transient behavior has been made.

Consider the coupled transmission lines in region 2 (Fig. 4-1) having the admittance matrix:

$$[Y]_2 = [Y_0] = \begin{bmatrix} Y_{11} & Y_{12} \\ Y_{12} & Y_{22} \end{bmatrix} = \frac{1}{\sqrt{\mu s}} \begin{bmatrix} C_{11} & -C_m \\ -C_m & C_{22} \end{bmatrix} \qquad (4.1)$$

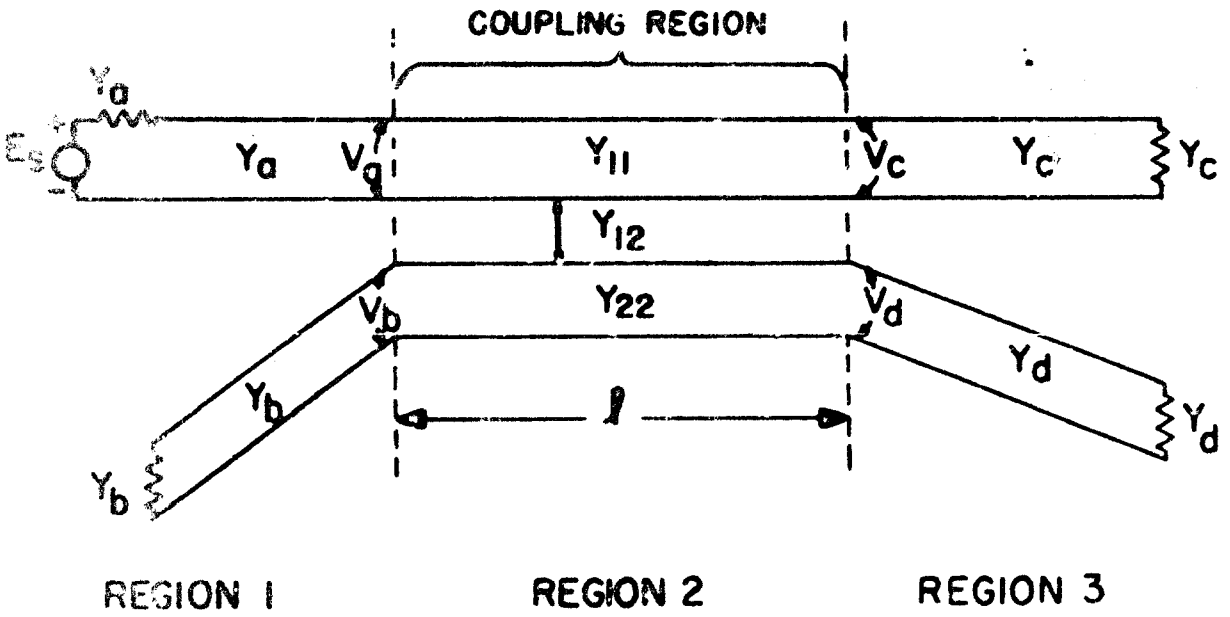

FIG. 4-1 A parallel-line coupler.

where the mutual capacitance C_m is

$$C_m = k\sqrt{C_{11}\,C_{22}}$$

$$0 < k < 1$$

Let the uncoupled transmission lines in regions 1 and 3 be terminated in their characteristic admittances. The admittance matrices of regions 1 and 3 are then

$$[Y]_1 = \begin{bmatrix} Y_a & 0 \\ 0 & Y_b \end{bmatrix} \qquad \text{(region 1)} \qquad (4.2)$$

$$[Y]_3 = \begin{bmatrix} Y_c & 0 \\ 0 & Y_d \end{bmatrix} \qquad \text{(region 3)} \qquad (4.3)$$

From these admittance matrices we can find the reflection matrix of a wave incident on the junction between any two regions.[25] These are

$$[\Gamma]_{21} = -[\Gamma]_{12} = \left[[Y]_1 + [Y]_2\right]^{-1}\left[[Y]_1 - [Y]_2\right] \qquad (4.4)$$

$$[\Gamma]_{23} = -[\Gamma]_{32} = \left[[Y]_3 + [Y]_2\right]^{-1}\left[[Y]_3 - [Y]_2\right] \qquad (4.5)$$

where $[\Gamma]_{ij}$ = reflection matrix for a wave incident from region j onto region i

Upon substitution of Eqs. 4.1, 4.2 and 4.3 into Eqs. 4.4 and 4.5, one obtains the expressions for the reflection matrix in terms of the line parameters; i.e.

$$[\Gamma]_{12} = -[\Gamma]_{21} = \begin{bmatrix} \Gamma_{aa} & \Gamma_{ab} \\ \Gamma_{ba} & \Gamma_{bb} \end{bmatrix} \qquad (4.6)$$

$$[\Gamma]_{32} = -[\Gamma]_{23} = \begin{bmatrix} \Gamma_{cc} & \Gamma_{cd} \\ \Gamma_{dc} & \Gamma_{dd} \end{bmatrix} \tag{4.7}$$

where

$$\Gamma_{ca} = \frac{(Y_{11} - Y_a)(Y_{22} + Y_b) - Y_{12}^2}{(Y_{11} + Y_a)(Y_{22} + Y_b) - Y_{12}^2}$$

$$\Gamma_{bb} = \frac{(Y_{11} + Y_a)(Y_{22} - Y_b) - Y_{12}^2}{(Y_{11} + Y_a)(Y_{22} + Y_b) - Y_{12}^2}$$

$$\Gamma_{ab} = \frac{2 Y_b Y_{12}}{(Y_{11} + Y_a)(Y_{22} + Y_b) - Y_{12}^2}$$

$$\Gamma_{ba} = \frac{2 Y_a Y_{12}}{(Y_{11} + Y_a)(Y_{22} + Y_b) - Y_{12}^2}$$

$$\Gamma_{cc} = \frac{(Y_{11} - Y_c)(Y_{22} + Y_d) - Y_{12}^2}{(Y_{11} + Y_c)(Y_{22} + Y_d) - Y_{12}^2}$$

$$\Gamma_{dd} = \frac{(Y_{11} + Y_c)(Y_{22} - Y_d) - Y_{12}^2}{(Y_{11} + Y_c)(Y_{22} + Y_d) - Y_{12}^2}$$

$$\Gamma_{cd} = \frac{2 Y_d Y_{12}}{(Y_{11} + Y_c)(Y_{22} + Y_d) - Y_{12}^2}$$

$$\Gamma_{dc} = \frac{2 Y_c Y_{12}}{(Y_{11} + Y_c)(Y_{22} + Y_d) - Y_{12}^2}$$

The coupled line configuration in Fig. 4-1 is then equivalent to the simple cascade of transmission lines in Fig. 4-2, where

$[V]_1$ = complex voltage matrix of wave near junction of region 1 and region 2 traveling away from junction in region 1

$[V]_3$ = complex voltage matrix of wave near junction of region 2 and region 3 traveling away from junction in region 3

$[V]^+_{ij}$ = complex voltage matrix of wave near junction of region i and region j traveling to the right in region 2

$[V]^-_{ij}$ = complex voltage matrix of wave near junction of region i and region j traveling to the left in region 2

$[V]_S$ = complex voltage matrix of source wave near junction of region 1 and region 2 traveling toward the junction in region 1

The transient solution of the system in Fig. 4-2 can be solved in the same way as the corresponding case for simple transmission lines, where all of the operations performed must be matrix operations.

One way to solve the problem is to use signal flow graphs. The signal flow graph for the system in Fig. 4-2 is easily constructed and is shown in Fig. 4-3. Since the gains on the paths of the graph are matrices, it is not possible to use Mason's formula for the transmission between source and sink nodes directly. Instead, one must transform the graph by absorbing nodes and eliminating loops.[29,30,31] This leads to the following source-to-sink transmissions:

$$[V]^-_1 = \left\{[\Gamma]_{12} + \left[[1] + [\Gamma]_{12}\right][\Gamma]_{23}\left[[1] - [\Gamma]_{12}[\Gamma]_{32}e^{-2j\beta\ell}\right]^{-1} e^{-j2\beta\ell}\right\}[V]_S \tag{4.8}$$

$$[V]^+_3 = \left[[1] + [\Gamma]_{23}\right][\Gamma]_{32}\left[[1] - [\Gamma]_{12}[\Gamma]_{32}e^{-j2\beta\ell}\right]^{-1}\left[[1] + [\Gamma]_{21}\right][V]_S \tag{4.9}$$

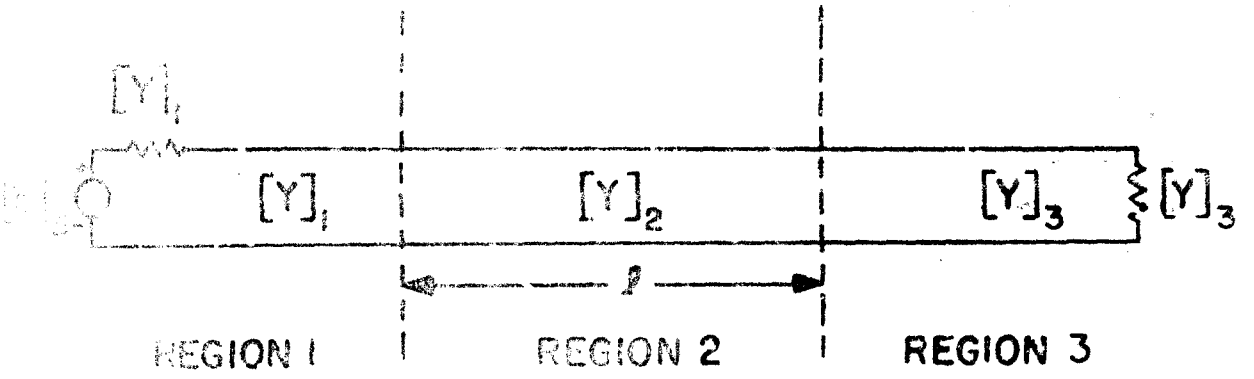

FIG. 4-2 The equivalent transmission line in matrix form.

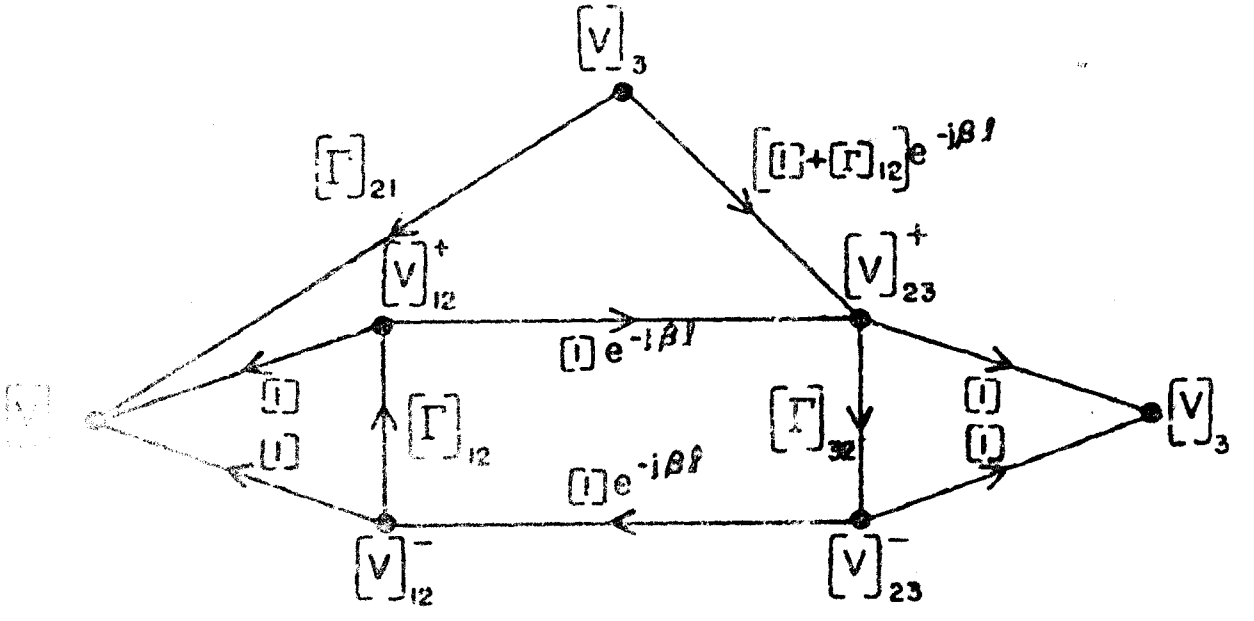

FIG. 4-3 Matrix flow graph.

$[1]$ = the identity matrix

First of all, note that Eqs. 4.8 and 4.9 are perfectly general and apply to any number of coupled lines. Secondly, since the evaluation of Eqs. 4.8 and 4.9 would be somewhat tedious, it would be judicious to choose to evaluate the transmissions by converting the matrix graph into an equivalent graph involving only scalar terms. When one considers the meaning of each part of the matrix graph, this can be done by inspection, yielding the graph in Fig. 4-4, where

$$[V]_S = \begin{bmatrix} V_S \\ 0 \end{bmatrix} \qquad [V]_3^+ = \begin{bmatrix} V_c \\ V_d \end{bmatrix}$$

$$[V]_1^- = \begin{bmatrix} V_a \\ V_b \end{bmatrix} \qquad [V]_{23}^{\pm} = \begin{bmatrix} V_c^{\pm} \\ V_d^{\pm} \end{bmatrix}$$

$$[V]_{12}^{\pm} = \begin{bmatrix} V_a^{\pm} \\ V_b^{\pm} \end{bmatrix}$$

We now are in a position to apply the Mason flow graph formula directly to Fig. 4-4. This results in

$$\frac{V_a}{V_S} = \frac{1}{\Delta}\left\{-\Gamma_{aa} + \left[\Gamma_{cc} + \Gamma_{ab}\Gamma_{dc} - \Gamma_{ba}\Gamma_{cd} - \Gamma_{dd}(\Gamma_{ab}\Gamma_{ba} - \Gamma_{aa}\Gamma_{bb})\right] e^{-j2\beta\ell}\right.$$

$$\left. + \Gamma_{bb}(\Gamma_{cd}\Gamma_{dc} - \Gamma_{cc}\Gamma_{dd})\, e^{-j4\beta\ell}\right\} \qquad (4.10)$$

$$\frac{V_b}{V_S} = \frac{1}{\Delta}\left\{-\Gamma_{ba} + \left[\Gamma_{ba}(\Gamma_{ab}\Gamma_{dc} + \Gamma_{cc} - \Gamma_{dd}) + \Gamma_{dc}(1 - \Gamma_{aa})(1 + \Gamma_{bb})\right] e^{-j2\beta\ell}\right.$$

$$\left. + \Gamma_{ba}(\Gamma_{cc}\Gamma_{dd} - \Gamma_{cd}\Gamma_{dc})\, e^{-j4\beta\ell}\right\} \qquad (4.11)$$

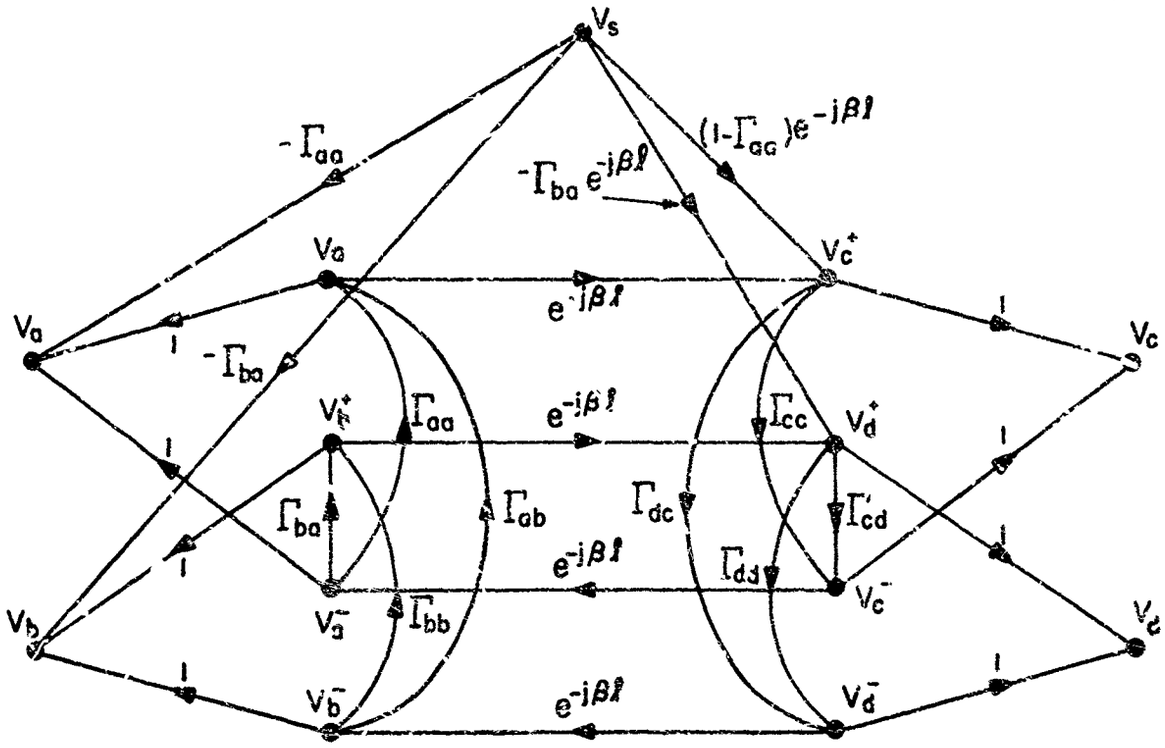

FIG. 4-4 Expanded scaler flow graph.

THIS
PAGE
IS
MISSING
IN
ORIGINAL
DOCUMENT

$$\Gamma_{bb}(\Gamma_{cc}\Gamma_{dc} - \Gamma_{cc}\Gamma_{dd}) = 0 \tag{4.17}$$

Equation 4.17 has two possible solutions; we will use only the solution

$$\Gamma_{bb} = 0 \tag{4.18}$$

since the alternate solution corresponds to an active termination which will not be treated here. Substituting the expressions for Γ_{aa} and Γ_{bb} into Eqs. 4.15 and 4.18 yields

$$(Y_{11} - Y_a)(Y_{22} + Y_b) - Y_{12}^2 = 0 \tag{4.19}$$

$$(Y_{11} + Y_a)(Y_{22} - Y_b) - Y_{12}^2 = 0 \tag{4.20}$$

Equations 4.19 and 4.20 lead to the following values for the input line admittances

$$Y_a = Y_{11}\sqrt{1 - k^2} \tag{4.21}$$

$$Y_b = Y_{22}\sqrt{1 - k^2} \tag{4.22}$$

When the expressions for the reflection coefficients are substituted into the remaining condition (Eq. 4.16) together with Eqs. 4.21 and 4.22, the result is

$$\frac{2Y_a(Y_a - Y_c)(Y_b + Y_d)(Y_b + Y_{22})}{Y_aY_b + Y_cY_{22} + Y_dY_{22} + Y_cY_d} = 0 \tag{4.23}$$

Equation 4.23 has two possible solutions:

$$Y_c = Y_a \tag{4.24}$$

$$Y_b = -Y_d \tag{4.25}$$

We shall not study the solution represented by Eq. 4.25 here, since again it leads to an active rather than a passive device.

From this analysis we have thus found that the most general conditions under which the coupler lines (Fig. 4-1) are perfectly matched are

$$Y_c = Y_a = Y_{11}\sqrt{1-k^2} \quad \text{and} \quad Y_b = Y_{22}\sqrt{1-k^2}$$

Significantly, we note that these conditions are completely independent of the characteristic admittance Y_d of line d. This should suggest that the voltage excited at port d is zero, since otherwise the admittance at port d would be expected to have an effect on the matching condition. When, in fact, the expressions for the reflection coefficients are substituted together with Eqs 4.21, 4.22 and 4.23 in Eq. 4.13, we find that

$$\frac{V_d}{V_s} = 0 \tag{4.26}$$

Thus, not only is this device perfectly matched at all frequencies, it also has perfect directivity at all frequencies. We can also conclude that all voltages and currents on the lines must be independent of the admittance of port d , since no voltage is excited across line d and the admittance then can have no effect on the rest of the lines. Therefore, let us assume, without loss in generality, that $Y_b = Y_a$ in order to simplify the algebra, since that has no effect on the resulting expressions in terms of admittances. Then

$$\Gamma_{aa} = \Gamma_{bb} = \Gamma_{cc} = \Gamma_{dd} = 0 \tag{4.27}$$

$$\Gamma_{ab} = \Gamma_{cd} \tag{4.28}$$

$$\Gamma_{ba} = \Gamma_{dc} \tag{4.29}$$

The remaining voltage expressions become

$$\frac{V_b}{V_s} = \frac{-\Gamma_{bg}(1 - e^{-j2\beta\ell})}{1 - \Gamma_{ab}\Gamma_{ba}e^{-j2\beta\ell}} \tag{4.30}$$

$$\frac{V_c}{V_s} = \frac{(1 - \Gamma_{ab}\Gamma_{ba})e^{-j\beta\ell}}{1 - \Gamma_{ab}\Gamma_{ba}e^{-j2\beta\ell}} \tag{4.31}$$

Substituting for the reflection coefficients, we get expressions which are independent of Y_d, i.e.

$$\frac{V_b}{V_s} = jk\sqrt{\frac{Y_{11}}{Y_{22}}}\,\frac{\sin\beta\ell}{\sqrt{(1-k^2)}\cos\beta\ell + j\sin\beta\ell} \tag{4.32}$$

$$\frac{V_c}{V_s} = \frac{\sqrt{1-k^2}}{\sqrt{(1-k^2)}\cos\beta\ell + j\sin\beta\ell} \tag{4.33}$$

Remembering that $\beta = \frac{\omega}{c}$, we can rewrite Eqs. 4.32 and 4.33 as

$$\frac{V_b}{V_s} = jk\sqrt{\frac{Y_{11}}{Y_{22}}}\,\frac{\sin\omega\tau}{\sqrt{(1-k^2)}\cos\omega\tau + j\sin\omega\tau} \tag{4.34}$$

$$\frac{V_c}{V_s} = \frac{\sqrt{1-k^2}}{\sqrt{(1-k^2)}\cos\omega\tau + j\sin\omega\tau} \tag{4.35}$$

where $\tau = \frac{\ell}{c}$, the one-way time delay in the coupling region.

We can recognize the above equations as the system functions of the networks evaluated along the $j\omega$ axis. The magnitude and phase of the above functions are plotted in Fig. 4-5 for three values of k. These functions reduce to those found by Oliver[26] when the coupling is symmetric, i.e., $Y_{11} = Y_{22}$.

In order to find the impulse response of the network, we merely have to take the Fourier transform of Eqs. 4.34 and 4.35. This may be done

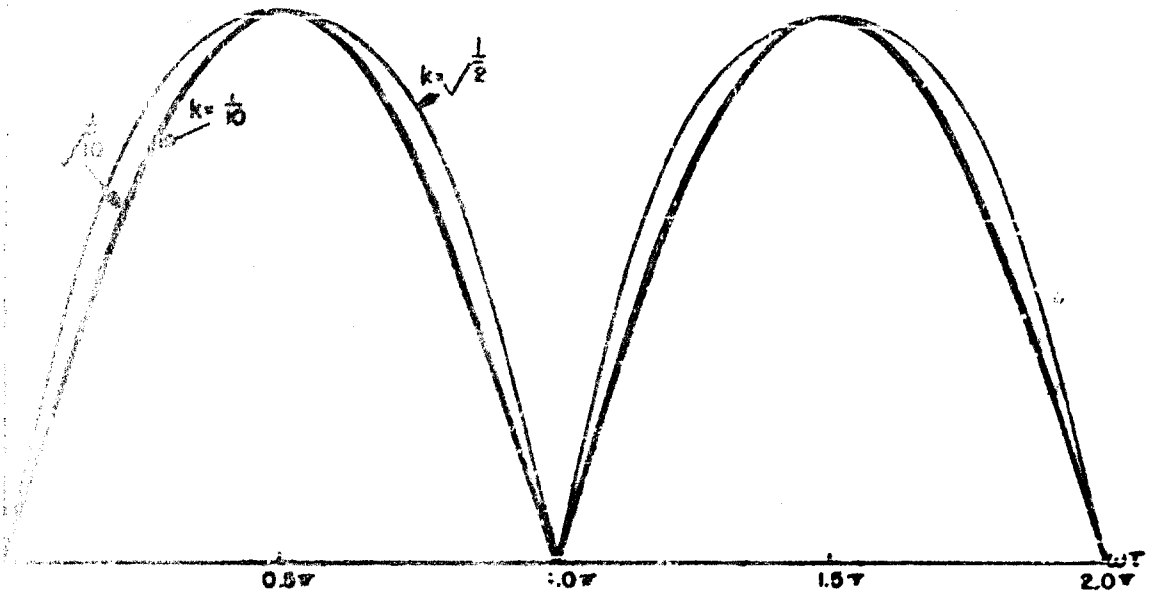

a. Amplitude spectrum.

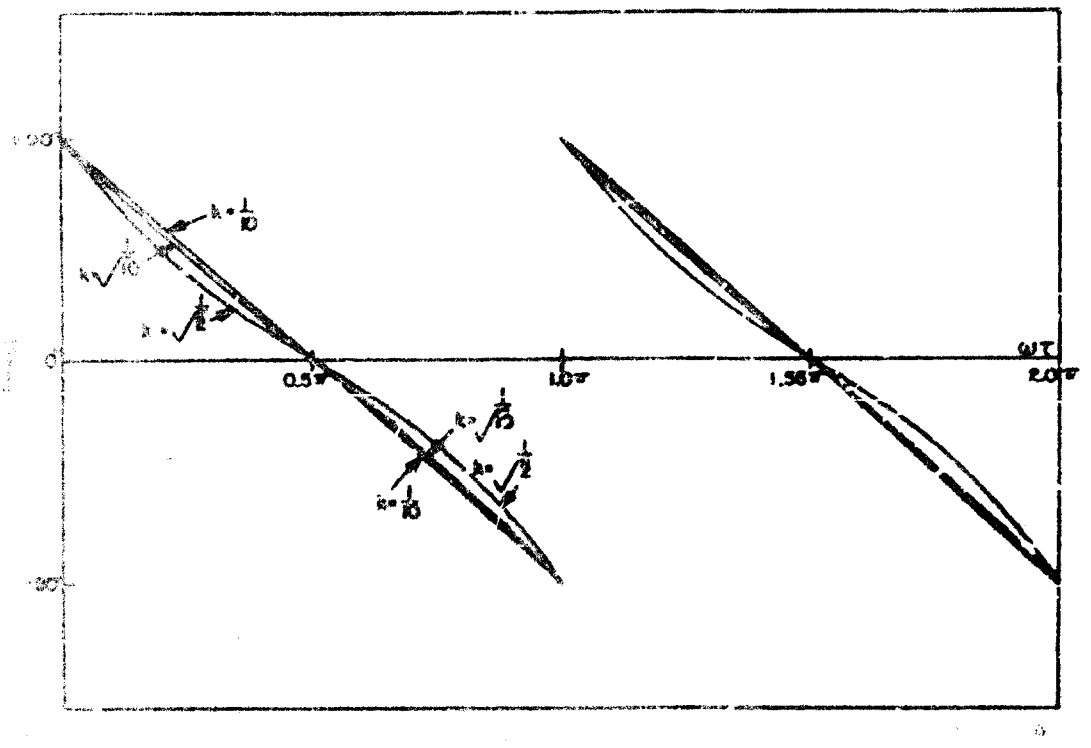

b. Phase function.

FIG. 4-3 Amplitude spectrum and phase function of a parallel-line sampler.

more easily if we first rewrite the equations in the following more convenient form:

$$\frac{V_b}{V_s} = \sqrt{\frac{Y_{11}}{Y_{22}}}\ \frac{\rho(1 - e^{-j2\omega\tau})}{1 - \rho^2 e^{-j2\omega\tau}} \tag{4.36}$$

$$\frac{V_c}{V_s} = \frac{(1 - \rho^2)e^{-j\omega\tau}}{1 - \rho^2 e^{-j2\omega\tau}} \tag{4.37}$$

where

$$\rho = \frac{k}{1 + \sqrt{1 - k^2}}$$

Expanding the denominator as an infinite series, one obtains

$$\frac{V_b}{V_s} = \sqrt{\frac{Y_{11}}{Y_{22}}}\ \rho\left[1 - (1 - \rho^2) \sum_{n=1}^{\infty} \rho^{2n-2}\, e^{-j2n\omega\tau}\right] \tag{4.38}$$

$$\frac{V_c}{V_s} = (1 - \rho^2) \sum_{n=0}^{\infty} \rho^{2n}\, e^{-j(2n+1)\omega\tau} \tag{4.39}$$

The impulse response is then

$$h_{V_b}(t) = \sqrt{\frac{Y_{11}}{Y_{22}}}\ \rho\left[\delta(t) - (1 - \rho^2) \sum_{n=1}^{\infty} \rho^{2n-2}\delta(t - 2n\tau)\right] \tag{4.40}$$

$$h_{V_c}(t) = (1 - \rho^2) \sum_{n=0}^{\infty} \rho^{2n}\delta(t - [2n+1]\tau) \tag{4.41}$$

where $\delta(t)$ is the unit impulse.

From the impulse response we can easily find the step-modulated response to an input of the form

$$V_a(t) = (\sin \omega_0 t)\, u(t) \tag{4.42}$$

where $\omega_0 = \pi/2\tau$ and $u(t)$ denotes a unit step. That is

$$V_b(t) = \sqrt{\frac{Y_{11}}{Y_{22}}}\, \rho \left[u(t) - (1-\rho^2) \sum_{n=1}^{\infty} \rho^{2n-2}(-1)^n u(t-2n\tau) \right] \sin \omega_0 t \tag{4.43}$$

$$V_c(t) = (1-\rho^2) \sum_{n=0}^{\infty} \rho^{2n}(-1)^{n+1}\, u(t-[2n+1]\tau) \cos \omega_0 t \tag{4.44}$$

Equations 4.43 and 4.44 are the response to a wideband signal whose frequencies are centered around the center frequency of the network (Fig. 4-5). Thus, such factors as the rise time and the settling time of the step-modulated response should give us a good grasp of the wideband transient behavior of the network.

Let us consider the transient response for the three values of k used in Fig. 4-5. These three values of k, namely $1/\sqrt{2}$, $1/\sqrt{10}$, and 1/10, correspond to a 3 dB, a 10 dB, and a 20 dB coupler, respectively. The transient responses for the symmetric coupler are as follows:

For $k = \frac{1}{\sqrt{2}}$ (3 dB coupler)

$$h_{V_0}(t) = .414\,\delta(t) - .343\,\delta(t-2\tau) - .0589\,\delta(t-4\tau) - .0101\,\delta(t-6\tau) - \cdots\cdots \tag{4.45}$$

$$h_{V_e}(t) = .828\,\delta(t-\tau) + .142\,\delta(t-3\tau) + .0244\,\delta(t-5\tau) + .00418\,\delta(t-7\tau) + \cdots\cdots \tag{4.46}$$

$$V_b(t) = \left[.414\,u(t) + .343\,u(t-2\tau) - .0589\,u(t-4\tau) + .0101\,u(t-6\tau) - \cdots\cdots \right] \sin \omega_0 t \tag{4.47}$$

$$v_c(t) = -\left[.828\,u(t-\tau) - .142\,u(t-3\tau) + .0244\,u(t-5\tau) - .00418\,u(t-7\tau) + \ldots\ldots \right] \cos \omega_0 t \qquad (4.48)$$

For $k = \frac{1}{\sqrt{10}}$ (10 dB coupler)

$$v_0(t) = .162\,\delta(t) - .158\,\delta(t-2\tau) - .00416\,\delta(t-4\tau) - 1.09 \times 10^{-4}\,\delta(t-6\tau) - \ldots\ldots \qquad (4.49)$$

$$v_c(t) = .974\,\delta(t-\tau) + .0256\,\delta(t-3\tau) + 6.77 \times 10^{-4}\,\delta(t-5\tau) + 1.78 \times 10^{-5}\,\delta(t-7\tau) + \ldots. \qquad (4.50)$$

$$v_0(t) = \left[.162\,u(t) + .158\,u(t-2\tau) - .00416\,u(t-4\tau) + 1.09 \times 10^{-4}\,u(t-6\tau) - \ldots\ldots \right] \sin \omega_0 t \qquad (4.51)$$

$$v_c(t) = -\left[.974\,u(t-\tau) - .0256\,u(t-3\tau) + 6.77 \times 10^{-4}\,u(t-5\tau) - 1.78 \times 10^{-5}\,u(t-7\tau) + \ldots\ldots \right] \cos \omega_0 t \qquad (4.52)$$

For $k = \frac{1}{10}$ (20 dB coupler)

$$v_0(t) = .050\,\delta(t) - .050\,\delta(t-2\tau) - 1.26 \times 10^{-4}\,\delta(t-4\tau) - 3.5 \times 10^{-7}\,\delta(t-6\tau) - \ldots\ldots \qquad (4.53)$$

$$v_c(t) = .997\,\delta(t-\tau) + .00251\,\delta(t-3\tau) + 6.30 \times 10^{-6}\,\delta(t-5\tau) + 1.58 \times 10^{-8}\,\delta(t-7\tau) + \ldots. \qquad (4.54)$$

$$v_0(t) = \left[.050\,u(t) + .050\,u(t-2\tau) - 1.26 \times 10^{-4}\,u(t-4\tau) + 3.15 \times 10^{-7}\,u(t-6\tau) - \ldots\ldots \right] \sin \omega_c t \qquad (4.55)$$

$$V_c(t) = -\left[.977\ u(t-\tau) - .00251\ u(t-3\tau) + 6.30\times10^{-6}\ u(t-5\tau)\right.$$

$$\left. - 1.58\times10^{-8}\ u(t-7\tau) + ...\right] \cos\omega_0 t \qquad (4.56)$$

The impulse responses and the envelopes of the step-modulated responses are plotted in Figs. 4-6 and 4-7, respectively. If one defines the settling time as the time it takes the step-modulated response to reach and remain within 5% of the steady-state value, then by comparing Fig. 4-5a and Fig. 4-7, we note that as the apparent steady-state bandwidth increases, the settling time increases. Thus, in a real sense the transient response of the network actually is made worse by increasing the network bandwidth. We also note that the phase function becomes more nonlinear as the bandwidth is increased, which indicates that the transient response is quite sensitive to phase variations. Thus, it appears that describing the wideband properties of a device by its bandwidth is not sufficient: one must also include the effects of phase distortion. (This matter is more fully discussed in Section III of this report.) In this coupler the transient theoretically lasts indefinitely, although practically speaking only a few terms of the infinite series in Eqs. 4.38-4.44 are important.

4.4 TIME-LIMITED TRANSIENT RESPONSE

We wish to consider the possibility of eliminating the infinite series in Eqs. 4.38 through 4.44 as a means of improving the transient response. In this particular coupler, the infinite series will vanish only if the coefficient of $e^{-j2\beta\ell}$ in the denominator of Eqs. 4.36 and 4.37 vanishes. For the constraints already imposed this will only occur for zero coupling between the lines. Thus, to examine the case of time-limited responses one has to remove the above constraints and start again with Eqs. 4.10 through 4.13.

We recall that we developed the directional coupler by assuming that the input was matched at all frequencies, and we found, as an additional bonus, that the network had infinite directivity at all frequencies as well. We know now that the condition of a perfect match at the input at all frequencies is too strong a restriction and results in a transient which lasts

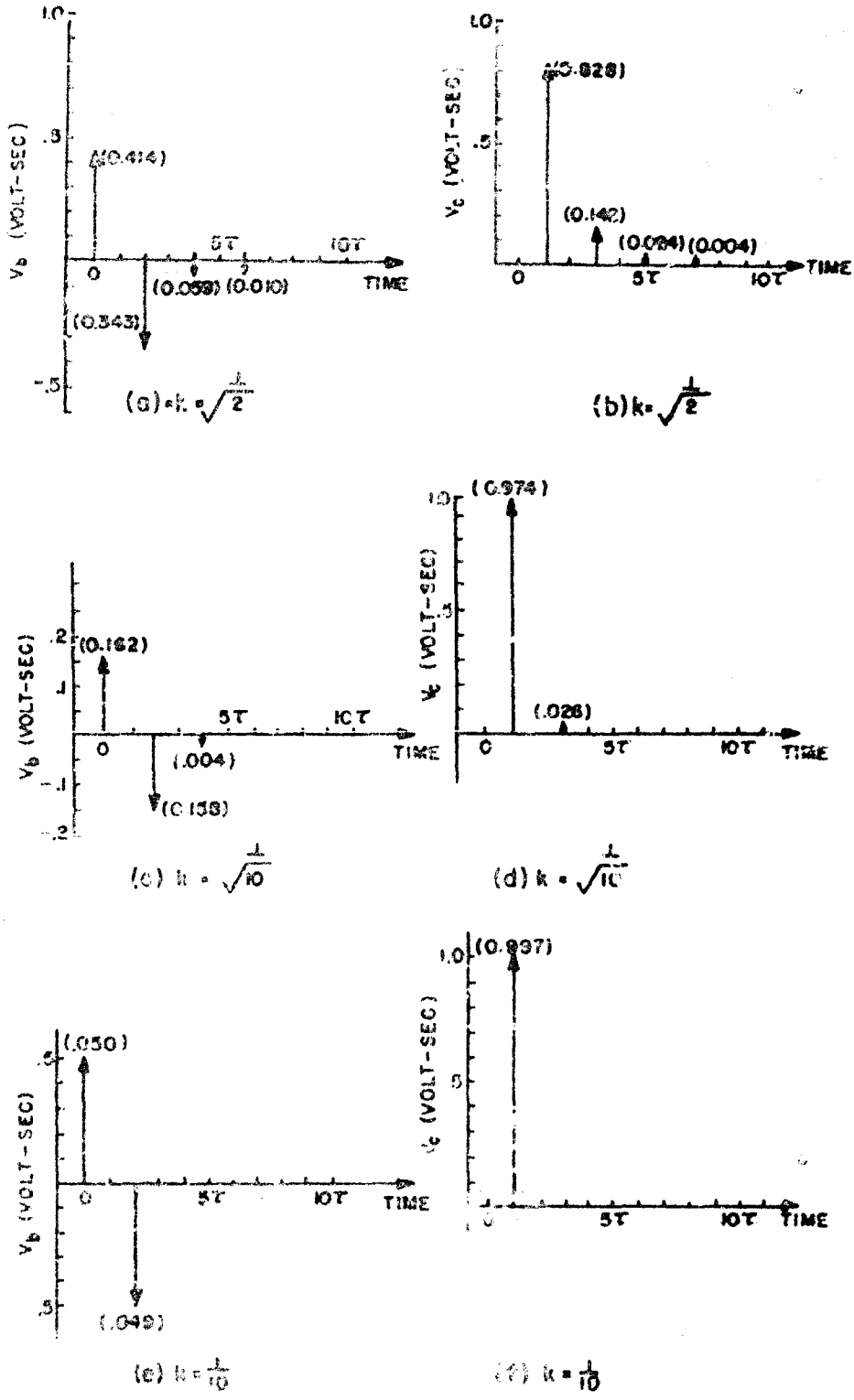

FIG. 4-6 The impulse response of a parallel-line coupler.

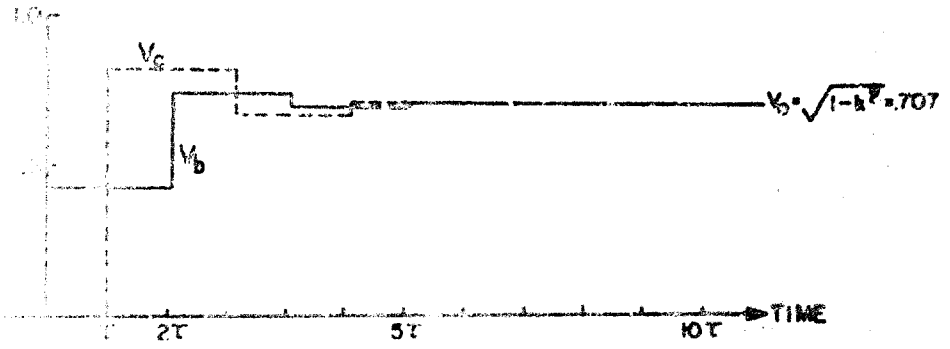

(a) $k = \frac{1}{\sqrt{2}}$

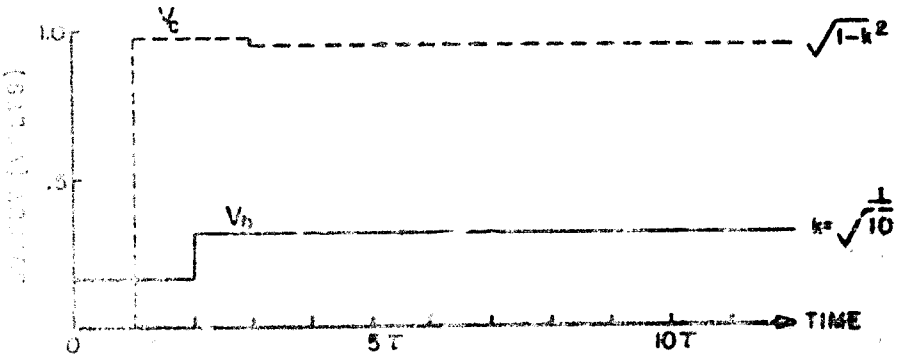

(b) $k = \sqrt{\frac{1}{10}}$

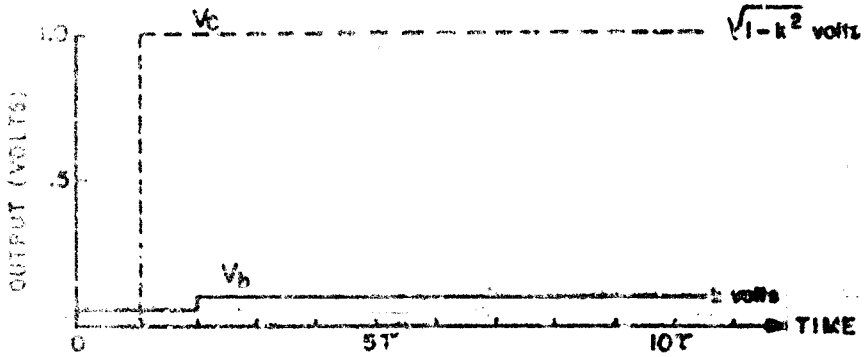

(c) $k = \frac{1}{10}$

FIG. 4-7 The peak magnitude of the step-modulated response of a parallel-line coupler.

definitely. Removing this restriction, requiring only that the coupler have infinite directivity, gives us an additional degree of freedom which allows us to eliminate the indefinitely continuing transient.

We require that

$$\frac{V_d}{V_s} = 0 \tag{4.57}$$

Therefore the coefficients of $e^{-jn\beta\ell}$ in the numerator of Eq. 4.13 must vanish identically; i.e.

$$(1 - \Gamma_{aa})\Gamma_{dc} - \Gamma_{ba}(1 + \Gamma_{dd}) = 0 \tag{4.58}$$

$$\Gamma_{ba}(\Gamma_{cc} + \Gamma_{ab}\Gamma_{dc} + \Gamma_{cc}\Gamma_{dd} - \Gamma_{cd}\Gamma_{dc}) + (1 - \Gamma_{aa})\Gamma_{dc}\Gamma_{bb} = 0 \tag{4.59}$$

Ordinarily the solution of the two equations above would be very difficult. Fortunately, we can make use of symmetry and reciprocity to simplify the above equations. First, note that all excitations at port a produce no voltage at port d by Eq. 4.57. Therefore, no change in the admittance at port d can have an effect on the voltage elsewhere in the network when excited from port a. This allows us to conclude that the condition for infinite directivity is independent of the admittance Y_d at port d. Now if we consider an excitation from port d, we will find that the voltage at port a must be zero by the reciprocity theorem. By the same argument we used above, we can conclude that the condition for infinite directivity is independent of Y_a. Therefore, the condition for infinite directivity depends only on Y_b and Y_c.

Since the condition for infinite directivity does not depend on Y_a and Y_d, for mathematical convenience we can choose

$$Y_a = Y_c \tag{4.60}$$

$$Y_d = Y_b \tag{4.61}$$

Then

$$\Gamma_{aa} = \Gamma_{cc} \tag{4.62}$$

$$\Gamma_{bb} = \Gamma_{dd} \tag{4.63}$$

$$\Gamma_{ab} = \Gamma_{cd} \tag{4.64}$$

$$\Gamma_{ba} = \Gamma_{dc} \tag{4.65}$$

Equations 4.58 and 4.59 now simplify to

$$-\Gamma_{ba}(\Gamma_{aa} + \Gamma_{bb}) = 0 \tag{4.66}$$

$$\Gamma_{ba}(\Gamma_{aa} + \Gamma_{bb}) = 0 \tag{4.67}$$

Substituting for the reflection coefficients in Eq. 4.61 yields

$$\begin{aligned} Y_b Y_c &= Y_{11}Y_{22} - Y_{12}^2 \\ &= Y_{11}Y_{22}(1 - k^2) \end{aligned} \tag{4.68}$$

We note that this condition is satisfied for the directional coupler we have previously discussed. However, in this case Y_a and Y_d are arbitrary, thus giving us an additional degree of freedom.

Since the voltages in the network are independent of Y_a, let us choose Y_d such that

$$Y_a Y_d = Y_b Y_c = Y_{11}Y_{22}(1 - k^2) \tag{4.69}$$

This will simplify the calculation of the transfer functions without affecting the results. The resulting reflection coefficients now satisfy the relations

$$\Gamma_{aa} + \Gamma_{dd} = 0 \tag{4.70}$$

$$\Gamma_{bb} + \Gamma_{cc} = 0 \tag{4.71}$$

$$\Gamma_{ab} = \Gamma_{cd} \tag{4.72}$$

$$\Gamma_{ba} = \Gamma_{dc} \tag{4.73}$$

The transfer functions now become

$$\frac{V_a}{V_s} = \frac{-(\Gamma_{aa} + \Gamma_{bb}e^{-j2\beta\ell})}{1-(\Gamma_{ab}\Gamma_{ba} - \Gamma_{aa}\Gamma_{bb})e^{-j2\beta\ell}} \tag{4.74}$$

$$\frac{V_b}{V_s} = \frac{-\Gamma_{ba}(1-e^{-j2\beta\ell})}{1-(\Gamma_{ab}\Gamma_{ba} - \Gamma_{aa}\Gamma_{bb})e^{-j2\beta\ell}} \tag{4.75}$$

$$\frac{V_c}{V_s} = \frac{[(1-\Gamma_{aa})(1-\Gamma_{bb}) - \Gamma_{ab}\Gamma_{ba}]e^{-j\beta\ell}}{1-(\Gamma_{ab}\Gamma_{ba} - \Gamma_{aa}\Gamma_{bb})e^{-j2\beta\ell}} \tag{4.76}$$

As in the case for the previous directional coupler, we can see that in general the impulse response will contain an infinite sequence of impulses. Thus, in general, the transient will last indefinitely. We can improve the transient response by eliminating the infinite series that results from the exponential term in the denominator of Eqs. 4.74 - 4.76. This may be done by setting

$$\Gamma_{aa}\Gamma_{bb} - \Gamma_{ab}\Gamma_{ba} = 0 \tag{4.77}$$

Then the responses simplify to

$$\frac{V_a}{V_s} = -(\Gamma_{aa} + \Gamma_{bb}e^{-j2\beta\ell}) \tag{4.78}$$

$$\frac{V_b}{V_s} = -\Gamma_{ba}(1 - e^{-j2\beta\ell}) \tag{4.79}$$

$$\frac{V_c}{V_s} = (1 - \Gamma_{aa} - \Gamma_{bb})e^{-j\beta\ell} \tag{4.80}$$

The impulse responses corresponding to Eqs. 4.78 and 4.79 have at most two impulses. Thus we have obtained improved transient response. It now remains to be shown that we can, in fact, meet the condition imposed by Eq. 4.77.

When the expressions for the reflection coefficient are substituted into Eq. 4.77 we get

$$\left(1 - \frac{Y_a}{Y_{11}}\right)\left(1 - \frac{Y_b}{Y_{22}}\right) = k^2 \tag{4.81}$$

This is indeed realizable. As a matter of fact, we still have some freedom in choosing Y_a and Y_b. Let us choose

$$\frac{Y_a}{Y_{11}} = \frac{Y_b}{Y_{22}} \tag{4.82}$$

Then from Eqs. 4.69 and 4.81 we obtain

$$\frac{Y_a}{Y_{11}} = \frac{Y_b}{Y_{22}} = 1 \pm k \tag{4.83}$$

$$\frac{Y_c}{Y_{11}} = (1 \mp k) \tag{4.84}$$

Upon substitution of these conditions into the expressions for the reflection coefficients in Eqs. 4.78 through 4.80 we find

$$\frac{V_a}{V_s} = \pm \frac{k}{2}(1+e^{-j2\beta\ell}) \tag{4.85}$$

$$\frac{V_b}{V_s} = \sqrt{\frac{Y_{11}}{Y_{22}}}\ \frac{k}{2}(1-e^{-j2\beta\ell}) \tag{4.86}$$

$$\frac{V_c}{V_s} = (1 \pm k)e^{-j\beta\ell} \tag{4.87}$$

Letting $\beta\ell = \omega\tau$ as before, we find that system functions are

$$\frac{V_a}{V_s} = \pm k(\cos\omega\tau)e^{-j\omega\tau} \tag{4.88}$$

$$\frac{V_b}{V_s} = \sqrt{\frac{Y_{11}}{Y_{22}}}\ jk(\sin\omega\tau)e^{-j\omega\tau} \tag{4.89}$$

$$\frac{V_c}{V_s} = (1 \pm k)e^{-j\omega\tau} \tag{4.90}$$

The impulse response can be easily found from Eqs. 4.85 through 4.87 to be

$$h_{V_a}(t) = \pm\frac{k}{2}\Big[\delta(t) + \delta(t-2\tau)\Big] \tag{4.91}$$

$$h_{V_b}(t) = \sqrt{\frac{Y_{11}}{Y_{22}}}\frac{k}{2}\Big[\delta(t) - \delta(t-2\tau)\Big] \tag{4.92}$$

$$h_{V_c}(t) = (1 \pm k)\,\delta(t-\tau) \tag{4.93}$$

The step-modulated response to the signal given by Eq. 4.42 is

$$V_a(t) = \pm\frac{k}{2}\Big[u(t) - u(t-2\tau)\Big]\sin\omega_0 t \tag{4.94}$$

$$V_b(t) = \sqrt{\frac{Y_{11}}{Y_{22}}}\,\frac{k}{2}\left[u(t)+u(t-2\tau)\right]\sin\omega_0 t \qquad (4.95)$$

$$V_c(t) = -(1 \pm k)\,u(t-\tau)\cos\omega_0 t \qquad (4.96)$$

The transient responses are plotted in Figs. 4-8 and 4-9 for a symmetric coupler and for the + case in Eqs. 4.91 through 4.96. We see that the transient is time limited and fully completed within half of a cycle of the carrier. Thus this device always has a better settling time than the standard directional coupler discussed in the beginning of this section.

In a real sense we can argue that this new coupler has the optimum transient response at the output. The coupler response can be made no faster since it experiences pure delay with no reflections. Now consider the response at the input to the coupler; this contains two reflections. If its response were to be improved, it would contain one or no reflections. If it contains no reflections, then it would behave like the standard directional coupler, whose transient response we know is not better, discussed at the beginning of this section. The only alternative is one reflection at the input. However, this case must reflect energy in the steady state, and hence could not be matched in the steady state. Therefore, we can conclude that our new coupler is "optimum."

We have stated that this new coupler is optimum only for systems in the form of Fig. 4-1. The question arises: "Can the response be improved by cascading several sections of coupled lines?" We know that this technique is used to give a broadband equal ripple amplitude characteristic.[32,33] One can show that this technique cannot improve the transient response over the "optimum" coupler.

The amplitude and phase characteristics of the coupled arm coincide with the graph plotted in Fig. 4-5 for $k = 1/10$ within the accuracy of the graph. It is interesting to note that optimum coupler has the narrowest bandwidth and the best settling time; this fact is discussed in Section 3.

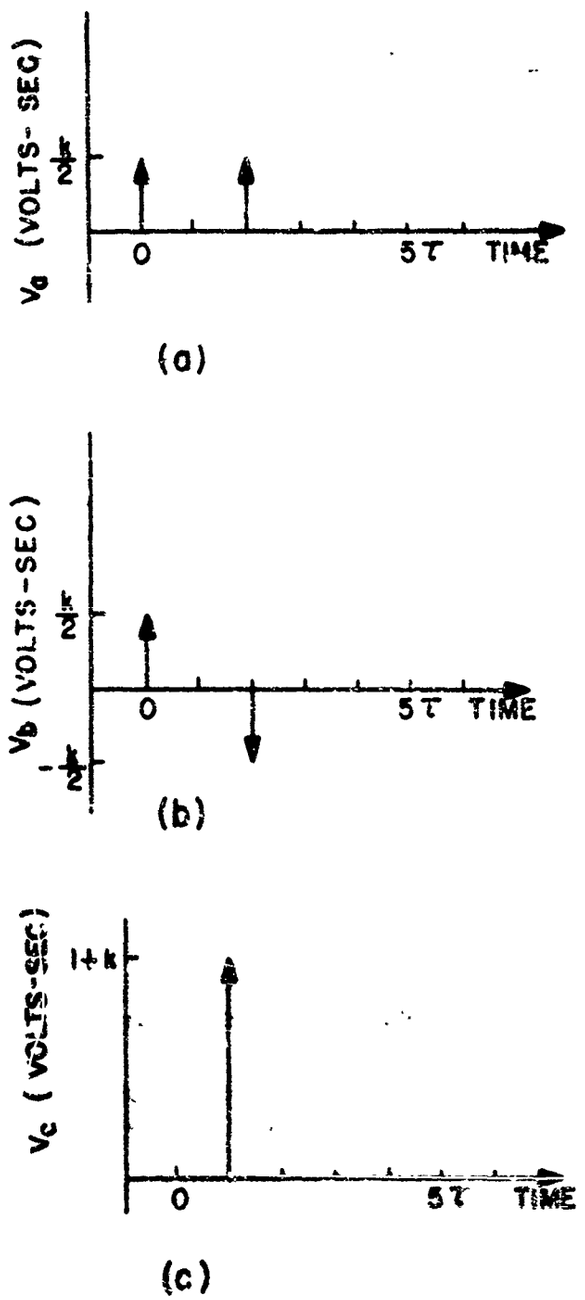

FIG. 4-8 The impulse response of an "optimum" parallel-type coupler.

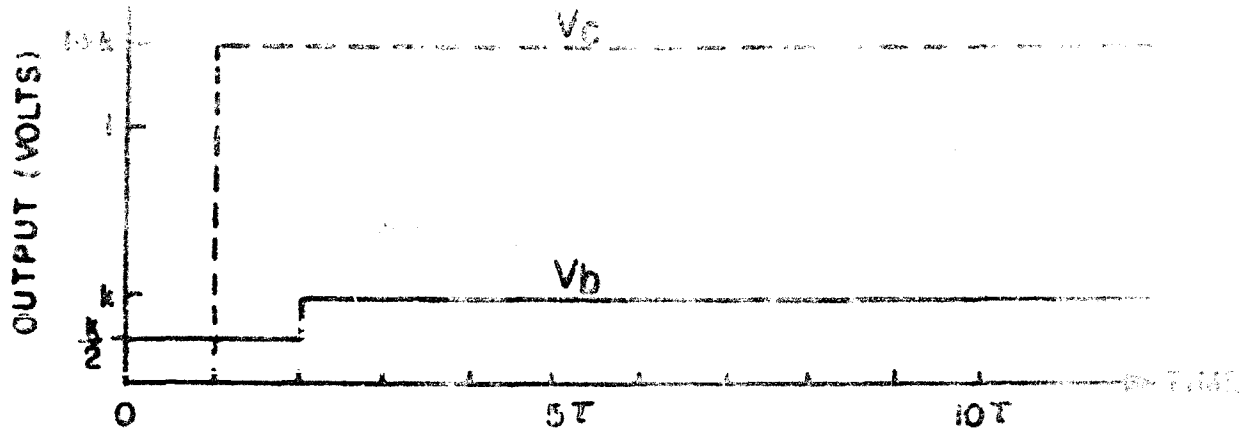

(a) Direct and Coupled arms

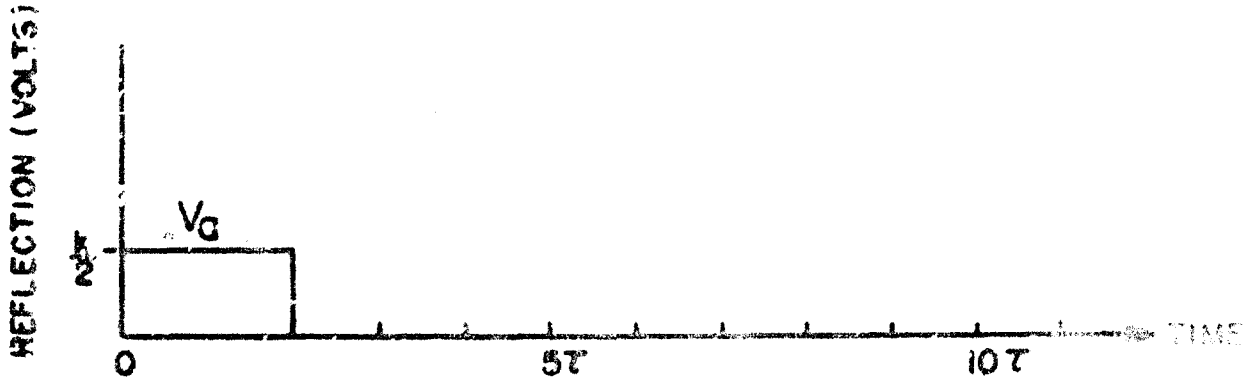

(b) Reflection at Input

FIG. 4-9 The peak magnitude of the step-modulated response of an optimum parallel-line coupler.

Practically speaking, the transient response of the standard 3 dP coupler is very good, since its settling time is on the order of 1½ cycles of the carrier, as opposed to 1/2 cycle for the optimum coupler. This indicates that for many applications the conventional quarter-wavelength coupler is sufficient. In other applications, however, where a cascade of such devices is required and time residue levels must be very low, the new time-limited coupler should be preferred. Note that the "optimum" coupler requires changes in the impedance level, since it is not possible to have the same impedance terminating all four ports.

4.5 EXPERIMENTAL RESULTS

The pulse response for three different experimental couplers is shown in Figs. 4-10 through 4-13. We can see that the agreement with experimental results and the corresponding impulse responses given in Fig. 4-6 is quite good for all three couplers. The improvement of settling time with decreasing coupling coefficients (k) is clearly evident. The step-modulated response of a 1.35 GHz carrier for the different couplers is shown in Figs. 3-12, 3-13, 4-14, and 4-15. We see, again, that the experimental data agree quite well with the corresponding theoretical results given in Fig. 4-7.

In the theory for the directional coupler, we predicted that there would be no reflection at the input and no output at point d (uncoupled output). In actual practice we find that there are outputs at these ports. These outputs are depicted in Fig. 4-16 for the 3 dB coupler. The outputs are superimposed on the corresponding input pulse with an increase in gain of 5 to 1. We note that in both figures there is a large component which is apparently proportional to the derivative of the input pulse. This differentiation of the input pulse is characteristic of radiating antennas.†

---

† This subject is discussed in related antenna papers to be presented by G. Ross and J. DeLorenzo at the 1967 NEREM Conference.

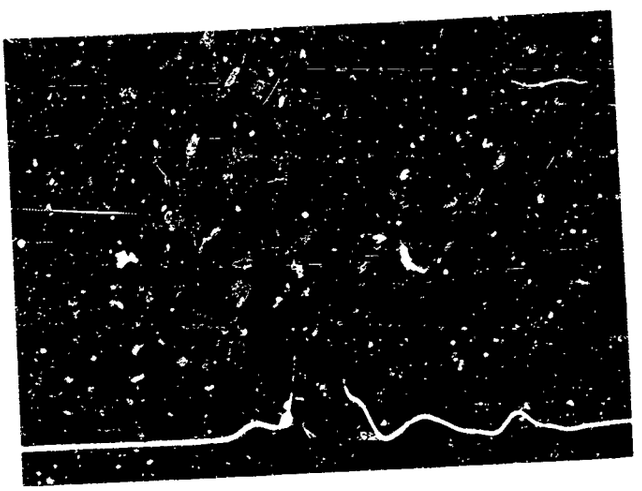

0.4 nsec./sec
0.05 p*/div

* p is proportional to volts

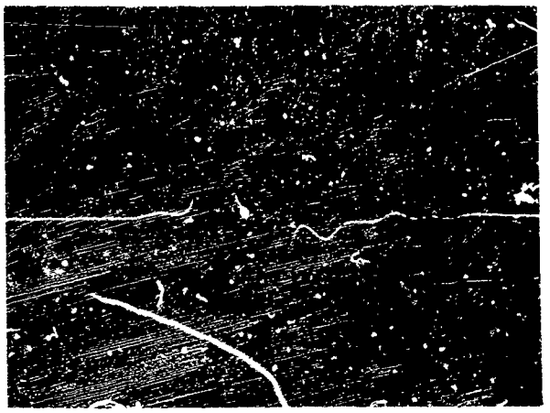

0.4 nsec / div
0.05 p* / div

(a) Port B, Coupled Output

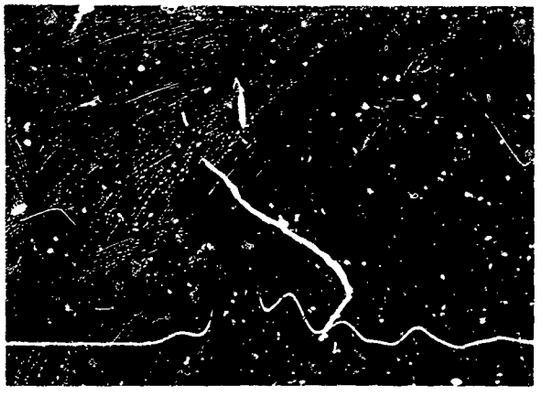

0.4 nsec/div
0.05 p* / div

(b) Port C, Direct Output

*p is proportional to volts

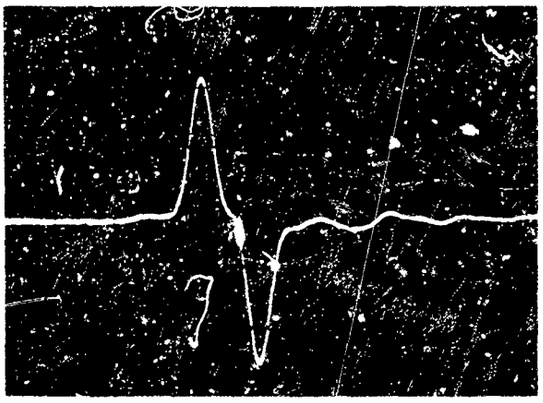

0.4 nsec / div
0.02 p* / div

(a) Port B, Coupled Output

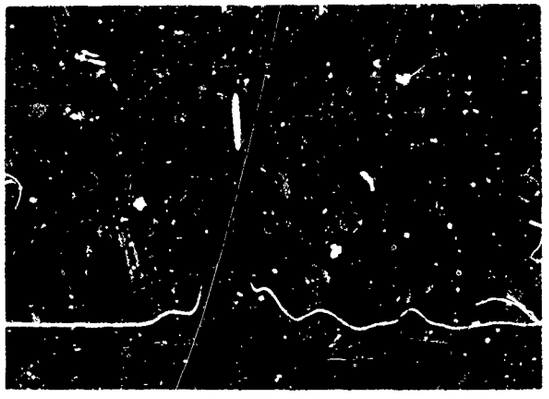

0.4 nsec / div
0.05 p* / div

(b) Port C, Direct Output

* p is proportional to volts

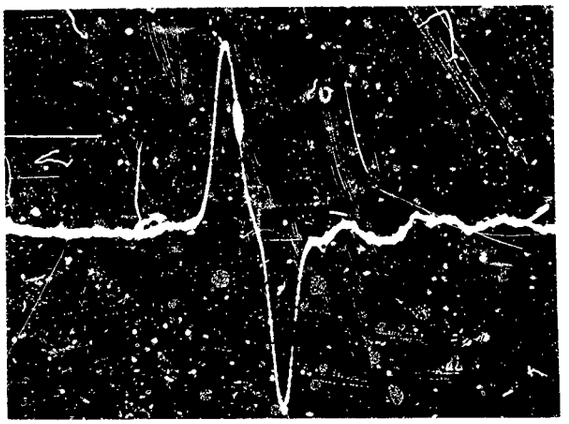

0 4 nsec / div
0 005 p*/div
(a) Port B, Coupled Output

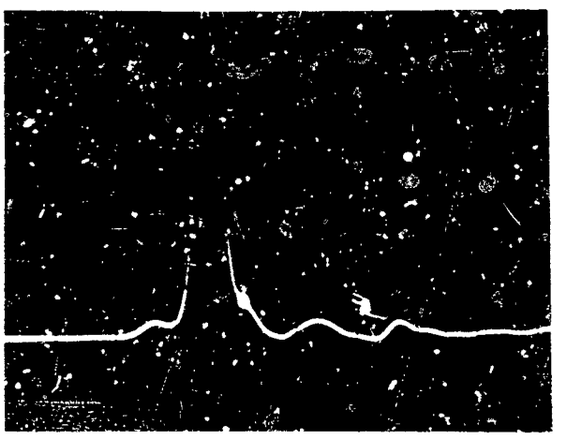

0. 4 nsec / div
0. 05 p*/div
(b) Port C, Direct Output

*p is proportional to volts

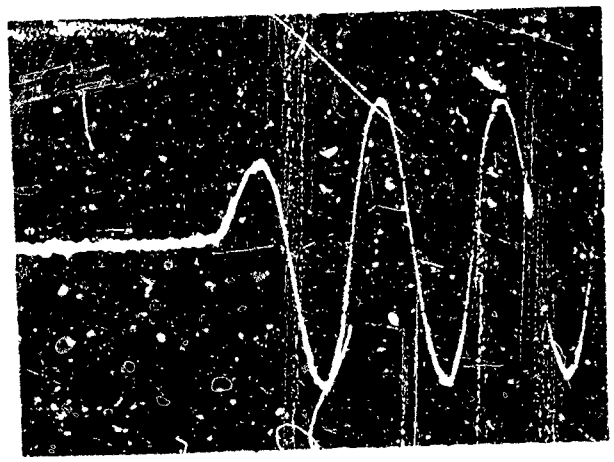

0 4 nsec / div
0 005 p*/ div
(a) Port B, Coupled Output

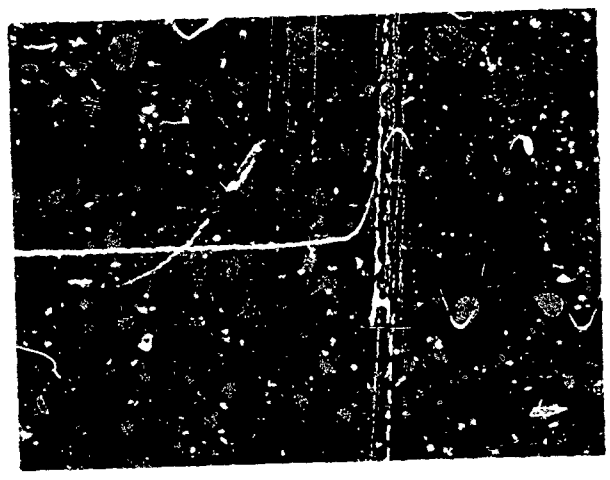

0 4 nsec / div
0 C2p*/div

(b) Port C, Direct Output

*p is proportional to volts

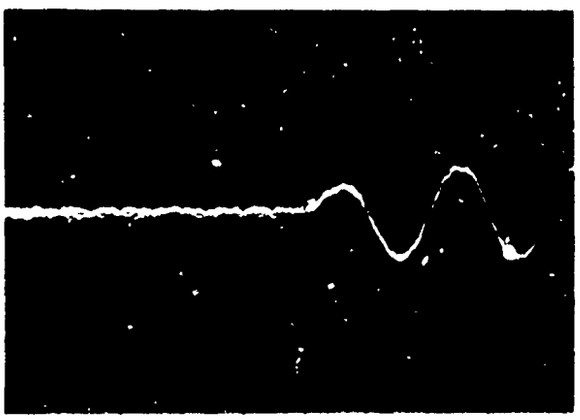

0.4 nsec / div
0.005 p* / div
(a) Port B, Coupled Output

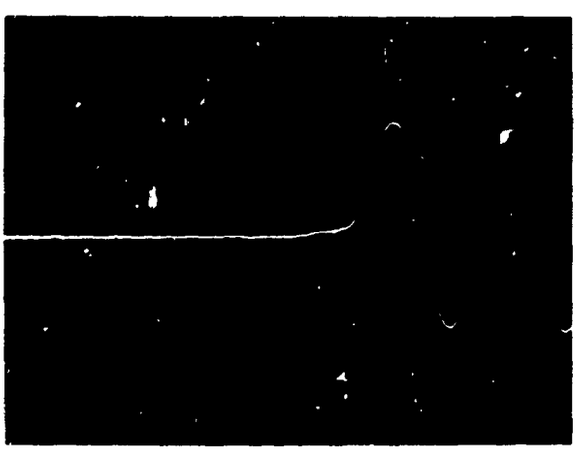

0.4 nsec / div
0.02 p* / div
(b) Port C, Direct Output

*p is proportional to volts

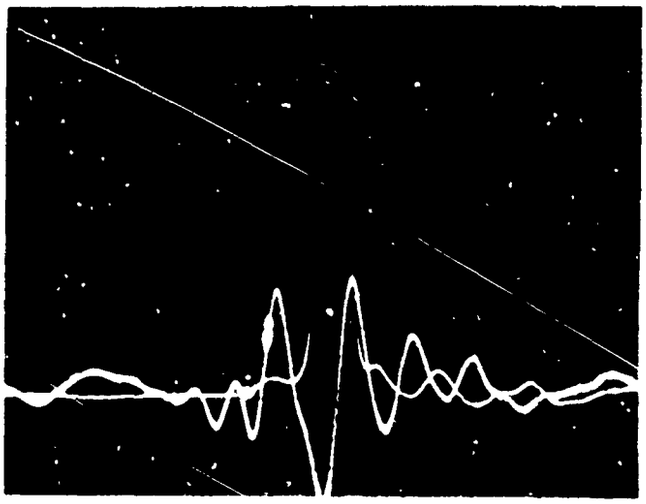

0.4 nsec / div

(a) Input Pulse And Input Reflection

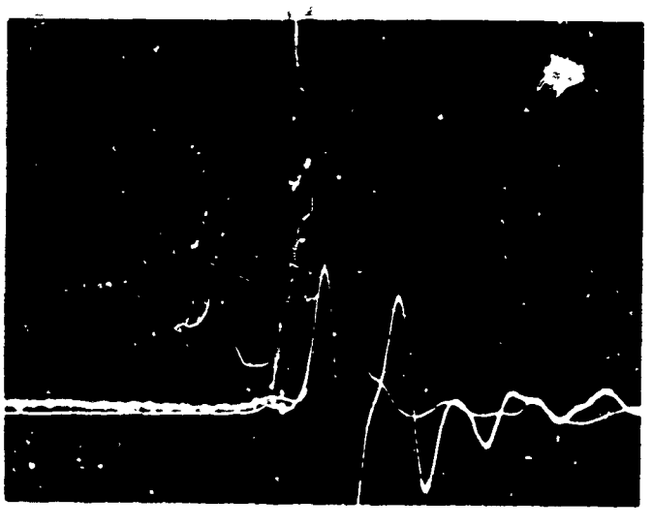

0.4 nsec / div

(b) Input Pulse And Uncoupled Output

such radiation within the coupler involves the excitation of non-TEM modes as should be excited by a transition within the coupler. This leads us to conclude that the deviations from the theory are due mainly to the excitation of non-TEM modes.

4.6 SUMMARY AND CONCLUSIONS

In this section we first derived the general expressions for the voltages occurring at the ports of a pair of coupled transmission lines terminated by uncoupled transmission lines. The conditions necessary for a perfect match at the input, independent of frequency, were derived and found to be the same as the conditions for the conventional coupled-transmission-line directional coupler.

The transient response of the conventional coupler was studied in detail. It was found that the settling time improved and the bandwidth decreased as the coupling of the lines was decreased. We considered the possibility of improving the transient response by relaxing the restrictive condition that the device be perfectly matched at the input. When this requirement was removed, it was found possible to develop a directional coupler whose impulse response was time-limited and whose transient response was optimum.

When values of coupling less than 3 dB were considered, we found that the conventional quarter-wavelength directional coupler has a transient response that approaches the "optimum" coupler as $k \to 0$; this is supported by the experimental results. The real importance of the new coupler lies in the fact that it suggests the investigation of a new class of elements which have a time-limited impulse response. Such a class of networks would, for example, be important in problems of time-domain equalization.

SECTION V

SIDEWALL COUPLERS

(L. Susman, Sperry Gyroscope Co.)

5.1 INTRODUCTION

The wideband properties of a microwave network can be deduced by examining the behavior of the device over all frequency or by its time response to particularly simple inputs such as an impulse or step function. Until recently, the frequency-domain description has been entirely adequate for almost all engineering applications for which these devices are commonly used. This is because the input signals most often used have been, to a very good approximation, narrow band. Thus, a complete representation, valid for all frequencies, was unnecessary; only a good representation valid over the range of operating frequencies was required. With the present emphasis on the use of wideband signals in modern radar systems and the recognition of the potential high-resolution capability that can be realized, the problem of signal distortion becomes very pertinent as one of the limitations to the resolution that can be obtained. To analyze the behavior of microwave networks in a way which makes clear the wideband behavior, one can revert from the frequency domain to a real-time description of the network's behavior. This point of view has been adopted in previous contracts[34] where the investigation of the transient behavior of microwave structures commonly used in arrays was initiated. The work performed under this contract can be viewed as a logical extension of the previous studies of the transient response of waveguides, magic tee's, branch-wall couplers, etc.

In particular, this section discusses the real-time response of sidewall couplers. Although the analysis presented is applied here to one particular device, the mathematical techniques presented, and certainly the point of view adopted, are applicable to many more commonly used microwave structures. Section 5.2 briefly reviews the work done on the transient response of straight waveguides. Section 5.3 considers, in some detail, the analysis of the sidewall coupler; i.e., the real-time behavior of two uniform waveguides coupled through a large aperture in a common sidewall. The

fact that the aperture is large is quite pertinent, since the complementary problem of rectangular waveguides coupled by small apertures involves quite different mathematical representations. Section 5.4 presents the results of experimental work on the step, impulse and step-modulated response of an L-band sidewall coupler.

5.2 REVIEW OF STRAIGHT SECTIONS OF WAVEGUIDES

In previous reports[34] the transient solution for a section of waveguide was examined from a number of points of view. The general discussion and results are reviewed here, since they form an integral part of the analysis of sidewall couplers contained in Sec. 5.3.

As explained in previous reports, the analysis of waveguide components differs conceptually from nondispersive microwave structures in that the input-output quantities are in general vector field components rather than scalar voltages. To interrelate these various output field quantities to input variables requires a dyadic system function. From a formal point of view, the impulse response contains all the information about the transient and steady-state response to any arbitrary input. Knowing the impulse response allows one (in principle at least) to compute the complete response to any other input excitation. Finally, asymptotic estimates of the settling time can be obtained by examining either the impulse response or the step response.

5.2.1 Transient Response

Consider the case of most practical importance, a rectangular waveguide operating in the dominant mode TE_{10}. One can show that the system function corresponding to the ratio of the H_z components at $z = z_0$ and $z = 0$ is given by

$$\frac{H_z(x,y,z_0,p)}{H_z(x,y,0,p)} = e^{-\frac{z_0}{c}\sqrt{p^2+\omega_c^2}} = e^{-\gamma z_0} \qquad (5.1)$$

where ω_c is the cutoff radian frequency of the guide, $\phi(x,y)$ gives the transverse spatial distribution of H_z, c is the velocity of light, $\gamma = \sqrt{p^2 + \omega_c^2}/c$, and p is the complex frequency variable; $p = \sigma + j\omega$. The transverse components of the field can be shown to be

$$E_y(x,y,z,p) = pH_z(x,y,z,p)$$
$$H_x(x,y,z,p) = \gamma H_z(x,y,z,p) \tag{5.2}$$

To find the impulse response corresponding to Eq. 5.1, the inverse Laplace transform of Eq. 5.1 is required. This is found to be

$$e^{-\frac{z}{c}\sqrt{p^2 + \omega_c^2}} \Leftrightarrow \delta(t - \tau) - \frac{\omega_c \tau}{\sqrt{t^2 - z\tau^2}} J_1\left(\omega_c \sqrt{t^2 - \tau^2}\right) u(t - \tau) \tag{5.3}$$

where $u(t)$ is the unit step function $\tau = \frac{z}{c}$.

The general character of this impulse response follows the computed impulse response of an ideal high-pass filter. First, there is an impulse term minus some oscillatory function. It should also be noted that the output for $t < \tau$ is zero. For $t \gg \tau$, Eq. 5.3 reduces to

$$h(t) = \omega_c \tau \frac{J_1(\omega_c t)}{t} \tag{5.4}$$

This form of the equation resembles the output of the high-pass filter, since as $t \to \infty$, $J_1(\omega_c t)$ approaches $\sin \omega_c t$.

Returning to the system function of the transverse components, it can be seen from Eq. 5.2 that the impulse response for $E_y(z,t)$ can be found by differentiating Eq. 5.3 with respect to t. (These expressions have been given in previous reports.) The various impulse responses consist of impulses and their derivatives (i.e., doublets), as well as oscillatory Bessel functions. Figure 5-1 shows the response $H(z,t)$ to

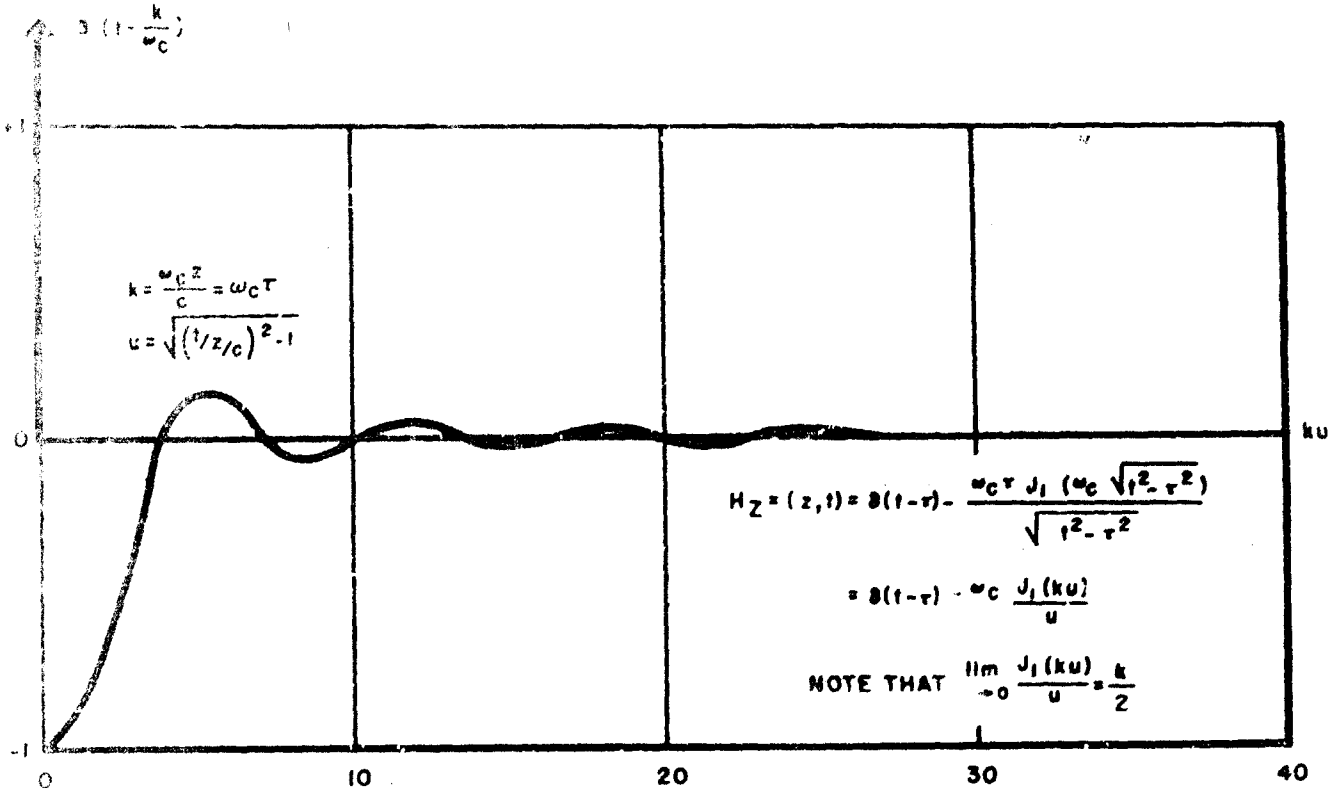

FIG. 5-1 The normalized waveguide impulse response to excitation of H_z at $z=0$.

an impulsive H_z field applied at $z = 0$. The transient response of a straight length of rectangular waveguide was computed by treating the structure as a two-port network.

The explicit assumption that the impulsive response corresponds to an impulsive excitation of one of the field components, say H_z, E_y, or H_x, is not realistic in most practical cases. For example, if a laboratory setup designed to test waveguides is arranged with coaxial-to-waveguide transitions, it is unreasonable to expect that an impulsive voltage applied to the coaxial line will result in impulsive field components.

A more reasonable model results by assuming that an impulsive voltage produces (approximately) an impulsive current across the guide. This problem is important because it closely simulates the experimental setup used in evaluating the theoretical results. If the impulsive excitation of a coaxial system produces an impulsive current density across the waveguide, the transverse electric field E_y that propagates down the guide is then given by Collin[35] as

$$E_y(z,t) = \delta(t - \tau) - \frac{c\omega_c t}{\sqrt{t^2 - \tau^2}} J_1\left(\omega_c \sqrt{t^2 - \tau^2}\right) u(t - \tau) \tag{5.5}$$

The step response can also be found in this case and is given by

$$a(t) = cJ_0\left(\omega_c \sqrt{t^2 - \tau^2}\right) u(t - \tau) \tag{5.6}$$

The impulse and step responses are shown in Fig. 5-2. These solutions have been the basis for Saxton and Schmitt's experimental verification of the transient response of waveguides.[36]

5.2.2 Step-Modulated Response

The previous section reviewed the results already obtained for the transient response of a uniform waveguide. There is much more literature

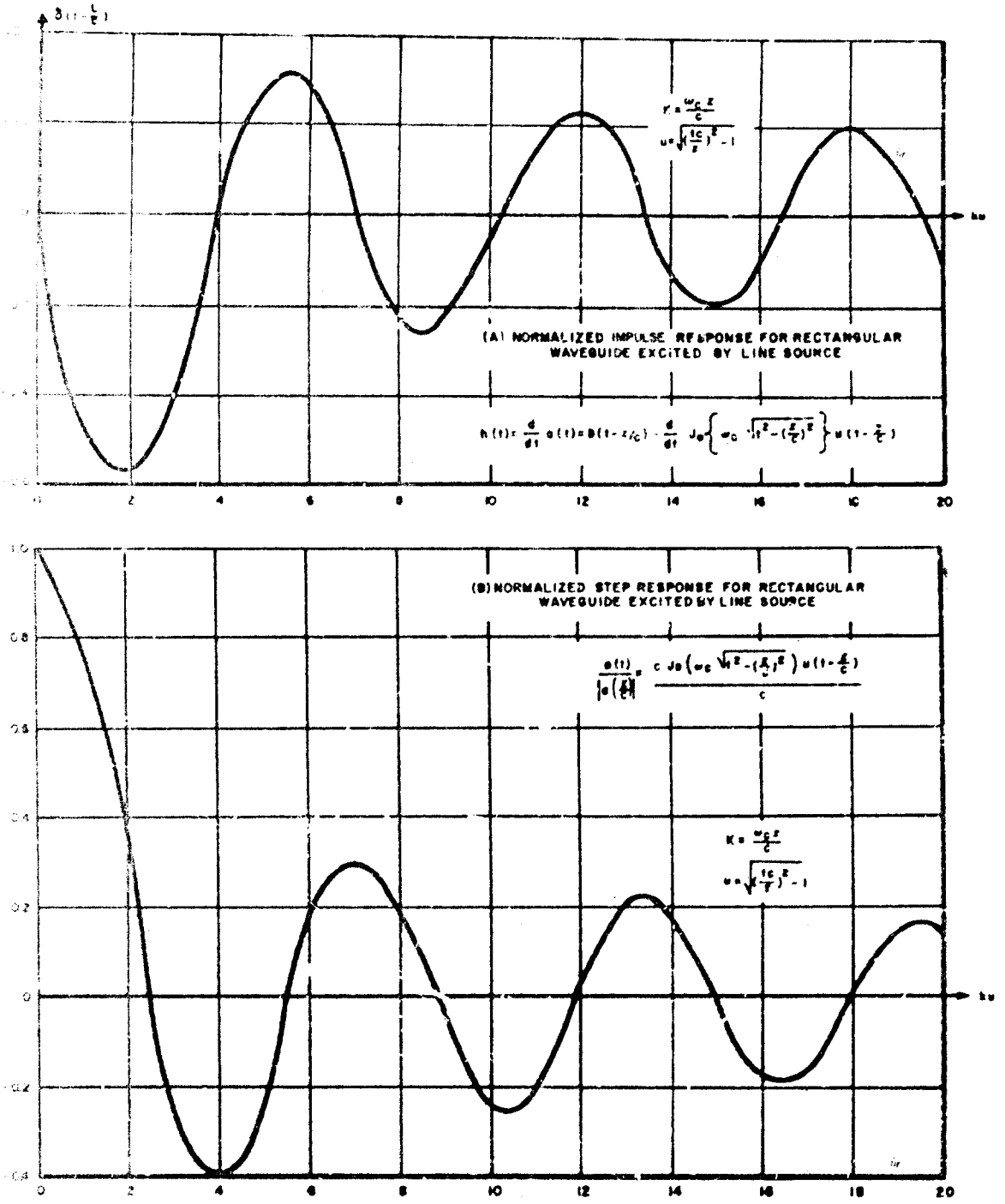

FIG. 5-2 The normalized impulse and step responses for a rectangular waveguide excited by a line source.

available on the step-modulated response of uniform waveguides. It is rather unfortunate that so basic and seemingly straightforward a problem should turn out to be extremely unwieldly from a mathematical point of view. The original work on this problem (and still the most complete) is contained in Cerrillo's dissertation.[37] He shows (among other things) that the step-modulated response of a uniform waveguide can be expressed in terms of Lommel functions. For the range of values of usual interest no tables of these functions are available. Recently, several investigators have reopened this complex problem and have added to it considerably by applying the mathematical results to cases of particular practical importance. In principle, the response of an ideal waveguide to a step-modulated input of the form

$$e(t) = \sin \omega_0 t \; u(t) \tag{5.7}$$

is given by the well known inversion formula

$$r(t) = \frac{1}{2\pi j} \int_{\Gamma} \frac{\omega_0 \, e^{-\frac{z}{c}\sqrt{p^2 + \omega_c^2}}}{p^2 + \omega_0^2} \, e^{+pt} dp \tag{5.8}$$

One notices that the integrand has a branch cut at $p = \pm j\omega_c$ and a pole at $p = \pm j\omega_0$. Karbowiak[38] obtained asymptotic expressions for the step-modulated response in essentially three regions of time: a) a region of antecedents, b) a main signal region, and c) the posterior transient region. His approach makes use of branch-point integration in the complex plane. More recently, Wait and Spies[39] treated the problem of propagation between parallel plates and were able to derive a power-series solution which is basically equivalent to Cerrillo's. Wait and Spies compare their results to the use of Fresnel integral approximations to the transfer function of the waveguide. Sueman previously treated the step-modulated response of a waveguide by starting from the impulsive response in the time domain and deriving an upper bound on the buildup time which agrees well with experiment.[40]

Since the major emphasis in this report is on the transient performance of microwave structures, several remarks that indicate how this work can be related to broadband behavior seem in order. When the excitation to a waveguide is relatively narrow band and not too close to cutoff, it seems expedient to rely on frequency-domain concepts in analyzing the distortions introduced by the waveguide. However, when very broadband signals are used (or signals extending close to cutoff), accurate results can be obtained only by using exact results, and one is forced to use either Cerrillo's exact expressions or the time-domain approach via a convolution with the impulsive response of the waveguide. Either of these approaches requires the use of a high-speed digital computer.

The following section treats the transient response of sidewall couplers. The emphasis here is placed on obtaining a clear picture of the mode coupling in the transient case. The step-modulated response of a real coupler is discussed in Sec. 5.4 but, as might be expected, only qualitative agreement can be claimed for these results.

5.3 ANALYSIS OF SIDEWALL COUPLERS

Consider the ideal sidewall coupler shown in Fig. 5-3. It consists of two rectangular, uniform waveguides coupled by an aperture across the narrow face of the adjacent walls. For analysis it is convenient to divide this four-port structure into three regions. Region I is the input section, region II is the coupling section, and region III is the output section. The device is designed to operate over a band of frequencies such that only the dominant TE_{10} mode can propagate in each of the waveguides in the input and output regions (I and III). In region II it is assumed that the dominant mode and the next higher-order mode (TE_{20}) are the only propagating modes.

In considering the interaction of the electromagnetic fields in the three regions of interest, it is best to start with the field configurations for the propagating modes. In regions I and III the field components are

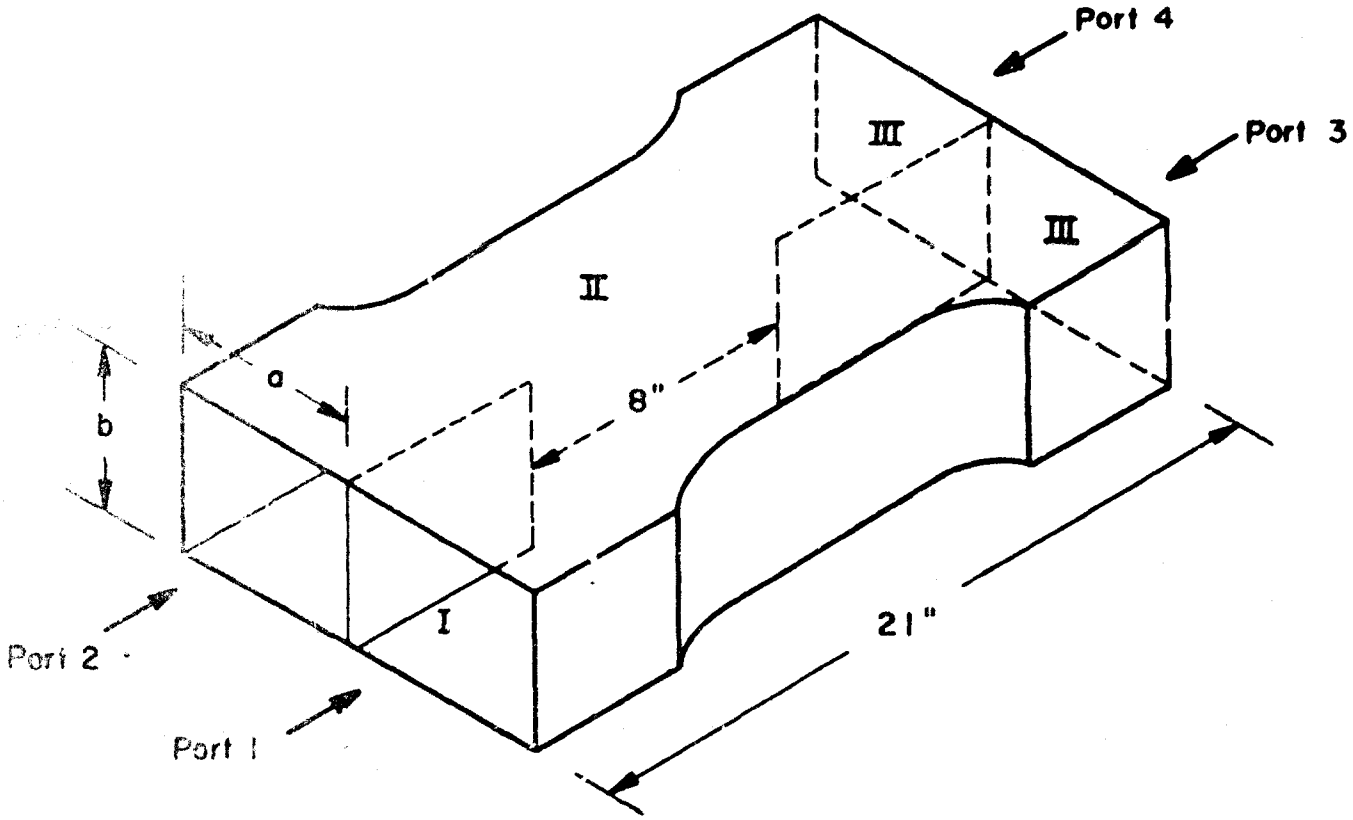

FIG. 5-3 An L-band waveguide sidewall coupler.

$$E_y = E_o \sin \frac{\pi x}{a} \qquad E_x = H_y = E_z = 0$$

$$H_x = \frac{-E_y}{Z_{TE}} \qquad H_z = j \frac{E_o}{\eta} \frac{f_c}{f} \cos \frac{\pi x}{a} \tag{5-9}$$

All the other field components are zero, Z_{TE} is the characteristic impedance of the guide and is given by

$$Z_{TE} = \frac{\eta}{\sqrt{1 - \left(\frac{f_c}{f}\right)^2}} \tag{5.10}$$

where f_c is the cutoff frequency of the guide and is given by

$$f_{c_1} = \frac{c}{2a} \text{ for the } TE_{10} \text{ mode.} \tag{5.11}$$

In the coupling region (region II) the expression for the field components are the same as Eqs. 5.9, with a replaced by 2a. That is

$$E_y = E_o \sin \frac{\pi x}{2a}$$

$$H_x = - \frac{E_y}{Z_{TE}} \tag{5.12}$$

$$H_z = j \frac{E_o}{\eta} \frac{f_{c_2}}{f} \cos \frac{\pi x}{2a}$$

where f_{c_2} is given by

$$f_{c_2} = \frac{c}{4a}$$

The field components corresponding to the TE_{20} mode in region II are given by the same expressions as Eqs. 5.9. In the normal mode of operation all higher-order modes are cut off. The resulting range of operation for the coupler is shown schematically in Fig. 5-4, which shows the relative cutoff frequencies for the higher-order modes (where it has been assumed that $a/b = 2$). In the actual sidewall coupler the "a" dimension of the coupling region is somewhat reduced. This is done to move the cutoff of the TE_{30} mode up, thereby extending the useful operating range of the device. A tuning post is also provided in the form of a bubble in the coupling region; this is needed to insure good isolation at the decoupled port.[41]

To understand the transient behavior of this rather complicated structure, it suffices to know the responses of the device to an impulsive excitation at one of its inputs. It is also convenient to take advantage of the inherent symmetry of the structure and consider the input at a single port, say port 1, as due to the sum of an "even-mode" and an "odd-mode" excitation at ports 1 and 2. The even-mode excitation consists of a TE_{10} field distribution at ports 1 and 2; the odd-mode excitation consists of a TE_{10} field distribution at port 1 and its negative at port 2. The desired response is seen to be due to the sum of the even-and odd-mode excitations and will simply be called the sum mode.

The convenience of this approach lies in the fact that one can assume that the odd mode propagates through the entire structure with virtually no distortion due to the discontinuities at the interfaces of the various regions. This is true as long as the dimensions of the inner wall are kept small. The effects of these discontinuities on the various modes are discussed in the following section.

5.3.1 Effects of Discontinuities

To quantitatively analyze the effects of the abrupt change in going from regions I to II and II to III generally requires the solution of an integral equation for the admittance of the junction. The particular model needed for the sidewall coupler corresponds to what is commonly called an H-plane bifurcation. Marcuwitz[42] treats this type of junction and derives

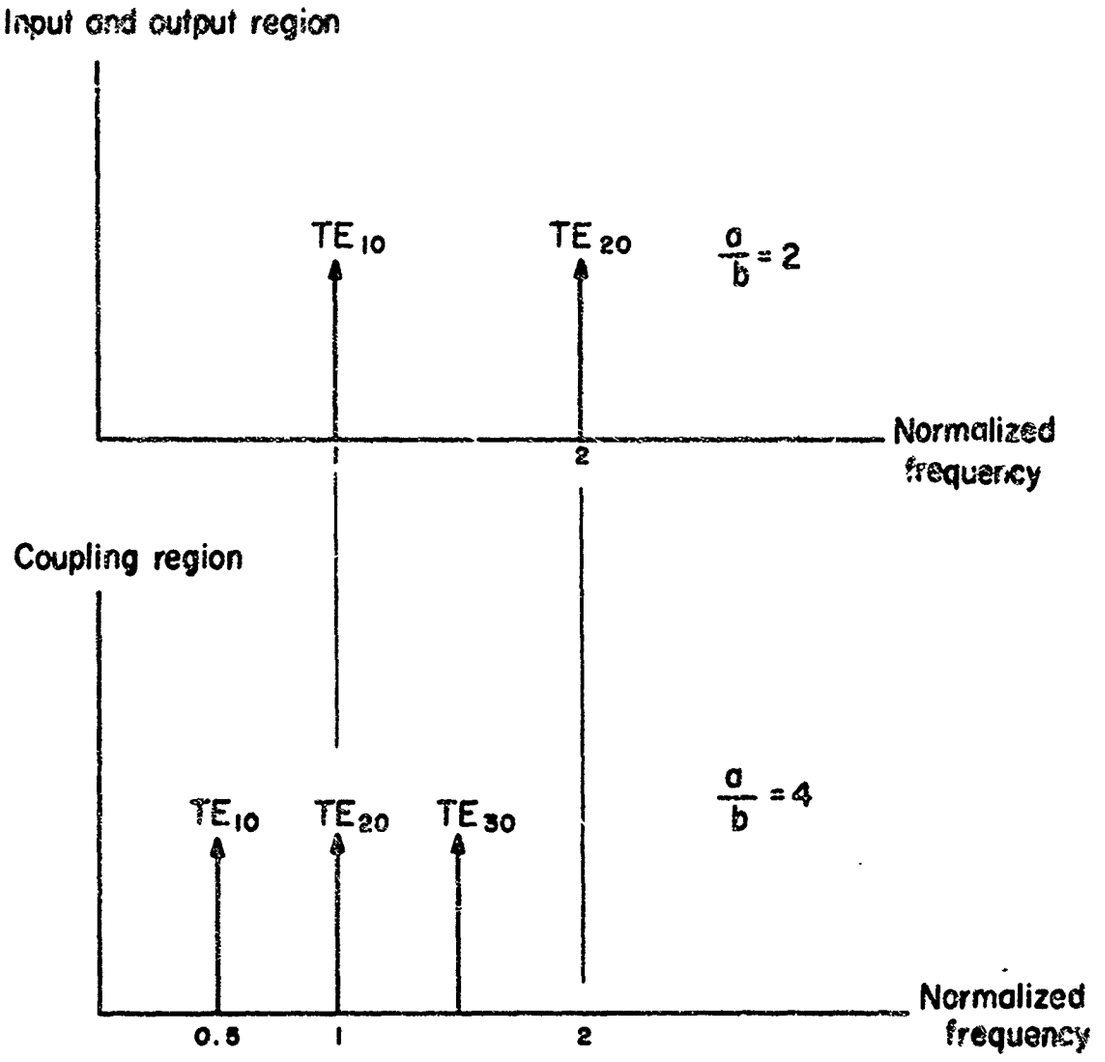

Note : Frequency axis is normalized to cutoff frequency of TE_{10} mode of input section

FIG. 5-4 The mode cutoffs for the ideal sidewall coupler.

an equivalent circuit which indicates that the junction is essentially equivalent to a hybrid coil arrangement. However, his range of values of the equivalent circuit is limited in the frequency domain to the usual operating range of the waveguide. An exact solution, using the Weiner-Hopf integral equation approach, can be found in Jones,[43] but here, too, Jones treats the case where the smaller waveguides are cut off at the operating frequency. In order to apply the results of this classical boundary-value problem to the distortion of transient signals we need an approach which gives the correct junction behavior at high frequencies (since it is this portion of the frequency band which determines the behavior of the incident field). For this purpose we have chosen to use the Schwinger-Lewin variational method.[44]

Consider first the case where the even-mode excitation in region I is incident on region II. It can be shown that the junction admittance is given by[41]

$$y = \frac{Y_1 \left[\int_0^a E_y \cos \frac{\pi x}{2a} \, dx \right]^2 + \sum_{m=3,5,7,\ldots}^{\infty} Y_m \left[\int_0^a E_y \cos \frac{m\pi x}{2a} \, dx \right]^2}{k_1 \left[\int_0^a E_y \sin \frac{\pi x}{a} \, dx \right]^2} \qquad (5,13)$$

where

$$Y_m = \sqrt{\left(\frac{m\pi}{2a}\right)^2 - k^2} \qquad k_n = \sqrt{\left(\frac{n\pi}{a}\right)^2 - k^2} \qquad k = \frac{\omega}{c}$$

Because of the stationarity of this expression for the admittance, one can approximate E_y (the field distribution at the junction) by $\sin \frac{\pi x}{a}$. With this approximation the real and imaginary parts of the junction admittance become

$$G = \frac{Y_1}{k_1} \frac{64}{9\pi^2} \; ; \quad jB = \frac{64}{\pi^2 k_1} \sum_{m=3,5,7,\ldots}^{\infty} \frac{Y_m}{(m^2 - 4)^2} \qquad (5,14)$$

Knowing y we can find the reflection and transmission coefficients; they are

$$R = \frac{1 - y}{1 + y} \qquad T = \frac{32}{3\pi} \frac{1}{1 + y} \tag{5.15}$$

The meaning of R is clear, the meaning of T requires a note of explanation. T gives the transmission coefficient relating the incident even mode to the TE_{10} mode in region II.

In a completely analogous way, one can derive the equivalent admittance for the TE_{10} mode in region II incident on region III; the resulting admittance is

$$G' = \frac{k_1}{\gamma_1} \frac{9\pi^2}{64} \qquad jB' = \frac{9}{\gamma_1} \sum_{m=3,5,7}^{\infty} \frac{\gamma^m}{(4-m^2)^2}$$

$$R' = \frac{1 - y'}{1 + y'} \qquad T' = \frac{3\pi}{8(1 + y')} \tag{5.16}$$

We could also derive the equivalent admittance for the odd mode, but, as we indicated before, one can verify that the odd mode does not encounter any distortion due to the discontinuities at the interface of the various sections.

5.3.2 Matrix Analysis of Sidewall Coupler

To make effective use of the calculations in the previous section the following mathematical artifice is used. A scattering matrix S′ describing the junction effects is first formulated.* The S′ matrix is then modified to take into account one-half the length of waveguide in

* A detailed discussion of the use of scattering matrix techniques to determine the transient response of microwave networks is presented in Appendix D.

region II. The resulting structure is then cascaded with its mirror image by using the well known formulas for cascade connections.[12] The use of scattering matrices for a description of discontinuities is well known, but the development here is unconventional in the sense that it has been found advantageous to use, not the incident and reflected voltages at the various ports, but independent linear combinations of these so that the elements of the resulting scattering matrix are exactly the quantities computed in Sec. 5.3.1.

Consider then the mathematical model shown in Fig. 5-5. The input port quantities correspond to even- and odd-mode excitations at ports 1 and 2 of the sidewall coupler. The output quantities are the wave amplitudes of the TE_{10} and TE_{20} mode signals in the coupling region of the coupler. For our purposes we have taken the network representation to be a 4-port network. To be completely rigorous would require a doubly infinite number of input and output ports to handle not only the mode which propagates but also those that are cut off.[45] This additional complication has been avoided, since it can be shown that it will have only a minor effect on the results. (Notice that the presence of cutoff modes was considered in the calculation of R, R', T and T'.) Denoting a_1b_1, a_2b_2, a_3b_3, and a_4b_4 as the incident and reflected scattering variables at the even mode input port, odd mode input port, TE_{10} output port, and TE_{20} output port, respectively, the scattering matrix for the junction is then seen to be

$$\begin{bmatrix} b_1 \\ b_2 \\ -- \\ b_3 \\ b_4 \end{bmatrix} = \left[\begin{array}{cc:cc} R & 0 & T' & 0 \\ 0 & 0 & 0 & 1 \\ \hdashline T & 0 & R' & 0 \\ 0 & 1 & 0 & 0 \end{array}\right] \begin{bmatrix} a_1 \\ a_2 \\ -- \\ a_3 \\ a_4 \end{bmatrix} \qquad (5.17)$$

For convenience, we shall write this matrix relation in the partitioned form

$$\begin{bmatrix} \underset{\sim}{b}^1 \\ -- \\ \underset{\sim}{b}_0 \end{bmatrix} = \left[\begin{array}{c:c} \underset{\sim}{S}'_{11} & \underset{\sim}{S}'_{12} \\ \hdashline \underset{\sim}{S}'_{21} & \underset{\sim}{S}'_{22} \end{array}\right] \begin{bmatrix} \underset{\sim}{a}^1 \\ -- \\ \underset{\sim}{a}_0 \end{bmatrix} \qquad (5.18)$$

It is well known that adding lengths of waveguide to various ports results in a new scattering matrix given by

$$S = \theta S' \theta \tag{5.19}$$

where θ is a diagonal matrix with entries $e^{-j\gamma_i \ell}$; here ℓ is the length of the waveguide and γ is the propagation constant. If the length of the coupling region is ℓ , then the resulting scattering matrix is

$$S = \theta S' \theta = \left[\begin{array}{c|c} \underset{\sim}{1} & \underset{\sim}{0} \\ \hline \underset{\sim}{0} & e^{-j\gamma\ell/2} \end{array}\right] \left[\begin{array}{c|c} \underset{\sim}{S}'_{11} & \underset{\sim}{S}'_{12} \\ \hline \underset{\sim}{S}'_{21} & \underset{\sim}{S}'_{22} \end{array}\right] \left[\begin{array}{c|c} \underset{\sim}{1} & \underset{\sim}{0} \\ \hline \underset{\sim}{0} & e^{-j\gamma\ell/2} \end{array}\right] \tag{5.20}$$

where $\underset{\sim}{1}$ is the 2×2 identity matrix, $\underset{\sim}{0}$ is the 2×2 zero matrix, and $e^{-j\gamma\ell/2}$ is a diagonal matrix $\left\{e^{-j\gamma_1\ell/2}, e^{-j\gamma_2\ell/2}\right\}$. When Eq. 5.20 is combined with Eq. 5.17 the resulting overall scattering matrix is

$$\left[\begin{array}{c} b_1 \\ b_2 \\ \hline b_3 \\ b_4 \end{array}\right] = \left[\begin{array}{cc|cc} R & 0 & \lambda_1 T' & 0 \\ 0 & 0 & 0 & \lambda_2 \\ \hline \lambda_1 T & 0 & \lambda_1^2 R' & 0 \\ 0 & \lambda_2 & 0 & 0 \end{array}\right] \left[\begin{array}{c} a_1 \\ a_2 \\ \hline a_3 \\ a_4 \end{array}\right] \tag{5.21}$$

where

$$\lambda_1 = e^{-j\gamma_1\ell/2} \quad \text{and} \quad \lambda_2 = e^{-j\gamma_2\ell/2}$$

This overall network is then cascaded with its mirror image. The derivation for the resulting scattering is well known and is reviewed in Appendix D. The final result corresponding to Fig. 5-6 is

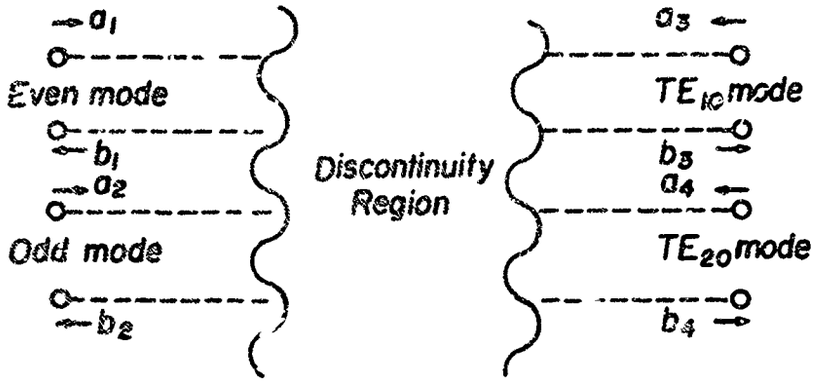

FIG. 5-5 Scattering matrix formulation.

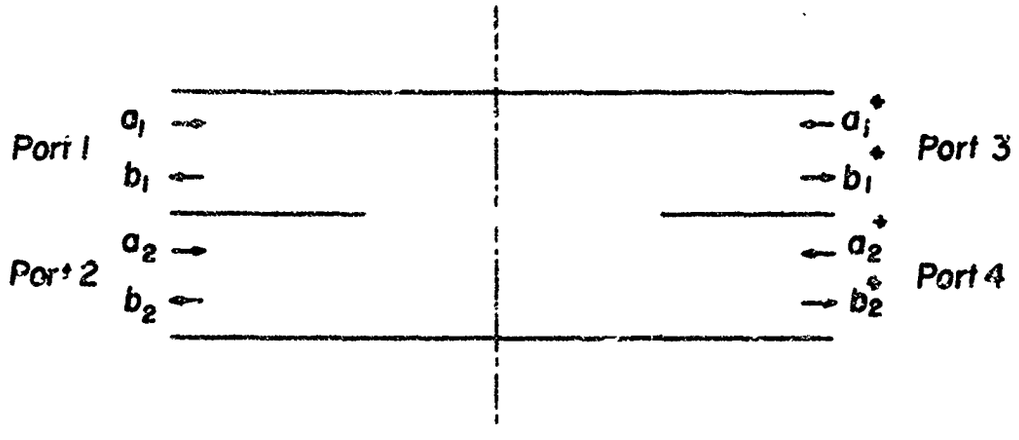

FIG. 5-6 The sidewall coupler as a cascade connection.

$$\begin{bmatrix} b_1 \\ b_2 \\ -- \\ b_1^* \\ b_2^* \end{bmatrix} = \begin{bmatrix} \underset{\sim}{S}_{11} & \underset{\sim}{S}_{12} \\ \\ \underset{\sim}{S}_{21} & \underset{\sim}{S}_{22} \end{bmatrix} \begin{bmatrix} a_1 \\ a_2 \\ -- \\ a_1^* \\ a_2^* \end{bmatrix} \tag{5.22}$$

where the starred quantities denote the scattering variables and

$$\underset{\sim}{S}_{12} = \underset{\sim}{S}_{21} = \begin{bmatrix} \dfrac{T'T\lambda_1^2}{1 - R'^4\lambda_1^2} & 0 \\ 0 & \lambda_2^2 \end{bmatrix} \tag{5.23}$$

$$\underset{\sim}{S}_{11} = \underset{\sim}{S}_{22} = \begin{bmatrix} \dfrac{R + T'T\lambda_1^4 R'}{1 - R'^2\lambda_1^4} & 0 \\ 0 & 0 \end{bmatrix} \tag{5.24}$$

To use the above development for a case of practical interest, assume that the output of the coupler is matched (that is, $a_1^* = a_2^* = 0$) and that port 1 is excited with an input of unit amplitude. Then $a_1 = +\frac{1}{2}$ and $a_2 = +\frac{1}{2}$ because this sum of the even and odd modes yields a single unit input at port 1. The reflected variables can then easily be found to be

$$b_1 = \frac{1}{2}\ \frac{R + T'T\lambda_1^4 R'}{1 - R'^2\lambda_1^4}$$

$$b_2 = 0$$

$$b_1^* = \frac{1}{2}\ \frac{T'T\lambda_1^2}{1 - R'^2\lambda_1^4} \qquad (5.25)$$

$$b_2^* = \frac{1}{2}\ \lambda_2^2$$

These are the outputs, but expressed in terms of an even and odd modal decomposition. In terms of actual output variables we need $b_1 \pm b_2$ and $b_1^* \pm b_2^*$; thus

$$b_1 \pm b_2 = \frac{1}{2}\ \frac{R + T'T\lambda_1^2 R'}{1 - R'^2\lambda_1^4}$$

$$b_1^* \pm b_2^* = \frac{1}{2}\ \frac{TT'\lambda_1^2}{1 - R'^2\lambda_1^4} \pm \frac{\lambda_2^2}{2} \qquad (5.26)$$

It should be recognized that R, R', T and T' are all functions of frequency. For any one frequency, Eqs. 5.26 contain all the information needed. For example, the condition that the sidewall coupler be a 3 dB coupler is

$$|b_1^* + b_2^*| = b_1^* - b_2^* \qquad (5.27)$$

For our purposes it is convenient to formally expand the denominator term in Eqs. 5.26. This leads to

$$b_1^* \pm b_2^* = \pm \frac{1}{2}\lambda_2^2 + \frac{1}{2}TT'\lambda_1^2\left\{1 + R'^2\lambda_1^4 - \left(R'^2\lambda_1^4\right)^2 + \left(R'^2\lambda_1^4\right)^4 + \ldots\right\} \qquad (5.28)$$

Since λ_1^2 is of the form $e^{-\frac{\ell}{c}\sqrt{p^2+\omega_c^2}}$ in the p domain, the output is seen to be a train of distorted waveforms similar to the transient solution for a straight section of waveguide (see Sec. 5.2). Additional distortion is introduced since the reflection and transmission factors are also functions of p. Some quantitative data can be obtained by applying a modified initial-value theorem (see Appendix D) but since the solution is known to be highly oscillatory the first few terms of the power series that results give very little information. It is clear from Eq. 5.28 that successive reflections are separated in time by $2\left(\frac{\ell}{c}\right)$ seconds, where ℓ is the length of the coupling region.

5.4 EXPERIMENTAL RESULTS - SIDEWALL COUPLER

To experimentally verify the suitability of some of the approximations made in Sec. 5.3 and to obtain meaningful results for real sidewall couplers, an L-band sidewall coupler was tested. The experiments consisted of displaying both the impulse and step-modulated responses for even- and odd-mode excitation between various ports. The means for generating these test signals have been discussed in previous reports.[34] To summarize, the test signals used for the waveguide sidewall coupler were: (1) a 0.2 nsec video pulse, and (2) 16 cycles of a 1350 MHz step-modulated signal. These signals were synthesized from the output of the Hewlett-Packard time-domain reflectometer and were applied to the waveguide through an L-band coax-to-waveguide adapter. The sidewall coupler is 21 inches long, coupled over a region of 8 inches by a large aperture in the sidewall.

The impulse response of the sidewall coupler was examined experimentally by applying the 0.2 nsec pulse to port 1 of the coupler (see Fig. 5-3) and measuring the response at the other three ports. This was done for three types of modal excitation, the even, odd, and sum modes; the results are shown in Figs. 5-7, 5-8 and 5-9, respectively. During the tests all unused ports were terminated in a matched load. In Fig. 5-7 one notes that the responses at ports 3 and 4 for the even-mode excitation are identical. The presence of distortion due to multiple reflections is evident after approximately 1.6 nsec, while the overall transient is basically zero after 20 nsec. From this one can conclude that an upper bound

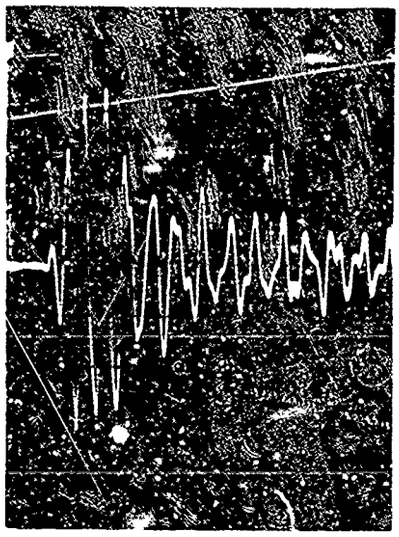

(a)

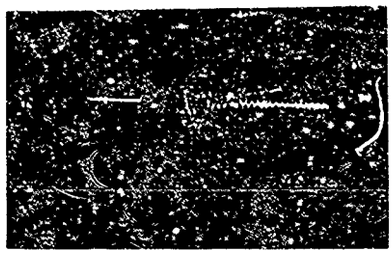

4 nsec / maj. div.

Time scale : 1 nsec/maj.div.

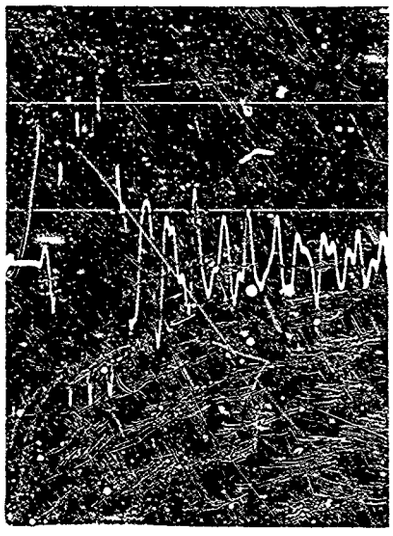

(b)

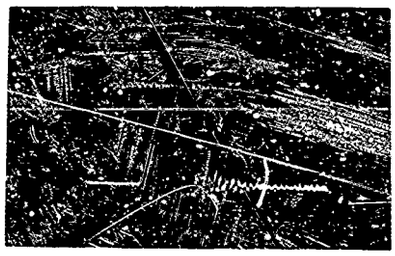

4 nsec / maj.div.

Time scale : 1 nsec/maj. div.

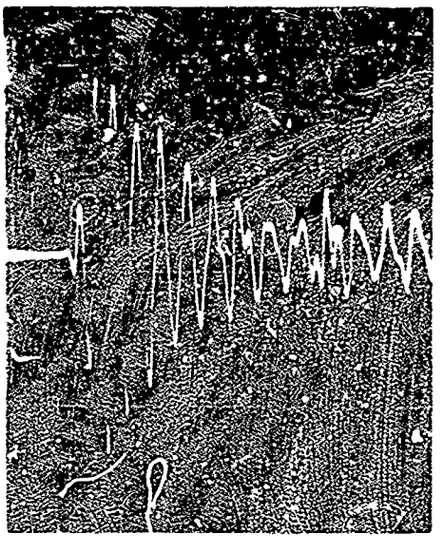

(a)

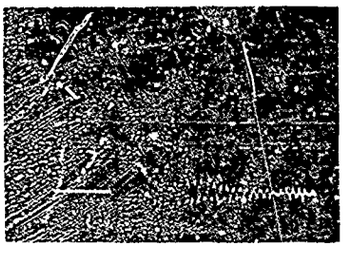

4 nsec / maj.div.

Time scale : 1 nsec / maj.div.

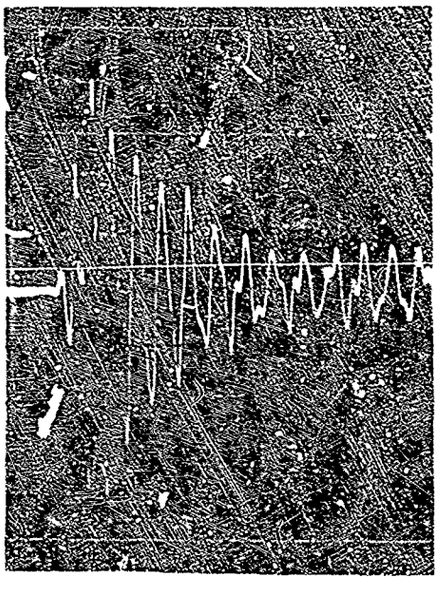

(b)

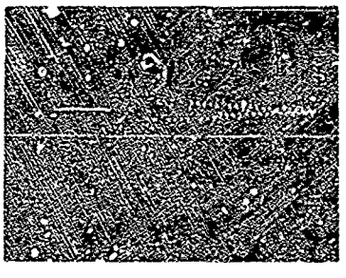

4 nsec / maj. div.

Time scale : 1 nsec / maj.div.

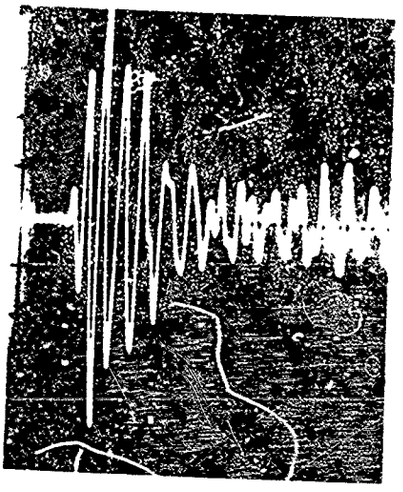

Output at port 3

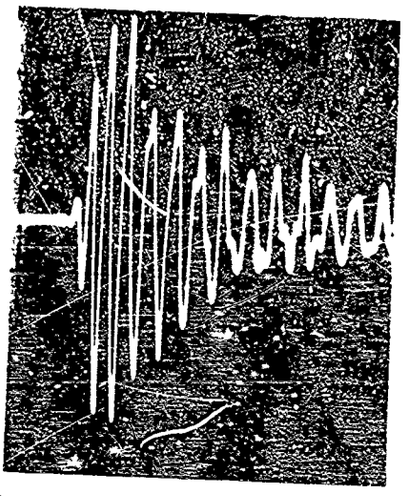

Output at port 4

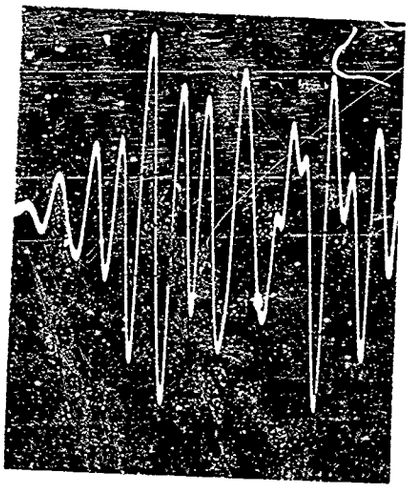

Output at port 2

Time scale : 1 nsec/maj. div.

on the buildup time for the step-modulated response is 20 nsec (as previous experience has shown, this is a rather gross upper bound, and one expects buildup times which are considerably shorter).

Figure 5-8 shows the impulse response of the L-band sidewall coupler for the odd-mode excitation, i.e., where the excitations at ports 1 and 4 are the negative of each other. From theory one would expect this type of excitation to create a minimum of distortion, since the transport mechanism from input to output involves only one modal configuration. From Fig. 5-8 it is evident that distortion due to internal re-reflections does not take place before 2.5 nsec of time delay. The compressed view in Fig. 5-8 shows that the transient response is somewhat longer for the odd mode, lasting approximately 24 nsec.

Figure 5-9 shows the transient response to the sum excitation (the even plus odd excitation). First of all, it should be noted that at ports 3 and 4 the initial output is positive. The outputs at ports 3 and 4 are not identical, but have the same general character. The output at port 2, the normally decoupled port, is quite different. First, the output is not zero, as might be predicted from the steady-state characteristics of the device. The output at the decoupled port builds up gradually, with distortions due to re-reflections occurring 2.5 nsec after the initial excitation.

Figure 5-10 shows the step-modulated response of the sidewall coupler to a 1350 MHz signal applied as an even and odd excitation. We see that at port 3 the even and odd modes have opposite polarity. The odd mode has a slightly longer rise time as conjectured from the results of the transient excitation. The rise time is seen to be on the order of 2 nsec in all cases; the buildup time is much longer.

Figure 5-11 shows the response of the sidewall coupler to the 1350 MHz step-modulated signal applied in the sum mode. The outputs at ports 3 and 4 have almost identical rise times, but the buildup time at port 3 is slightly less than that at port 4. The output at port 2 is quite low, with no spurious level.

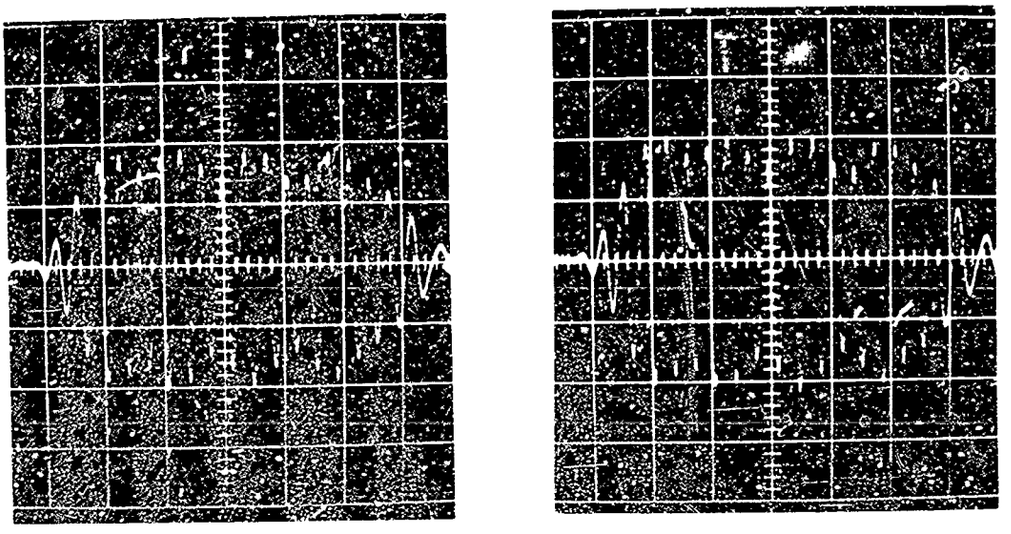

Even mode

Output at port 3 Output at port 4

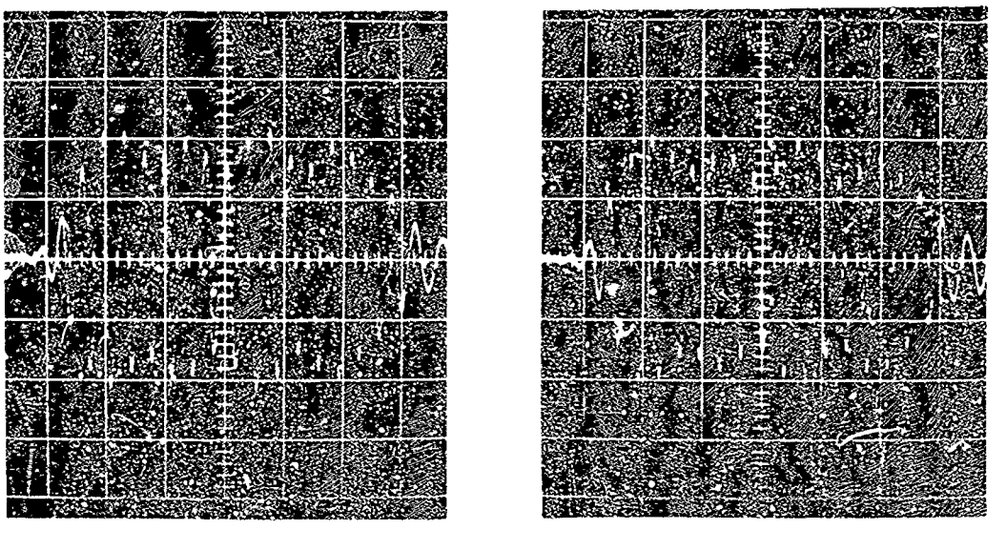

Odd mode

Scale : 5 mV / maj. div

Time scale: 2 nsec/maj.div.

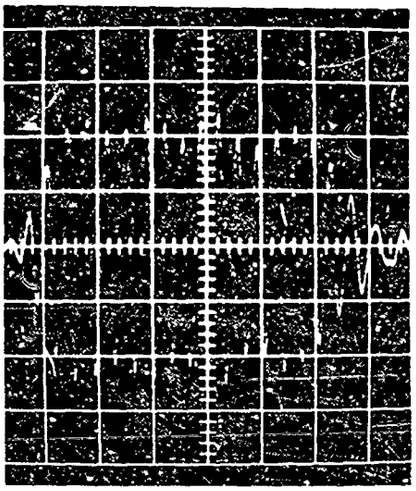

Output at port 3

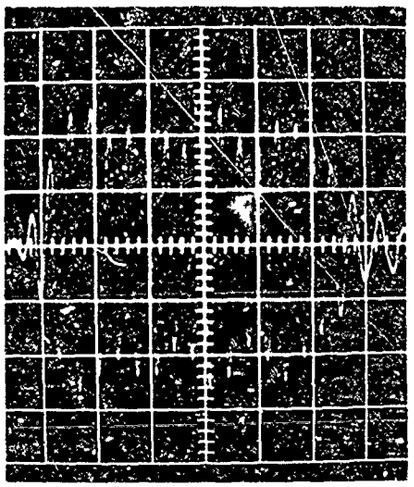

Output at port 4

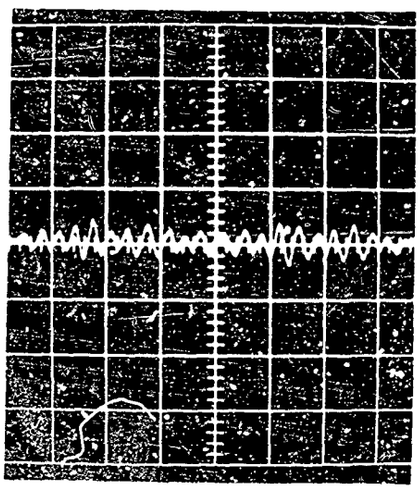

Output at port 2

Scale: 5 mV/maj.div.

Time scale : 2 nsec/maj. div.

5.5 CONCLUSIONS

The transient response of the sidewall coupler is similar in several respects to the transient response of interconnections to TEM-mode lines. The response consists of delayed, but now modified, versions of a basic form. The delays are governed by the electrical dimensions between discontinuities and depend on the reflection and transmission coefficients at the junction. The response is complicated by two inherent properties of the structure's geometry. First of all, the propagation through the straight sections of waveguide is affected by the dispersive nature of the propagating characteristics. The degree of dispersion depends on the cutoff frequency of the mode considered and, unfortunately, on the length of the waveguide. The second complexity arises from the fact that the junction effects, the reflection and transmission coefficients, depend on frequency in a complicated way. These two factors alone are sufficient to make any attempt at obtaining exact agreement between theory and experiment extremely difficult.

To add to the difficulty, the basic waveguide acts as a high-pass filter: since the display equipment has a high-frequency cutoff, there is an inevitable degree of rounding caused by the display equipment. For the case of TEM-mode structures, this distortion is not critical because the impulsive train is time separated; for waveguides, however, the transient response is not a train of impulses but a highly oscillatory waveform, and the distortion introduced by the display equipment effectively masks the details of the waveform.

The best that can be obtained from an investigation of the transient response of highly dispersive devices is a better and clearer understanding of the mechanism of transient behavior. This, we feel, has been accomplished. It is interesting to note that the analysis given in Sec. 5.3 relies heavily on the symmetry of the structure involved; this geometric property is independant of frequency and so is equally valuable in a frequency- or time-domain approach.

APPENDIX A

A NUMERICAL APPROACH FOR EVALUATING WAVE PROPAGATION THROUGH A SEMI-INFINITE FERRITE MEDIUM

The discussion below provides a method for inverting the Laplace transform (LT) of Eq. 2.2 numerically. Briefly summarized, the procedure involves the application of the initial value theorem (LT theory) to invert numerically the system function of a propagating medium. The significant feature of this method is the fact that because the signal is traveling through a distributed medium, it is delayed and no longer exists at $t=0$. Hence the response must be advanced by the signal front delay τ_{fr} (i.e., returned to the origin) before the initial value theorem can be applied. This technique is described in detail in a recent IEEE journal.[34] Thus, if the response of a network to a step excitation is given by

$$g(t) \overset{\mathcal{L}}{\longleftrightarrow} G(p) = F(p)\cdot H(p)$$

where

$$\begin{aligned} F(p) &= LT\,[u(t)] = 1/p \\ H(p) &= LT\,[h(t)] = H_1(p) + H_2(p) \\ H_1(p) &= \exp\{-pz\sqrt{\mu_0\,\epsilon(\mu + K)}\} \\ H_2(p) &= \exp\{-pz\sqrt{\mu_0\,\epsilon(\mu - K)}\} \end{aligned} \tag{A.1}$$

then

$$g(t) = \hat{g}(t - \tau_{fr}) = \left\{\hat{g}(0+) + \frac{\hat{g}^{(1)}(0+)(t - \tau_{fr})}{1!} + \frac{\hat{g}^{(2)}(0+)(t - \tau_{fr})^2}{2!} + \ldots\right\} u(t - \tau_{fr})$$

The Fourier transform of $h(t)$ can be found from $H(p)$ by substituting $j\omega$ for p in Eq. A.1. Thus

$$H(\omega) = H(p)\Big|_{p=j\omega} = A(\omega)\exp[-j\theta(\omega)]$$

Then by definition

$$\tau_{fr} = \lim_{\omega\to\infty} \frac{\theta(\omega)}{\omega}$$

This can be shown to be

$$\lim_{\omega\to\infty} \frac{\theta(\omega)}{\omega} = \tau_{fr} = z\sqrt{\mu_0}$$

Using the procedure outlined in ref. 34, the first four terms of the Maclaurin series expansion of $\hat{g}(t)$ are given by

$$\hat{g}(0+) = \exp\left[\frac{-k\hat{R}}{2}\right] + \exp\left[\frac{-k\hat{R}^*}{2}\right]$$

$$\hat{g}^{(1)}(0+) = \frac{k}{8a}\left[4b + a\right]\left\{\hat{R}^2\exp\left[\frac{-k\hat{R}}{2}\right] + \hat{R}^{*2}\exp\left[\frac{-k\hat{R}^*}{2}\right]\right\}$$

$$\hat{g}^{(2)}(0+) = -\frac{k}{16a^2}\left[8b^2 + 4ab + a^2\right]\left\{\hat{R}^3\exp\left[\frac{-k\hat{R}}{2}\right] + \hat{R}^{*3}\exp\left[\frac{-k\hat{R}^*}{2}\right]\right\}$$
$$+ \frac{k^2}{128a^2}\left[4b + a\right]^2\left\{\hat{R}^4\exp\left[\frac{-k\hat{R}}{2}\right] + \hat{R}^{*4}\exp\left[\frac{-k\hat{R}^*}{2}\right]\right\}$$

$$\hat{g}^{(3)}(0+) = \frac{k}{128a^3}\left[5a^3 + 24a^2b + 48ab^2 + 64b^3\right]\left\{\hat{R}^4\exp\left[\frac{-k\hat{R}}{2}\right] + \hat{R}^{*4}\exp\left[\frac{-k\hat{R}^*}{2}\right]\right\}$$
$$- \frac{k^2}{128a^3}\left[a^3 + 8a^2b + 24ab^2 + 32b^3\right]\left\{\hat{R}^5\exp\left[\frac{-k\hat{R}}{2}\right] + \hat{R}^{*5}\exp\left[\frac{-k\hat{R}^*}{2}\right]\right\}$$
$$+ \frac{k^3}{3072a^3}\left[a + 4b\right]^3\left\{\hat{R}^6\exp\left[\frac{-k\hat{R}}{2}\right] + \hat{R}^{*6}\exp\left[\frac{-k\hat{R}^*}{2}\right]\right\}$$

In order to adequately represent the function it is necessary to evaluate the n^{th} term of the expansion which is of the form

$$\hat{g}^{(n)}(0+) = \lim_{p\to\infty} \left\{ p^{n+1} G(p) e^{p\tau_{fr}} - p^n \hat{g}(0+) - \ldots - p^2 \hat{g}^{(n-2)}(0+) - p\hat{g}^{(n-1)}(0+) \right\}$$

The inversion intergral was approached directly by R. Church, Research Staff Member, SRRC, and has been programmed for the 7094 using a method to be described in a forthcoming Research Report.

Principal features of the method are:

(1) Choice of path of integration sufficiently to the right of the origin that singularities at the integrand are not troublesome.

(2) Use of the efficient high order Gaussian quadrature formulas for the near region.

(3) Use of the Euler transformation for a slowly converging alternating series for the tails.

The results of these methods are shown in Fig. A-1.

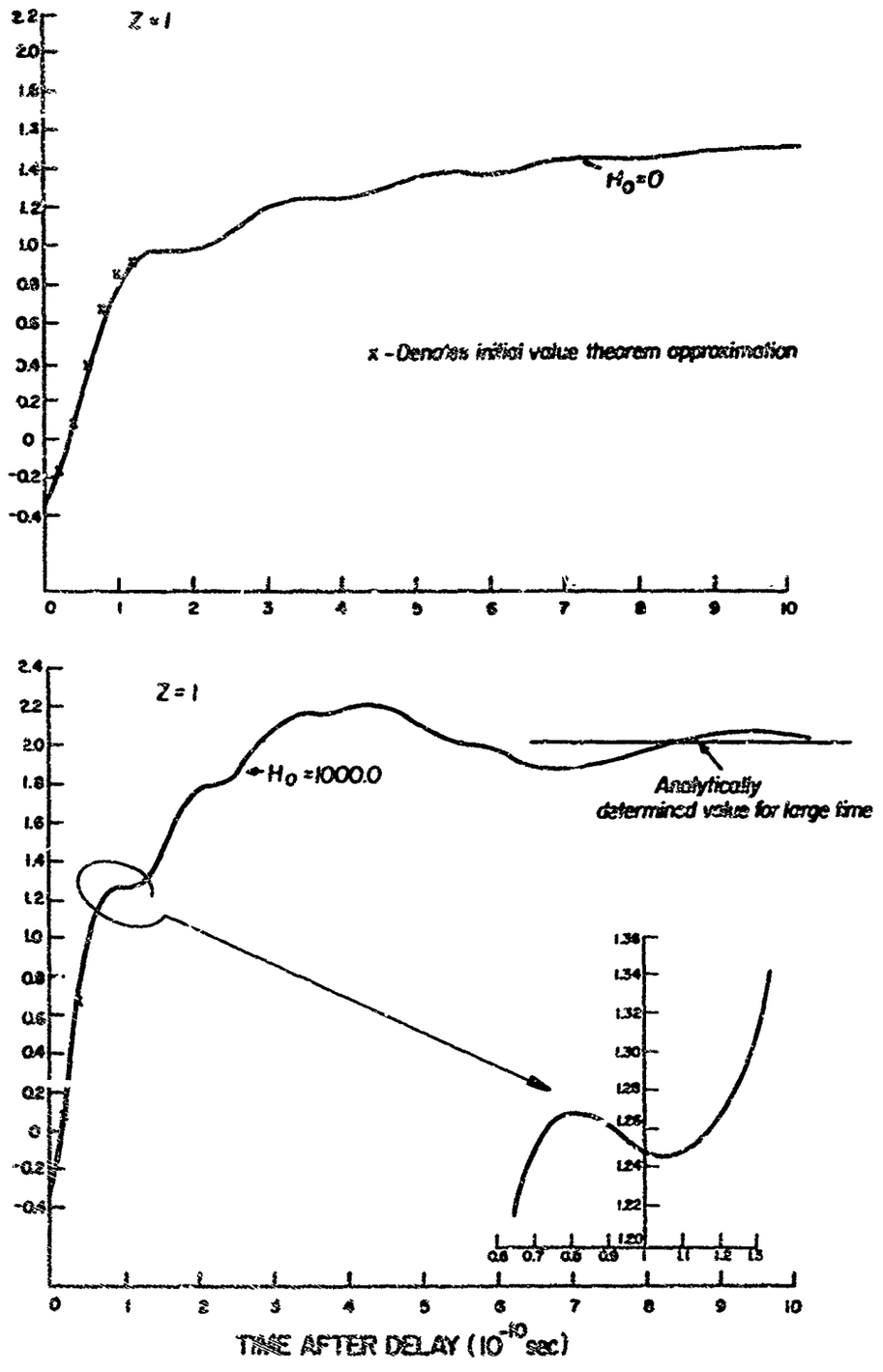

FIG. A-1 The step-response of a semi-infinite ferrite medium.

APPENDIX B

THE CONVENTIONAL QUALITY FACTOR Q

(G. F. Ross, Sperry Rand Research Center)

I. INTRODUCTION

In the narrow-band sense, Q is defined as

$$Q = \frac{\omega_o \langle W_{Total} \rangle|_{\omega_o}}{\langle Pd \rangle|_{\omega_o}} \tag{B.1}$$

where ω_o is the resonant frequency of the system, $\langle W_{Total} \rangle|_{\omega_o}$ is the time average of the total stored energy at ω_o, and $\langle Pd \rangle|_{\omega_o}$ is the time average of the power dissipated in the network. The definition is applied to driving-point (dp) impedance measurements and "loosely" to transfer-function measurements. A more general definition of Q can be obtained by using the relationship

$$\frac{1}{2} V_{IN} I_{IN}^{*} = \langle Pd \rangle + j2\omega \left(\langle W_m \rangle - \langle W_e \rangle \right)$$

It is not difficult to show that this relationship is given by

$$Q = \frac{\omega_o \frac{d}{d\omega} \left\{ \omega \left(\langle W_m \rangle - \langle W_e \rangle \right) \right\} |_{\omega=\omega_o}}{\langle Pd \rangle|_{\omega=\omega_o}} \tag{B.2}$$

and the method used to obtain this solution will be demonstrated here.

---

*This definition is still a narrowband approximation, as will soon become evident.

In the very narrowband case, the impedance or transfer function in question may be represented by an equivalent circuit consisting of a single resistor R, an inductor L, and a capacitor C, all connected in series. Then, for a given current magnitude $|I|$ it is clear that the time average of the power dissipated in the resistor is given by

$$\langle P_d \rangle = |I|^2 R$$

while

$$\langle W_m \rangle = \frac{1}{4} L |I|^2 \tag{B.3}$$

and

$$\langle W_e \rangle = \frac{1}{4} \frac{|I|}{\omega^2 C}$$

Substituting the values given in Eq. B.3 into Eq. B.2, we obtain

$$Q = \frac{\omega_0 \frac{d}{d\omega}\left\{\omega\left[\frac{1}{4}|I|^2 - \frac{1}{4}\frac{|I|^2}{\omega^2 C}\right]\right\}\Big|_{\omega=\omega_0}}{\langle P_d \rangle|_{\omega=\omega_0}} \tag{B.4}$$

which reduces to

$$Q = \frac{\omega_0 \left\{\frac{1}{4}\frac{|I|}{\omega_0^2 C} + \frac{1}{4} L |I|^2\right\}}{\langle P_d \rangle|_{\omega=\omega_0}}$$

$$= \frac{\omega_0 \left\{\langle W_{Total} \rangle\right\}\Big|_{\omega=\omega_0}}{\langle P_d \rangle|_{\omega=\omega_0}} \tag{B.5}$$

This is identical to Eq. B.1.

II. STORED ENERGY AND THE TRANSFER FUNCTION FOR A LOSSLESS TWO-PORT

For the special case where a network is lossless and reciprocal, the unitary condition on the scattering matrix* can be applied, resulting in

$$|S_{21}|^2 = 1 - |S_{11}|^2 \tag{B.6}$$

We can evaluate $|S_{11}|^2$ since

$$S_{11} = \frac{Zdp - 1}{Zdp + 1} = \frac{\frac{2\langle Pd\rangle}{|I|^2} + j\left\{\frac{4\omega}{|I|^2}\left(\langle W_e\rangle - \langle W_m\rangle\right)\right\} - 1}{\frac{2\langle Pd\rangle}{|I|^2} + j\left\{\frac{4\omega}{|I|^2}\left(\langle W_e\rangle - \langle W_m\rangle\right)\right\} + 1} \tag{B.7}$$

Letting $\underline{P} = \frac{2\langle Pd\rangle}{|I|^2}$ and $\underline{W} = \frac{4\omega}{|I|^2}\left(\langle W_e\rangle - \langle W_m\rangle\right)$ we have from Eq. B.6

$$|S_{11}|^2 = \frac{(\langle \underline{P}\rangle - 1)^2 + \underline{W}^2}{(\langle \underline{P}\rangle + 1)^2 + \underline{W}^2} \tag{B.8}$$

and

$$|S_{21}|^2 = 1 - |S_{11}|^2 = \frac{4\langle \underline{P}\rangle}{[\langle \underline{P}\rangle + 1]^2 + \underline{W}^2} \tag{B.9}$$

Next we define ω_0, the resonant frequency of the network, as that frequency where the time average of the stored electric and magnetic energies are equal.[20] Thus, in Eq. B.9 we have, at resonance,

---

* $S\ S^{*T} = I$, the identity matrix.

$$|S_{21}|^2_{\omega=\omega_c} = \frac{4\langle P\rangle}{[\langle P\rangle + 1]^2}\Big|_{\omega=\omega_0} \qquad (B.10)$$

Normalizing Eq. B.9 with respect to Eq. B.10, we obtain

$$\frac{|S_{21}|^2}{|S_{21}|^2_{\omega=\omega_c}} = |S_{21}|^2_{Norm} = \frac{[\langle P\rangle + 1]^2}{[\langle P\rangle + 1]^2 + \underline{W}^2} \qquad (B.11)$$

Expanding $\underline{W}$ in a Taylor series about the resonant frequency ω_0, we have

$$\underline{W} = \frac{4\omega}{|I|^2}\left[\langle W_e\rangle - \langle W_m\rangle\right]$$

$$= \frac{4}{|I|^2}\left\{\left[\left[\langle W_e\rangle - \langle W_m\rangle\right]\right]_{\omega=\omega_0} + \left[\omega\frac{d}{d\omega}\left(\langle W_e\rangle - \langle W_m\rangle\right)\right.\right.$$

$$\left.\left. + \left(\langle W_e\rangle - \langle W_m\rangle\right)\right]_{\omega=\omega_0}(\omega-\omega_0) + \ldots\right\} \qquad (B.12)$$

$$\approx \frac{4}{|I|^2}\left[\omega_0\frac{d}{d\omega}\left(\langle W_e\rangle - \langle W_m\rangle\right)\right]_{\omega=\omega_0}(\omega-\omega_0) + \ldots$$

because at resonance $\langle W_e\rangle = \langle W_m\rangle$. Substituting Eq. B.12 into Eq. B.11, we obtain

$$|S_{21}|^2_{Norm} = \frac{[\langle P\rangle + 1]^2}{|(\langle P\rangle + 1) + j\underline{W}|} \qquad (B.13)$$

$$= \frac{[\langle P\rangle + 1]^2}{\left|(\langle P\rangle + 1) + j\left\{\left[\frac{4\omega_0}{|I|^2}\frac{d}{d\omega}\left(\langle W_e\rangle - \langle W_m\rangle\right)\right]_{\omega=\omega_0}(\omega-\omega_0) + \ldots\right\}\right|}$$

Now again letting $P = \frac{2\langle Pd\rangle}{|I|^2}$

$$|S_{21}|^2_{Norm} = \frac{\left[\langle Pd\rangle + \frac{|I|^2}{2}\right]_{\omega=\omega_0}}{\left|\left(\langle Pd\rangle + \frac{|I|^2}{2}\right)_{\omega=\omega_0} + j\left\{\omega_0 2(\omega-\omega_0)\frac{d}{d\omega}\left\{\langle W_e\rangle - \langle W_m\rangle\right\}\Big|_{\omega=\omega_0} + \ldots\right\}\right|}$$

(B.14)

At the "half-power" frequencies, $|S_{21}|^2_{Norm} = 1/2$. This occurs at the frequencies for which

$$\langle Pd\rangle + \frac{|I|^2}{2} = \omega_0\, 2(\omega-\omega_c)\,\frac{d}{d\omega}\left\{\langle W_e\rangle - \langle W_m\rangle\right\}\Big|_{\omega=\omega_c} + \ldots$$

(B.15)

or (approximately) when

$$\text{Bandwidth} = \Delta\omega \simeq 2(\omega-\omega_0) = \frac{\langle Pd\rangle + \frac{|I|^2}{2}}{\omega_0\frac{d}{d\omega}\left[\left\{\langle W_e\rangle - \langle W_m\rangle\right\}\Big|_{\omega=\omega_0}\right]}$$

(B.16)

Using the narrow-band definition of Q, we have

$$Q = \frac{\omega_0}{\Delta\omega}$$

(B.17)

$$Q \simeq \frac{\omega_0^2\frac{d}{d\omega}\left\{\langle W_e\rangle - \langle W_m\rangle\right\}}{\langle Pd\rangle + \frac{|I|^2}{2}}$$

or, alternately,

$$Q = \frac{\omega_o \frac{d}{d\omega}\left\{\omega\left(\langle W_e\rangle - \langle W_m\rangle\right)\right\}\Big|_{\omega=\omega_o}}{\left[\langle Pd\rangle + \frac{|I|^2}{2}\right]_{\omega=\omega_o}} \qquad (B.18)$$

which is almost identical to the form given in Eq. B.2 and reduces (with interpretation) to the well known definition given in Eq. B.1 for the series RLC circuit resonant at ω_o. It is instructive to interpret the result given in Eq. B.18: the term $\langle Pd\rangle$ is clearly the power dissipated in the load and is equal to $|V_o|^2$. This follows, since the network was assumed lossless except for the termination; therefore,

$$\frac{|I|^2}{2}\,\mathrm{Re}\,Zdp = |S_{21}|^2 = \left\{\frac{|I|^2}{2}\right\}2\,\frac{\langle Pd\rangle}{|I|^2} = \langle Pd\rangle \qquad (B.19)$$

where I is the peak value of the total sinusoidal current entering the port. The term $\frac{|I|^2}{2}$, also in the denominator of Eq. B.18 is the power dissipated in the source impedance of the generator. If the network is "transparent" at resonance, we have

$$\left.\frac{|I|^2}{2}\right|_{\omega=\omega_o} = \langle Pd\rangle\Big|_{\omega=\omega_o} \qquad (B.20)$$

One can consider the "loaded Q" (or the Q including the loss introduced by both the load and source impedances) as given by

$$Q_L = \frac{\omega_o}{2}\,\frac{\frac{d}{d\omega}\left\{\omega\left(\langle W_e\rangle - \langle W_m\rangle\right)\right\}\Big|_{\omega=\omega_o}}{\langle Pd\rangle\Big|_{\omega=\omega_o}} \qquad (B.21)$$

where it will be remembered that the term $\frac{d}{d\omega}\left\{\omega\left(\langle W_e\rangle - \langle W_m\rangle\right)\right\}\Big|_{\omega=\omega_0}$ closely approximates the total energy stored in the network at ω_0. The quantity $\langle Pd\rangle$ is virtually an invariant function of frequency. This is not surprising in broadband lossless networks, since the magnitude squared of the transfer function (equal to $\langle Pd\rangle$) is by definition a "flat" function of frequency; the phase function, however, can be a nonlinear function of frequency.

APPENDIX C

THE TRANSMISSION COEFFICIENT AS A FUNCTION OF THE STORED ENERGY IN A NETWORK

(G. F. Ross, Sperry Rand Research Center)

I. THE ONE-PORT NETWORK

Consider the "black box" shown in Fig. C-1 enclosed by surface S_1: it is essentially a one-port network. It can be shown that for a one-port network[19]

$$\frac{1}{2} V_{IN} I_{IN}^{*} = \langle Pd \rangle + j2\omega \left(\langle W_m \rangle - \langle W_e \rangle \right) \qquad (C.1)$$

and, since $V_{IN} = I_{IN} Z_{dp}$, we have

$$Z_{dp} = \frac{2}{|I_{IN}|^2} \left\{ \langle Pd \rangle + j2\omega \left(\langle W_m \rangle - \langle W_e \rangle \right) \right\} \qquad (C.2)$$

If the one-port network is lossless, $\langle Pd \rangle = 0$ and the driving-point (dp) impedance is a strict function of the stored energy within the network. This relationship will be applied in the next section to study the transmission properties of the lossless two-port network.

II. THE TWO-PORT NETWORK

The network shown in Fig. C-1 and enclosed by the surface S_1 is defined as a two-port network. The network embedded in surface S_3 may be lossless, but the 1-ohm loads terminating ports 2, 3, 4, ...,i make the overall two-port a lossy network. This type of network has applications in many engineering problems where a system is excited at an input port and the response is observed at a specified output port; the other ports are "output" ports only with respect to surface S_3. The normalized scattering matrix of the two-port network is described by

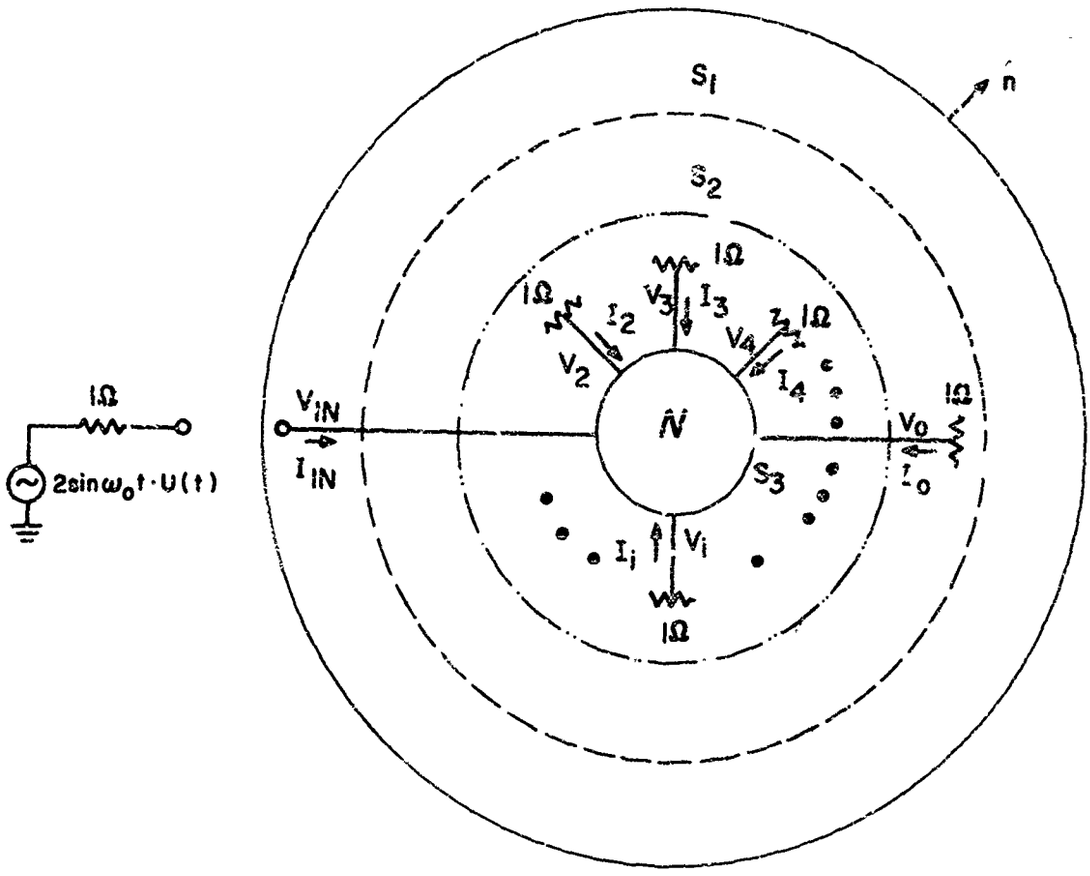

FIG. C-1 Poynting's vector and the n-port network.

$$S = \begin{bmatrix} S_{11}(\omega) & S_{12}(\omega) \\ S_{21}(\omega) & S_{22}(\omega) \end{bmatrix} \qquad (C.3)$$

where

$\underline{b} = S\,\underline{a}$

$\underline{b}$ is the column matrix representing the reflected waves

$\underline{a}$ is the column matrix representing the incident waves

Both $S_{11}(\omega)$ and $S_{22}(\omega)$ are defined by the relationships

$$S_{11}(\omega) = \frac{Zdp_1 - 1}{ZAdp_1 + 1} \quad ; \quad S_{22}(\omega) = \frac{Zdp_2 - 1}{Zdp_2 + 1} \qquad (C.4)$$

If we now short-circuit the output port, we have $b_2 = - a_2$ and, using Eq. C.3, we obtain

$$b_1 = S_{11}\, a_1 + S_{12}\, a_2 \qquad (C.5a)$$

$$-a_2 = S_{21}\, a_1 + S_{22}\, a_2 \qquad (C.5b)$$

Solving Eq. C.5b for a_2 and substituting the result into Eq. C.5a, we obtain

$$\left.\frac{b_1}{a_1}\right|_{SC} = S_{11} - \frac{S_{12}\,S_{21}}{1 + S_{22}} = S_{11} - \frac{S_{21}^2}{1 + S_{22}} \qquad (C.6)$$

for the special case where the network is reciprocal.

Defining $\left.\frac{b_1}{a_1}\right|_{SC} = \tilde{S}_{11}(\omega)$ and solving for $S_{21}(\omega)$, we obtain

$$S_{21}(\omega) = \sqrt{[S_{11}(\omega) - \tilde{S}_{11}(\omega)][1 + S_{22}(\omega)]}$$

$$= 2\sqrt{\frac{(Zdp_1 + \tilde{Z}dp)\, Zdp_2}{(1 + Zdp_1)(1 + Zdp_2)(1 + \tilde{Z}dp)}} \qquad (C.7)$$

with the aid of Eq. C.4 note that Eq. C.7 expresses the transfer function of interest (i.e., the ratio of the reflected voltage at the output port to the incident voltage at the input port) in terms of only the dp impedances of the network under matched and short-circuited conditions. It is therefore evident, using the results presented in Eq. C.2 , that the dp impedance can be expressed in terms of the time average of the power dissipated and the energy stored in the network. Assuming that the time average of the power dissipated in the network is a constant within the band of interest (in broadband networks this is a reasonable assumption), then $S_{21}(\omega)$ is given (approximately) as a function of the energy stored in the network. If we multiply $S_{21}(\omega)$, given in Eq. C.7 , by its conjugate, we obtain the magnitude squared of the transfer function; this is also only a function (to a close approximation) of the energy stored in the network.

In certain cases of practical importance (e.g., a lossless four-port coupler) it is possible to express the general transfer function $S_{ij}(\omega)$ between two ports as an exact function of the stored energy in the network. The procedure is to measure the dp impedance $\tilde{Z}_{ii}$ with all output ports either open- or short-circuited and relate the results to $S_{ij}(\omega)$, the scattering parameter obtained under matched conditions. Since the network is lossless, $\tilde{Z}_{ii}$ can only have an imaginary part and is therefore a strict function of the stored energy. Even when the network is reciprocal*, however,

* Reciprocity is defined by the relationship $S=S^T$.

we must obtain the solution to ten simultaneous, nonlinear algebraic equations having ten unknowns, making the solution of the problem impractical in general (see the next section).

III. SPECIAL CASE - THE LOSSLESS RECIPROCAL TWO-PORT NETWORK

Assume the scattering matrix of a passive, linear, reciprocal two-port network is to be determined only from open- and short-circuit tests. In particular, we are interested in evaluating the transfer coefficient $S_{21}(\omega)$ in terms of only the open- and short-circuit parameters; the driving impedance of a lossless network under open- or short-circuit conditions must be only reactive, and from Eq. C.2 we know that the reactive component is a function of the stored energy in the network.

If the output terminals of the two-port network are short-circuited then

$$\frac{b_1}{a_1} = S_{11} + S_{21}\frac{a_2}{a_1} \tag{C.8}$$

$$\frac{a_2}{a_1} = S_{21} + S_{22}\frac{a_2}{a_1} \tag{C.9}$$

Solving Eq. (C.9) for $\frac{a_2}{a_1}$ and substituting the result into Eq. C.8, we obtain

$$\left.\frac{a_1}{a_1}\right|_{SC} = S_{11}\,{}_{SC} = S_{11} - \frac{S_{21}^2}{S_{22}+1} \equiv A \tag{C.10}$$

Similarly, with the output terminals open-circuited we have

$$\left.\frac{b_1}{a_1}\right|_{OC} = S_{11}\Big|_{OC} = S_{11} - \frac{S_{21}^2}{S_{22} - 1} = b \qquad (C.11)$$

and

$$\left.\frac{b_2}{a_2}\right|_{SC} = S_{22}\Big|_{SC} = S_{22} - \frac{S_{21}^2}{S_{11} + 1} = C \qquad (C.12)$$

Adding Eqs. C.10 and C.11, we obtain

$$\frac{A + B}{2} = S_{11} - \frac{S_{22} S_{21}^2}{S_{22}^2 - 1} = E \qquad (C.13)$$

Subtracting Eq. C.11 from Eq. C.10, we obtain

$$\frac{B - A}{2} = \frac{S_{21}^2}{1 - S_{22}^2} = D \qquad (C.14)$$

Substituting Eq. C.14 into Eq. C.13 and solving for S_{11}, we obtain

$$S_{11} = E - S_{22}D \qquad (C.15)$$

Solving for S_{21}^2 and substituting the result together with Eq. C.15 into Eq. C.12, we obtain

$$C = S_{22} = \frac{D(1 - S_{22}^2)}{E - S_{22}D + 1} \tag{C.16}$$

Solving for S_{22}, we find that

$$S_{22} = \frac{CE + C + D}{1 + CD + E} \tag{C.17}$$

and, finally, using Eq. C.14,

$$S_{21}^2 = D\left\{1 - \left[\frac{CE + C + D}{CD + E + 1}\right]^2\right\} \tag{C.18}$$

The interpretation of Eq. C.18 is of interest. The result holds for any lossy reciprocal two-port network and should be identical to Eqs. C.7 and C.6 after mathematical manipulation. However, if we allow the network to be <u>lossless</u>, then A, B, and C must have a magnitude of unity: the quantities A, B, and C are in reality the dp reflection coefficients, which can be related to a purely reactive dp input impedance through Eq. C.4. From Eq. C.1 it is clear that the reactive component of the dp impedance is a function of the energy stored in the network. Hence, we have shown that $S_{21}^2(\omega_1)$ of a lossless two-port network can be described by the stored energy at that frequency. Note also that $S_{21}(\omega)$ or $S_{21}^2(\omega)$ is, in general, a complex number: A, B, and C have unity magnitude but in general are complex numbers. Hence, as we would expect, the numerator and denominator of Eq. C.18 are complex quantities.

APPENDIX D

MATRIX ANALYSIS OF MICROWAVE NETWORKS

(L. Susman, Sperry Gyroscope Co.)

I. INTRODUCTION

The use of matrix techniques allows one to formulate and solve the transient response in a strictly mathematical but straightforward way and has the advantage of being a familiar technique to microwave engineers. The formulation presented below is based on the use of a scattering matrix description of the microwave network, and follows closely the development of Laemmel.[47]

The scattering matrix formulation is used to compute the overall scattering representation of a cascade connection of an n-port and k-port microwave network (where in general n and k need not be identical). It should be noted from the outset that the scattering matrix used here is a representation of the microwave network that is valid over all of ω. This differs substantially from the scattering matrix techniques most often encountered by microwave engineers-where a single frequency representation of the device is usually used.

II. INTERCONNECTION OF NETWORKS

Given an N-port network and an M-port network, each described by scattering matrices S^N and S^M, respectively, we are interested in finding the scattering matrix S of the network formed when k of the n ports are connected to K of the m ports (as shown in Fig. D-1a) to form an $(n + m - 2k)$-port network. Let b_1^N, a_1^N, b_2^N, a_2^N, b_1^M, a_1^M, b_2^M, a_2^M be the n-k, k, k, and m-k column vectors denoting the variables of networks N and M.

Then

$$\begin{bmatrix} b_1^N \\ \hline b_2^N \end{bmatrix} = \begin{bmatrix} S_{11}^N & S_{12}^N \\ \hline S_{21}^N & S_{22}^N \end{bmatrix} \begin{bmatrix} a_1^N \\ \hline a_2^N \end{bmatrix} \qquad \text{(D.1a)}$$

and

$$\begin{bmatrix} b_1^M \\ \hline b_2^M \end{bmatrix} = \begin{bmatrix} S_{11}^M & S_{12}^M \\ \hline S_{21}^M & S_{22}^M \end{bmatrix} \begin{bmatrix} a_1^M \\ \hline a_2^M \end{bmatrix} \qquad \text{(D.1b)}$$

are the scattering matrices of the networks N and M. When the networks are interconnected as shown in Figure D-1b,

$$b_2^N = a_1^M \quad \text{and} \quad a_2^N = b_1^M \qquad \text{(D.2)}$$

Matrix S for the overall matrix can be written in the form

$$\begin{bmatrix} b_1^N \\ \hline b_2^M \end{bmatrix} = \begin{bmatrix} S_{11} & S_{12} \\ \hline S_{21} & S_{22} \end{bmatrix} \begin{bmatrix} a_1^N \\ \hline a_2^M \end{bmatrix} \qquad \text{(D.3)}$$

From equations D.1 and D.2 it follows that

$$[a_1^M] = [b_2^N] = [S_{21}^N \; a_1^N] + [S_{22}^N \; a_2^N] = S_{21}^N \; a_1^N + S_{22}^N \; S_{11}^M \; a_1^M + S_{22}^N \; S_{12}^M \; a_2^M$$

or (D.4)

$$[a_1^M] = [1 - S_{22}^N \; S_{11}^M]^{-1} \left\{ S_{21}^N \; a_1^N + S_{22}^N \; S_{12}^M \; a_2^M \right\}$$

In a similar way, a_2 can be found to be

$$[a_2^N] = [I - S_{11}^M \; S_{22}^N]^{-1} \left\{ S_{11}^M \; S_{21}^N \; a_1^N + S_{12}^M \; a_2^M \right\} \qquad (D.5)$$

From Eqs. D.4 and D.5 we arrive at the final result for the overall scattering matrix S; i.e.,

$$S = \left[\begin{array}{c|c} S_{11}^N + S_{12}^N [I - S_{11}^M \; S_{22}^N]^{-1} \; S_{11}^M \; S_{21}^N & S_{12}^N [I - S_{11}^M \; S_{22}^N]^{-1} \; S_{12}^M \\ \hline S_{21}^M [I - S_{22}^N \; S_{11}^M]^{-1} \; S_{21}^N & S_{22}^M + S_{21}^M [I - S_{22}^N \; S_{11}^M]^{-1} \; S_{22}^N \; S_{12}^M \end{array}\right]$$

D.6

III. ANALYSIS OF SPECIAL CASES

A. Special Case 1 - Cascade of Two Ports

Consider the cascade of two ports shown in Fig. D-2. Then from Eq. D.6 the overall scattering matrix is simply

$$S = \left[\begin{array}{c|c} S_{11}^{(1)} + \dfrac{S_{12}^{(1)}\, S_{11}^{(2)}\, S_{21}^{(1)}}{1 - S_{11}^{(2)}\, S_{22}^{(1)}} & \dfrac{S_{12}^{(1)}\, S_{12}^{(2)}}{1 - S_{11}^{(2)}\, S_{22}^{(1)}} \\ \hline \dfrac{S_{21}^{(2)}\, S_{21}^{(1)}}{1 - S_{11}^{(2)}\, S_{22}^{(1)}} & \dfrac{S_{22}^{(2)} + S_{21}^{(2)}\, S_{22}^{(1)}\, S_{21}^{(2)}}{1 - S_{11}^{(2)}\, S_{22}^{(1)}} \end{array}\right]$$

B. Special Case 2 - Cascade of Identical Structures with Mirror Symmetry

Consider the cascade connection shown in Fig. D-3. Here the two networks are identical and are interconnected to form a symmetric structure. It is easy to see that the scattering matrix for the individual networks can be written for network I as

$$\begin{bmatrix} b_1 \\ \hline b_2 \end{bmatrix}^{I} = \left[\begin{array}{c|c} S_{11} & S_{12} \\ \hline S_{21} & S_{22} \end{array}\right] \begin{bmatrix} a_1 \\ \hline a_2 \end{bmatrix}^{I}$$

and for network II

$$\begin{bmatrix} b_2 \\ \hline b_1 \end{bmatrix}^{II} = \left[\begin{array}{c|c} S_{22} & S_{21} \\ \hline S_{12} & S_{11} \end{array}\right] \begin{bmatrix} a_1 \\ \hline a_2 \end{bmatrix}^{II}$$

It then follows from Eq. D.6 that the overall scattering matrix is given by

$$S = \left[\begin{array}{c|c} S_{11} + S_{12}[I - S_{22}^2]^{-1} S_{22} S_{21} & S_{12}[I - S_{22}^2]^{-1} S_{21} \\ \hline S_{12}[I - S_{22}^2]^{-1} S_{21} & S_{11} + S_{12}[I - S_{22}^2]^{-1} S_{22} S_{21} \end{array}\right]$$

This particular matrix was shown to be of considerable value in the analysis of the sidewall coupler (see Sec. 5.3).

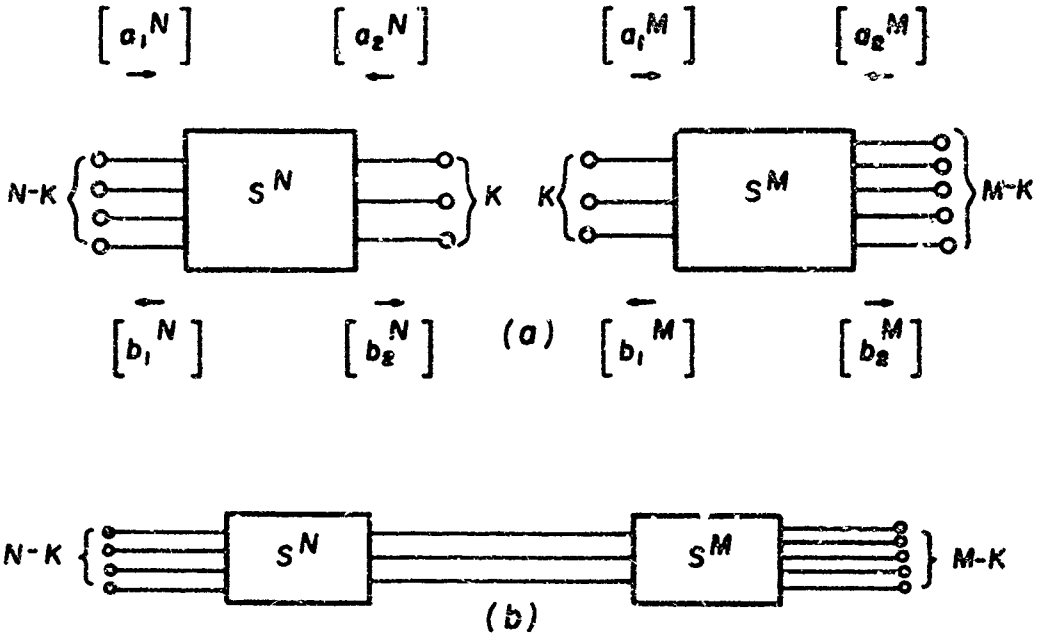

FIG. D-1 Interconnection of networks.

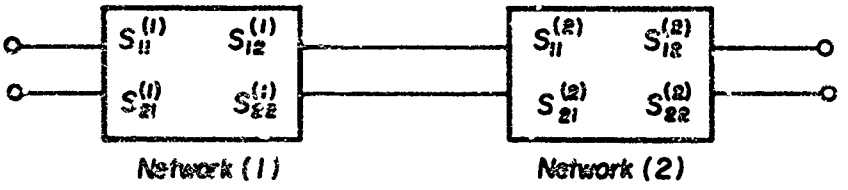

FIG. D-2 Cascade of two ports.

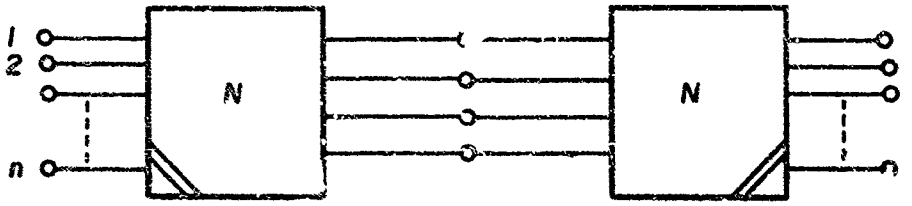

FIG. D-3 Cascade of identical networks with mirror symmetry.

BIBLIOGRAPHY

1. M. Ito, Dispersion of Very Short Microwave Pulses in Waveguide, IEEE Trans. on Microwave Theory and Techniques (May 1965), p. 357.

2. H. J. Shaw, et al., Microwave Generation in Pulsed Ferrites, J. Appl. Phys. 37, No. 3 (March 1966), p. 1060.

3. F. R. Morgenthaler, Microwave Radiation from Ferrimagnetically Coupled Electrons in Transient Magnetic Fields, Trans. IRE, PGMTT (January 1959), p. 6.

4. E. Schloemann, Ferromagnetic Resonance at High Power Levels, Raytheon Report No. R-48 (October 1959).

5. K. J. Harker, Final Precession Angles for Pulsed Ferrite Samples, IEEE Trans. Magnetics (March 1960).

6. K. J. Harker and H. J. Shaw, Transient Spinwave Buildup in Ferrites, Microwave Lab. Report No. 1365, Stanford Univ. (Sept. 1965).

7. R. I. Joseph, et al., Transient Growth of Spin Waves Under Parallel Pumping, J. Appl. Phys. 37, No. 3 (March 1966), p. 1069.

8. H. Suhl, The Theory of Ferromagnetic Resonance at Signal Powers, J. Phys. Chem. Solids (1957), p. 209.

9. J. A. Stratton, Electromagnetic Theory, McGraw-Hill Book Company, Inc., New York (1941), p. 320.

10. R. F. Harrington, Time Harmonic Electromagnetic Fields, McGraw-Hill Book Co., Inc., New York (1961).

11. A. D. Berk, "Variational Principles for Electromagnetic Resonators and Waveguides," IRE Trans. on Ant. & Prop. (April 1956), p. 104.

12. B. Lax and K. J. Button, Microwave Ferrites and Ferrimagnetics, McGraw-Hill Book Co., Inc., New York (1962).

13. E. Angelo, Electronic Circuits, McGraw-Hill Book Co., Inc., New York (1958), p. 353.

14. G. Valley, H. Wallman, Vacuum Tube Amplifiers, MIT Radiation Lab. Series, Vol. 18, McGraw-Hill Book Co., New York (1948), p. 169.

15. S. Goldman, Frequency Analysis, Modulation and Noise, McGraw-Hill Book Co., Inc., New York (1948), p. 254.

16. C. Helstrom, Statistical Theory of Signal Detection, Pergamon Press, New York (1960), p. 18.

17. G. Ross, The Transient Analysis of Certain TEM Mode Four-Port Networks, IEEE Trans. MTT, Vol. MTT-14, No. 11 (November 1966), pp. 528-541.

18. R. Adler, L. Chu and R. Fano, Electromagnetic Energy Transmission and Radiation, John Wiley & Sons, New York (1960), p. 273.

19. E. Jordan, Electromagnetic Waves and Radiating Systems, Prentice Hall, Inc., New York (1950), pp. 160-169.

20. R. Fano, L. Chu and R. Adler, Ref. 18, p. 296.

21. Air Force Contract No. F30602-67-C-0121, Transient Behavior of Microwave Networks, II.

22. J. Ragazzini and G. Franklin, Sampled Data Control Systems, McGraw-Hill Book Co., Inc., New York (1958), p. 78.

23. J. Aseltine, Transform Methods in Linear System Analysis, McGraw-Hill Book Co., Inc., New York (1958), p. 253.

24. A. Papoulis, The Fourier Integral and Its Applications, McGraw-Hill Book Co., Inc., New York (1962), pp. 134-138.

25. G. Ross, et al., Transient Behavior of Microwave Networks, Interim Report, Sperry Rand Research Center, Sudbury, Mass. (1967).

26. B. M. Oliver, Directional Electromagnetic Couplers, Proc. IRE 42, 1686-1642 (1954).

27. W. L. Firestone, Analysis of Transmission Line Directional Couplers, Proc. IRE 42, 1529-1538 (1954).

28. E. G. Cristal, Coupled-Transmission-Line Directional Couplers with Coupled Lines of Unequal Characteristic Impedances, 1966 PGMTT International Symposium, pp. 114-117 (1966).

29. S. Mason, Feedback Theory - Further Properties of Signal Flow Graphs, Proc. IRE 44, 920 (1956).

30. S. J. Mason and H. J. Zimmerman, Electronic Circuits, Signals and Systems, John Wiley and Sons, Inc., New York (1960), pp. 92.

31. K. L. Su, Active Network Synthesis, McGraw-Hill Book Co., Inc., New York (1965), pp. 340-342.

32. R. Levy, General Synthesis of Asymmetric Multi-Element Coupled Transmission Line Directional Couplers, IRE Trans. on Micro. Th. and Tech. MTT-11, 226-237 (1963).

33. E. G. Cristal and L. Young, Theory and Tables of Optimum Symmetrical TEM-Mode Coupled-Transmission-Line Directional Couplers, IEEE Trans. on Micro. Th. and Tech. MTT-13, 544-558 (1965).

34. G. F. Ross, et al., The Transient Analysis of Large Arrays, Technical Report No. RADC-TDR-64-509, Rome Air Development Center, Griffiss Air Force Base, Rome, New York, February 1965.

35. R. E. Collin, Field Theory of Guided Waves, McGraw-Hill Book Co., Inc., New York (1960).

36. W. A. Saxton and H. J. Schmitt, Transients in a Large Waveguide, Proc. IEEE 52, 405 (1963).

37. M. Cerrillo, Transient Phenomena in Waveguides, Research Laboratory of Electronics, MIT Technical Report No. 33 (1948).

38. A. E. Karbowiak, Propagation of Transients in Waveguides, Proc. IEES 104 (Part C), 329-349 (1957).

39. J. R. Wait and K. P. Spies, On the Theory of Transient Wave Propagation in a Dispersive Medium, Applied Scientific Research 16, 455-465 (1966).

40. G. L. Hanley and L. Susman, Sinusoidal Step Response of L-Band Waveguide, Proc. IEEE 53 (1965).

41. E. S. Sablin, Use of the Mirror-Image Method to Evaluate the Scattering Matrix of a Slot Waveguide Bridge, Izvestiya VUZ, Radiotekhnika, Vol. 8, No. 1, pp. 111-116 (1965).

42. N. Marcuvitz, Waveguide Handbook, Rad. Lab Series, Vol. 10, McGraw-Hill Book Co., New York.

43. D. S. Jones, The Theory of Electromagnetism, Pergamon Press, New York (1964).

44. L. Lewin, Advanced Theory of Waveguides, Iliffe and Sons, Ltd., London (1951).

45. J. R. Pace and R. Mittra, Generalized Scattering Matrix Analysis of Waveguide Discontinuity Problems, Proc. of the Symposium on Quasi-Optics, Polytechnic Press (1964).

46. G. F. Ross, An Extension of the Initial Value Theorem, IEEE Trans. CT, Vol. CT-13, No. 2, pp. 220-221 (1966).

47. A. E. Laemmel, Scattering Matrix Formulation of Microwave Networks, Symposium on Modern Network Synthesis, Polytechnic Press (1952).

UNCLASSIFIED

Security Classification

DOCUMENT CONTROL DATA - R&D

(Security classification of title, body of abstract and indexing annotation must be entered when the overall report is classified)

1. ORIGINATING ACTIVITY (Corporate author)	2a. REPORT SECURITY CLASSIFICATION
Sperry Rand Research Center Sudbury, Mass.	UNCLASSIFIED
	2b. GROUP

3. REPORT TITLE

TRANSIENT BEHAVIOR OF MICROWAVE NETWORKS

4. DESCRIPTIVE NOTES (Type of report and inclusive dates)

Final Report:

5. AUTHOR(S) (Last name, first name, initial)

Ross, Gerald F.; Allen, Lamar; Smith, Robert; Susman, Leon

6. REPORT DATE	7a. TOTAL NO. OF PAGES	7b. NO. OF REFS
August 1967	194	47

8a. CONTRACT OR GRANT NO.	9a. ORIGINATOR'S REPORT NUMBER(S)
AF30(602)-4180 b. PROJECT NO. 4506 c. Task No. 450602 d.	SRRC-CR-67-29 9b. OTHER REPORT NO(S) (Any other numbers that may be assigned this report) RADC-TR-67-370

10. AVAILABILITY/LIMITATION NOTICES This document is subject to special export controls and each transmittal to foreign governments, foreign nationals or representatives thereto may be made only with prior approval of RADC (EMLI) Griffiss AFB, NY 13440.

11. SUPPLEMENTARY NOTES	12. SPONSORING MILITARY ACTIVITY
RADC Project Engineer VINCENT C. VANNICOLA (EMATE) AC 315 330-4251	Air Force Systems Command Research and Technology Division Rome Air Development Center Griffiss Air Force Base, New York 13440

13. ABSTRACT

The purpose of this study is to investigate the transient behavior of non-reciprocal ferrite devices and coupled networks which are used in wideband radar and communications systems to process signals having wideband spectral content. This investigation should lead to a better understanding of the limitations imposed by the use of these components.

This final report is divided into three major component study areas. They are: (a) nonreciprocal ferrite devices (e.g., isolators, circulators); (b) coupled TEM-mode networks (e.g., the quarter-wavelengths or parallel-line coupler) and (c) coupled waveguide networks (e.g., the sidewall coupler). In addition, a major subsection is devoted to determining the utility of describing the transient behavior of a microwave network by a single paramter in the frequency domain, namely, "the bandwidth "

New methods are introduced to evaluate transients in microwave networks in both the study of ferrite and waveguide networks; in the former area a microstrip circulator is suggested for wideband application. A new definition of effective bandwidth for microwave networks is offered which considers energy stored in the modes of the device. Finally, a novel class of parallel-line couplers whose impulse response is time limited is introduced: the impulse response consists of two delayed impulses.

Both the theoretical and experimental portions of this study employ a time domain analysis as opposed to the conventional frequency domain approach. It is shown that a time domain analysis yields considerable insight and suggests new network models. The measurement and analysis techniques presented in this study are outgrowths of efforts on two previous Air Force sponsored programs, namely, "the Transient Behavior of Large Arrays" (AF30(602)-3348) and "the Transient Behavior of Radiating Elements" (AF30(602)-4250).

DD FORM 1473

UNCLASSIFIED

Security Classification

Unclassified
Security Classification

14 KEY WORDS	LINK A		LINK B		LINK C	
	ROLE	WT	ROLE	WT	ROLE	WT
Microwave Time-domain Wideband Waveguides Networks						

INSTRUCTIONS

1 ORIGINATING ACTIVITY. Enter the name and address of the contractor, subcontractor, grantee, Department of Defense activity or other organization (*corporate author*) issuing this report.

2a. REPORT SECURITY CLASSIFICATION: Enter the overall security classification of the report. Indicate whether "Restricted Data" is included. Marking is to be in accordance with appropriate security regulations.

2b. GROUP: Automatic downgrading is specified in DoD Directive 5200.10 and Armed Forces Industrial Manual. Enter the group number. Also, when applicable, show that optional markings have been used for Group 3 and Group 4 as authorized.

3. REPORT TITLE: Enter the complete report title in all capital letters. Titles in all cases should be unclassified. If a meaningful title cannot be selected without classification, show title classification in all capitals in parenthesis immediately following the title.

4. DESCRIPTIVE NOTES: If appropriate, enter the type of report, e.g., interim, progress, summary, annual, or final. Give the inclusive dates when a specific reporting period is covered.

5. AUTHOR(S): Enter the name(s) of author(s) as shown on or in the report. Enter last name, first name, middle initial. If military, show rank and branch of service. The name of the principal author is an absolute minimum requirement.

6. REPORT DATE: Enter the date of the report as day, month, year, or month, year. If more than one date appears on the report, use date of publication.

7a. TOTAL NUMBER OF PAGES: The total page count should follow normal pagination procedures, i.e., enter the number of pages containing information.

7b. NUMBER OF REFERENCES: Enter the total number of references cited in the report.

8a. CONTRACT OR GRANT NUMBER: If appropriate, enter the applicable number of the contract or grant under which the report was written.

8b, 8c, & 8d. PROJECT NUMBER: Enter the appropriate military department identification, such as project number, subproject number, system numbers, task number, etc.

9a. ORIGINATOR'S REPORT NUMBER(S): Enter the official report number by which the document will be identified and controlled by the originating activity. This number must be unique to this report.

9b. OTHER REPORT NUMBER(S): If the report has been assigned any other report numbers (*either by the originator or by the sponsor*), also enter this number(s).

10 AVAILABILITY/LIMITATION NOTICES: Enter any limitations on further dissemination of the report, other than those imposed by security classification, using standard statements such as:

(1) "Qualified requesters may obtain copies of this report from DDC."

(2) "Foreign announcement and dissemination of this report by DDC is not authorized."

(3) "U. S. Government agencies may obtain copies of this report directly from DDC. Other qualified DDC users shall request through _____."

(4) "U. S. military agencies may obtain copies of this report directly from DDC. Other qualified users shall request through _____."

(5) "All distribution of this report is controlled. Qualified DDC users shall request through _____."

If the report has been furnished to the Office of Technical Services, Department of Commerce, for sale to the public, indicate this fact and enter the price, if known.

11. SUPPLEMENTARY NOTES: Use for additional explanatory notes.

12. SPONSORING MILITARY ACTIVITY: Enter the name of the departmental project office or laboratory sponsoring (*paying for*) the research and development. Include address.

13 ABSTRACT: Enter an abstract giving a brief and factual summary of the document indicative of the report, even though it may also appear elsewhere in the body of the technical report. If additional space is required, a continuation sheet shall be attached.

It is highly desirable that the abstract of classified reports be unclassified. Each paragraph of the abstract shall end with an indication of the military security classification of the information in the paragraph, represented as (*TS*), (*S*), (*C*), or (*U*).

There is no limitation on the length of the abstract. However, the suggested length is from 150 to 225 words.

14 KEY WORDS: Key words are technically meaningful terms or short phrases that characterize a report and may be used as index entries for cataloging the report. Key words must be selected so that no security classification is required. Identifiers, such as equipment model designation, trade name, military project code name, geographic location, may be used as key words but will be followed by an indication of technical context. The assignment of links, rules, and weights is optional.

Unclassified
Security Classification